PNC TN941 82-53

SCOPE OF PRESENTATIONS (III)

Third Specialists' Meeting on Reactor Noise SMORN-III

October 26-30, 1981, Tokyo

1981 ASME Winter Annual Meeting

November 15-20, 1981, Washington D.C.

1981 ANS Winter Meeting

November 29-December 3, 1981, San Francisco

PNC-UKAEA Specialists' Meeting on Safety and Instrument

October 20-28, 1981, Oarai, Tokyo

March 1982

Power Reactor and Nuclear Fuel Development Corporation

PNC TN941 82-53
1982年 3 月

プレゼンテーションの記録（Ⅲ）

第3回炉雑音専門家会議（1981年10月26～30日，東京）
1981年 ASME冬の年会（1981年11月15～20日，ワシントン）
1981年 ASME冬の会議（1981年 11月29日～12月3日，サンフランシスコ）
日英安全性・計測専門家会議（1981年10月20～28日，大洗，東京）

監修：羽賀 一男*

要　　旨

本資料は1981年10月から12月にかけて開かれた国際会議，米国における学会，さらに英国との専門家会議における発表のうち，大洗工学センター高速炉安全性試験室で行なわれた試験研究の報告の記録をまとめたものである。

この時期，東京で開催された第3回炉雑音専門家会議（SMORN－Ⅲ）では，熱電対，うず電流型流量・温度計，音響検出器といった炉心計測器による燃料集合体内局所沸騰検知の可能性を検討する論文を提出した。米国機械学会（ASME）や米国原子力学会（ANS）の年会における計3件の発表でも局所閉塞に起因する事象を取り扱い，ガス放出の効果を含めた温度上昇割合の評価，ナトリウム局所沸騰現象について述べた。また，大洗および東京で開催された日英安全性・計測専門家会議では，ナトリウム過度沸騰・燃料破損伝熱試験の進捗状況を報告した。

各発表における提出論文，口頭発表原稿が本文中に収録されている。

* 大洗工学センター，蒸気発生器開発部，高速炉安全性試験室

PNC TN941 82-53
Mar. 1982

Scope of Presentations (III)

Edited by Kazuo HAGA[a)]

SUMMARY

The present report compiles submitted papers and their manuscripts of oral presentations in an international conference and two meetings in USA during 1981. Four papers in total were contributed to the meetings on experimental studies of local faults in the Fast Reactor Safety Section. That is, the one paper for the Third Specialists' Meeting on Reacotr Noise discussed the possibility of anomaly ditection using in-core monitor sensors, the two for the ASME Winter Annual Meeting treated the temperature rise behind blockage and the one for the ANS Winter Meeting discribed local boiling phenomena.

On the other hand, in this time period, the PNC-UKAEA specialists' meeting on safety and instrument was held at OEC. One chapter of this report is used for the record of presentation on the transient sodium boiling and fuel failure propagation tests status in PNC.

CONTENTS

a) Fast Reactor Safety Section, Steam Generator Division, Oarai Engineering Center, Power Reactor and Nuclear Fuel Development Corporation (OEC/PNC)

1. THIRD SPECIALISTS' MEETING ON REACTOR NOISE SMORN-III

1 Detection of Local Sodium Boiling in a Simulated LMFBR Fuel Subassembly*

H. Inujuma, T. Ogino, K. Haga and Y. Kikuchi

Edited by H. Inujima

* Present work was conducted by the collaborative research between PNC and Mitsubishi Electric Corp. (Contract number 560F002)

DETECTION OF LOCAL SODIUM BOILING IN A SIMULATED LMFBR FUEL SUBASSEMBLY

H. INUJIMA*, T. OGINO*, K. HAGA** and Y. KIKUCHI***

* Central Research Laboratory, Mitsubishi Electric Corporation, Japan

** O-arai Engineering Center, Power Reactor and Nuclear Fuel Development Corporation, Japan

*** Department of Nuclear Engineering, Kyoto University Japan

ABSTRACT

Out-of-pile experiments were carried out to study the feasibility of the local sodium boiling detection by use of temperature, flow and acoustic noises. The studies showed that the temperature fluctuation transferred the information of local sodium boiling to the end of the bundle, but little to the outlet. A new anomaly detection method, which used the algorithm of whiteness test of the residual time series data of autoregressive model, especially using flow fluctuation, was effective detecting the anomaly such as local sodium boiling. On the other hand, acoustic noises with local sodium boiling became much higher than the background such as the mechanical and flow noises. A waveguide method, which was utilized for the present experiments, was useful for the boiling detection.

KEYWORDS

Sodium boiling, temperature fluctuation, flow fluctuation, acoustic noises, anomaly detection method, autoregressive model, out-of-pile experiments.

INTRODUCTION

For the safety operation of liquid metal cooled fast breeder reactors (LMFBRs) it is very important to detect local boiling in a subassembly at its initial stage. Since flow blockage is one of the most typical causes of local boiling, many efforts (Fry and Levell, 1976; Ohlmer and Shwalman, 1975) have been concentrated on the study of detecting the flow blockage under non-boiling conditions by use of temperature fluctuations at the outlet of a subassembly.

In-pile and out-of-pile experiments have been made on the local boiling detection by use of temperature and flow fluctuations (Ogino, Inujima et al., 1979; Burton, Bentley, et al., 1979; Smith, et al. 1978). The results showed that the utilization of temperature fluctuations was promising for the early detection of sodium boiling in LMFBRs. Measurement of acoustic noise signals is also useful for the boiling detection. In the earlier papers (Kikuchi, Daigo, et al., 1975, 1977; Ozaki, et al., 1978), which dealt with the sodium boiling experiments in small geometries, it was revealed that the boiling caused a considerable increase in acoustic noise intensity. The peak observed at the low-frequency hertz ranges was due to the repetition of bubble formation and collapse. In the high-frequency kilohertz ranges, however, resonance peaks were superposed on a broad peak at approximately 10kHz.

In order to make it clear that these noise analyses are applicable to an actual anomaly detection method, larger scaled experiments have recently been carried out. This paper will give the experimental results obtained, especially of the following subjects.

(1) Statistical properties of temperature and flow fluctuations in the downstream of the blockage under local boiling conditions.

(2) Sensitivity of a newly developed anomaly detection method which uses the statistical

index of fluctuation signals.

(3) Statistical properties of acoustic noises under local boiling conditions.

(4) Sensitivity of an anomaly detection method using the acoustic noise.

EXPERIMENTAL EQUIPMENT

A series of sodium boiling experiments were carried out in the SIENA loop installed at the O-arai Engineering Center, Power Reactor and Nuclear Fuel Development Corporation (PNC). The details of the SIENA loop are described by Kikuchi, Diago and Ohtsubo, (1977).

Figure 1 shows a schematic representation of electrically heated LMFBR fuel subassembly mockups. The 61-pin wire-wrapped bundle was used for the study of temperature and flow fluctuations. Only 37 central pins were electrically heated and others were dummy pins. The diameter of each pins was 6.5mm and the pin pitch was 7.9mm. The 36% central type tight blockage was attached at the middle position of the heated section. On the other hand, the 37-pin grid-spaced bundle was used for the study of acoustic noises. Only 12 pins were electrically heated and others were dummy pins. The blocked area was 27% of the total flow area.

Chromel-Alumel thermocouples represented by T-XXXX in Fig.1 were located at various positions of the test section. T-004, T-10 and T-113 were ungrounded type sheathed thermocouples (4.8mm in diameter). The others were grounded type sheathed thermocouples (0.3mm in diameter). An eddy current type flowmeter FEC-1 was installed at the outlet of the bundle.

Three types of acoustic transducers were used in order to measure the boiling acoustic noise. The first were strain-gauge type pressure transducers P_N-106 and P_N-107 which were provided at the inlet and outlet of the test section, respectively, to measure pressure changes in boiling sodium. Secondly lead zirconate-titante(PZT) microphones M-103 and M-104 were mounted onto waveguides placed to the expansion tank and the inlet of the test section, respectively. The third were quartz accelerometers Ac-101 and Ac-102.

A data acquisition and processing system for boiling noise signals is shown in Fig.2. Temperature and flow signals were transmitted to the control room using double shielded cables. shielded cables. The fluctuation signals were recorded through specially designed measuring circuits. The circuits consisted of a low-noise AC amplifier and a band-pass filter. The specification of these components was as follows.

AC amplifier	gain	60dB(max)
	low cut-off frequency	0.01Hz
Band-pass filter	low cut-off frequency	0.01Hz
	slope	40dB/dec
	high cut-off frequency	15Hz
	slope	200dB/dec

The signals from the acoustic transducers were amplified and recorded on an analog tape recorder. The tape recordings of the acoustic signals were analyzed using a real time analyzer. An AC voltmeter was used for measuring the acoustic noise intensity, regulated by an active electric filter.

OPERATING PROCEDURE AND LOCAL BOILING EXPERIMENT

In the experiments of temperature and flow fluctuations, the flow velocity was initially maintained at the constant value of 1.5m/sec, and the heat flux of each pin was adjusted to be 61W/cm^2. After the steady state condition was attained, the flow velocity was decreased stepwise. Figure 3 shows typical signals obtained in a local boiling experiment (run 61WLB-101). FEC-1A is the flow fluctuation signal measured by the eddy current type flowmeter. T-024 and T-024A are the outlet temperature and its fluctuation signals, respectively. T-021G and T-021GA are the readings of the thermocouple whose location is 34mm downstream of the blockage. P-111 is the outlet pressure. The inception of boiling was monitored by this pressure signal. F-103 is the inlet flow signal.

The inlet flow was decreased stepwise at 62, 86, 157 and 251 sec. The local boiling was initiated at about 95 sec. Three types of steady-state local boiling were established under defferent condition; "Local Boiling I", "Local Boiling II" and "Local Boiling III". At the third reduction (157 sec) of flow rate, conspicious increases were found in both the temperature and its fluctuation signals measured at the position immediately behind the blockage (T-021G and T-021GA). During the types of Local Boiling II and III, T-021G had reached the sodium saturation temperature. On the other hand, the outlet temperature T-024 increased gradually by only 3 to 5°C at each step of flow reduction. Marked changes were hardly found in the outlet temperature fluctuation T-024A during the flow reductions, except the second one. The flow fluctuation FEC-1A did not show any visible changes not only during the flow reductions but also at the onset of boiling.

In the experiments of acoustic noise, however, the inlet temperature and flow rate were held constant and the heat flux was gradually increased to the boiling inception. After boiling had set in, the heat flux was further increased step by step. Figure 4 represents changes in the heat flux, void fraction, temperatures, flow velocities and pressure rise during a typical boiling run 37(12)LB-129. The experimental conditions were; inlet temperature 469°C, inlet flow velocity 0.98m/sec and cover gas pressure 1.05 bar. The inlet pressure transducer P_N-106 registers an abrupt change upon boiling inception followed by oscillations.

These oscillations indicate a repetition of bubble formation and collapse. It is clear from the outlet temperature T-10 that the liquid around the vapor bubble is highly subcooled. When the bubble enters the subcooled liquid, its growth is markedly inhibited. Thus the void meter(VoT-3) and the flowmeters(F-106 and F-107) cannot detect the boiling initiation. With the rise in heat flux the boiling region expands and a considerable amount of vapor forms, leading to violent oscillations in the pressure rise. Small oscillations are also observed in the signals from the void meter and the flowmeters. But the temperatures are still below saturation, and the boiling continues in a subcooled environment.

RESULTS OF ANALYSES

1. RMS Value of Temperature Fluctuation

Figure 5 shows the root-mean-square (RMS) values of temperature fluctuations measured at several axial positions behind the blockage. The following items were made clear from the figure.

(1) At the position (34mm) immediately behind the blockage, the RMS values of temperature fluctuations under local boiling conditions were about 15 times larger than those under a non-boiling condition.

(2) In the farther downstream of the blockage, noticable changes were not found in the RMS values of temperature although boiling condition changed.

(3) The RMS values of temperature fluctuations measured at the outlet were about 5 times larger than those at the end of the bundle.

2. PSD of Temperature Fluctuation

Figures 6 and 7 show the power spectral densities (PSDs) of the temperature fluctuations measured under the non-boiling and the boiling conditions, respectively. Peaks were observed around 4Hz during boiling, except in the outlet temperature T-024. These peaks were due to the respective cycle of bubble formation and collapse. On the other hand, the temperature fluctuation at the outlet had no spectral peak.

3. PSD of Flow Fluctuation

As shown in Fig.8, no conspicious feature of local boiling was found in the PSDs of flow fluctuations measured at the outlet.

4. Transfer and Coherence Functions of Temperature Fluctuations

Figures 9 and 10 show the transfer and coherence functions between several couples of temperature fluctuations under Local Boiling III condition. On of a couple is the signal

STEP 1

$$\varepsilon_n = \underline{X}_n - \sum_{i=1}^{M} \hat{a}_i \underline{X}_{n-1} \qquad (1)$$

M: order of AR model
ε_n: residual time series data of the AR-model fitting
$\underline{X}_n$: fluctuation signal to be diagnosed
a_i: preparatively determined AR model coefficients of fluctuation signal at normal state

STEP 2

$$\psi_{\varepsilon\varepsilon}(n,\tau) = \frac{1}{L} \sum_{j=1}^{No} \varepsilon_{n+j} \cdot \varepsilon_{n+j-\tau}, \quad \tau = 1,2,\ldots, \tau_{max} \qquad (2)$$

L: number of data used for computing $\phi_{\varepsilon\varepsilon}(n+N_o, \tau)$
No: number of sampled data in the monitored interval
τ_{max}: maximum lag number of autocovariance function $\phi_{\varepsilon\varepsilon}(n, \tau)$

STEP 3

$$\phi_{\varepsilon\varepsilon}(n+N_o, \tau) = \phi_{\varepsilon\varepsilon}(n,\tau) + \psi_{\varepsilon\varepsilon}(n,\tau) - \psi_{\varepsilon\varepsilon}(n-L,\tau) \qquad (3)$$

The values of L and No are chosen so that L/No shall be integer.

STEP 4

$$I(n+N_o, M, L, \tau_{max}) = \sum_{i=1}^{\tau_{max}} |\phi_{\varepsilon\varepsilon}(n+No, \tau)|^2 \qquad (4)$$

I (n+No, M, L,τmax) : AR-index

STEP 5

$$I^{\ell}_{lmt} \leq I(n+No, M, L, \tau_{max}) \leq I^{u}_{lmt} : \text{Normal} \qquad (5)$$

Otherwise : Anomaly

where I^{ℓ}_{lmt} and I^{u}_{lmt} are the lower and the upper alarm levels, respectively.

Figure 14 shows the AR-indexes obtained by applying the WTM to the temperature and flow fluctuations, where the sampling interval and averaging time were taken to be 0.016 and 8.0 seconds, respectively. In this figure the RMS values of fluctuations are also shown. Noticable changes were not found in the RMS value during the run, and then the RMS value method is insufficient to detect local boiling. In the AR-index of fluctuations remarkable increases were found immediately after the reduction of flow rate, and the AR-index maintains a higher level during local boiling than during non-boiling periods.

This tendency is more pronounced in Fig.15, which shows the ratio of the average AR-index under steady-state local boiling conditions to that under a non-boiling condition (averaging time of 32sec). The ratio of the temperature fluctuation increased from 1.5 to 1.8 with increasing boiling intensity (by decreasing the inlet flow rate at a constant heat flux).

As mentioned in the previous section, there was little correlation between the temperature fluctuation at the boiling position and that (or the flow fluctuation) at the outlet. Consequently local boiling may be detected only when the local boiling region is large enough to affect the temperature distribution at the outlet or to generate global flow oscillations due to the bubble formation and collapse.

(T-021GA) measured at immediately behind the blockage and another is chosen from those measured at various downstream locations.

Concerning the transfer functions, peaks around 4Hz appeared in the 66mm (T-021J) or less downstream of the blockage. In the farther downstream region, however the peak(4Hz) was attenuated remarkably. In the case of coherence functions, conspicious peaks were found along the whole bundle section. However, no distinct peaks were found at the outlet.

5. RMS of Acoustic Noise

Figure 11 shows the effect of changes in heat flux on the intensity ratio I/Io measured by the pressure transducer P_N-106 during a typical boiling run 37(12)LB-129. "I" is the noise intensity during boiling and "Io" is the noise intensity in the absence of boiling. The boiling caused a considerable increase in acoustic noise intensity, and the intensity then increased with rising heat flux. A similar effect of heat flux on the acoustic noise intensity was measured by the other transducers.

The present experimental conditions were in a state of developing nucleate boiling. In this state, the vapor bubble became larger with higher heat fluxes and then caused higher acoustic noise intensities since the liquid around the bubble was yet so highly subcooled that each bubble collapsed completely, leading to the generation of presure pulses due to sodium hammer phenomena. The noise intensity (approximately between 10 and 100 mbar in RMS value) in the present local boiling of sodium was much higher than that (approximately 0.5 mbar) obtained in the ordinary pool boiling in water.

6. PSD of Acoustic Noise

Figure 12 shows the PSDs of acoustic noise measured by the pressure transducer P_N-106 during the boiling run 37(12)LB-129. The frequency ranges from 0 to 100 Hz. The boiling caused a considerable increase in intensity at all frequencies. A distinct peak was observed at the frequency of 5.6Hz for the heat flux of 148.4W/cm^2. This was due to the repetition of bubble formation and collapse.

Figure 13 shows a comparison of PSDs of acoustic noises measured at the expansion tank (M-103) and at the inlet of the test section (M-104) during the same boiling run. The frequency ranges up to 25kHz and is higher than that in the former Fig.12. The boiling caused a considerable incese in intensity at all frequencies, as indicated more clearly in Fig.13(b), but frequency spectra did not change markedly during boiling. Several resonance peaks were observed in the inlet noises (Fig.13(b)). At the expansion tank, however, these peaks were attenuated as the noises were transmitted from the noise generation region to the measuring point since the transducer M-103 was approximately 13m apart from the noise generation region (while the transducer M-104 was only 1m distant).

But the waveguide method, which was utilized for the present experiment, is useful for sodium boiling detection since surface waves transmitted with smaller attenuation rate in intensity and/or energy than longitudinal waves (Ozaki, et al., 1978).

NEW ANOMALY DETECTION METHOD AND ITS APPLICATIONS

An anomaly detection method, which uses fluctuation signals, is generally based on the comparison of the typical statistical index of fluctuation signals at a normal state with that at an anomalous state. Statistical properties, such as PSD, RMS value, skewness factor etc., are usually used for this purpose. It is desirable that the anomaly detection method takes into account enough informations from fluctuation signals to know the operational status of a reactor, because the anomaly phenomena have not been thoroughly understood and the effect of the anomaly status on temperature (or flow) fluctuations has not been fully clarified. A new anomaly detection method has been developed, which uses the autoregressive model (AR-model) (Akaike, 1969). This method is called Whiteness Test Method (WTM) in this paper. Signal processing procedure of WTM is summerized as follow;

CONCLUSIONS

Analyses of temperature, flow and acoustic noises under local sodium boiling conditions yielded the following conclusions;

(1) The strong correlations are found between the temperature fluctuations measured at the boiling position and at the end of the bundle. But the correlation has not been clarified with regard to the fluctuations at the outlet.

(2) It will be promising to detect a local sodium boiling accident by temperature and flow fluctuations when the boiling intensity becomes fairly large.

(3) The whiteness test method (WTM) of fluctuation signals is sensitive and reliable for detecting local accidents in a subassembly.

(4) The intensity of boiling acoustic noise (approximately 10 and 100 mbar in RMS value) is much higher than the background noises such as mechanical and flow noises.

(5) The peak observed at the low-frequency hertz ranges is due to the repetition of bubble formation and collapse. In the high-frequenay kilohertz ranges, however, the spectra have several resonance peaks and do not change during boiling. The above observations confirm that the measurement of acoustic noise signals by using waveguides is promising for early detection of local sodium boiling in LMFBR fuel subassemblies.

ACKNOWLEDGMENT

The authors wish to acknowledge the contributions of Messrs. T. Isozaki, T. Komaba, M. Uotani and K. Yamaguchi throughout the performance of the experiments.

REFERENCES

(1) Akaike H. (1969), Fitting autoregressive models for prediction, Institute of Statistical Mathematics, 21, 243-247.

(2) Burton E.J., Bentley P.G., Cartwright D.K., Macleod I.D. and Mcknight J.A. (1979), An overview of the development of diagnostic techniques for fast reactor, Proc. Int. Meet. Fast Reactor Safety Technology,Seattle, 2651-2660.

(3) Fry D.N. and Leavell W.H. (1976), Temperature noise analysis at the exit of blocked and unblocked 19-pin electrically heated LMFBR fuel subassembly mockups, ORNL-TM-5464.

(4) Kikuchi Y., Daigo Y. and Ohtsubo A. (1977), Local sodium boiling behind local flow blockage in simulated LMFBR fuel subassembly, J. Nucl. Sci. Technol. 14, 774-790.

(5) Kikuchi Y., Haga K. and Takahashi T. (1975), Experimental study of steady-state boiling of sodium flowing in a single-pin annular channel, J. Nucl. Sci. Technol. 12, 83-91.

(6) Ogino T., Inujima H., Haga K., Ohtsubo A. and Akizuki K. (1979), Feasibility study of local core anomaly detection by use of temperature and flow fluctuations at LMFBR fuel subassembly outlet, Proc. Int. Meet. Fast Reactor Safety Technology, Seattle, 2630-2650.

(7) Ohlmer E. and Schwalm D. (1975), The use of the amplitude distribution function in a simulated reactor subassembly, Atomkernenergie, 25, 281-284.

(8) Ozaki Y, Haga K., Kikuchi Y., Morikawa T. and Hori M. (1978), Acoustic noises with loss-of-flow sodium boiling experiment in a 19-pin bundle, 8th Liquid Metal Boiling Working Group Meeting, Mol.

(9) Smith D., Bagley K., Gregory C., Leet G. and Tait D. (1978), DFR spectral experiment of demonstration LMFBR, IAEA, Int. Sympo. on design construction and operating experience of demonstration liquid metal fast breeder reactors, Volgano, IAEA-SM-225/49.

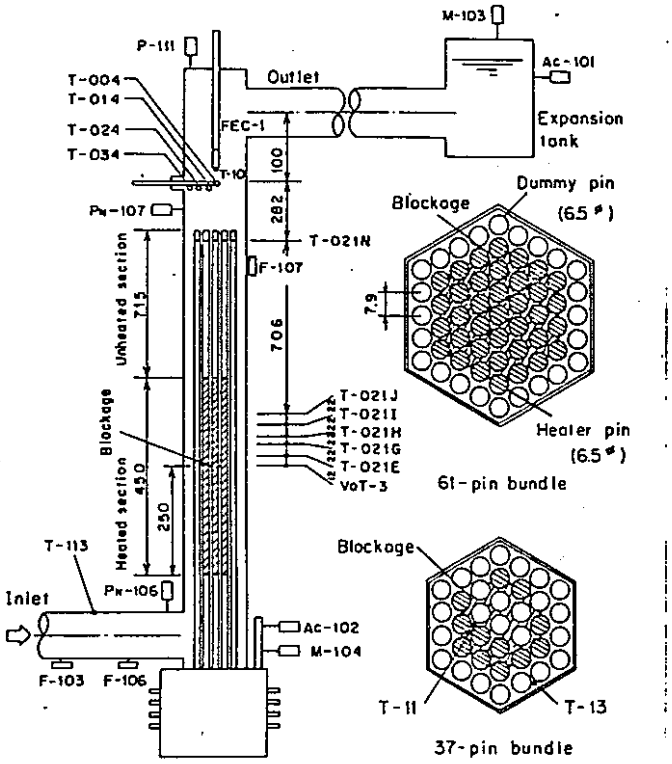

Fig. 1 Locally blocked 61- and 37-pin bundle test sections

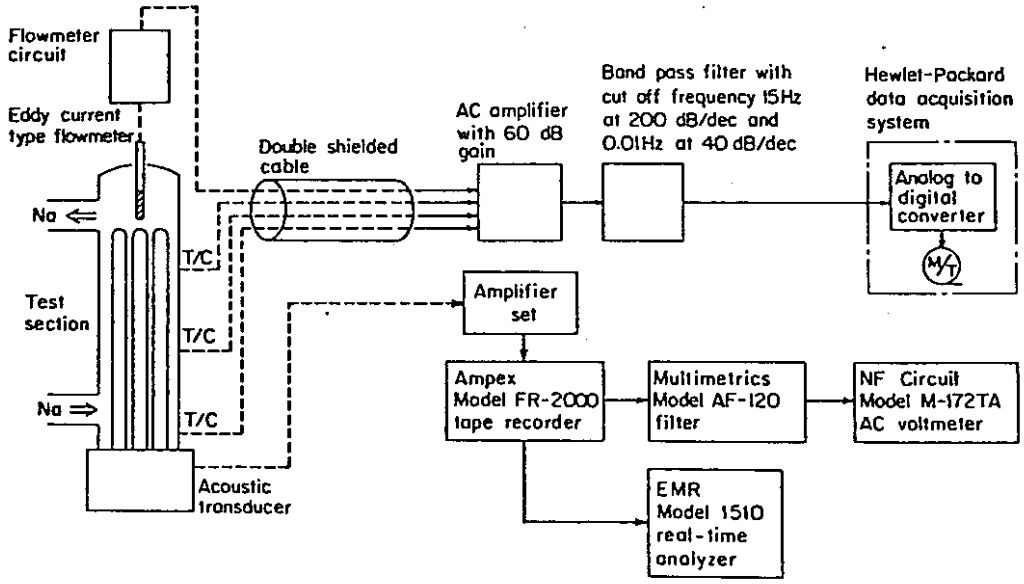

Fig. 2 Schematic diagram of data acquisition and processing system for boiling noise signals

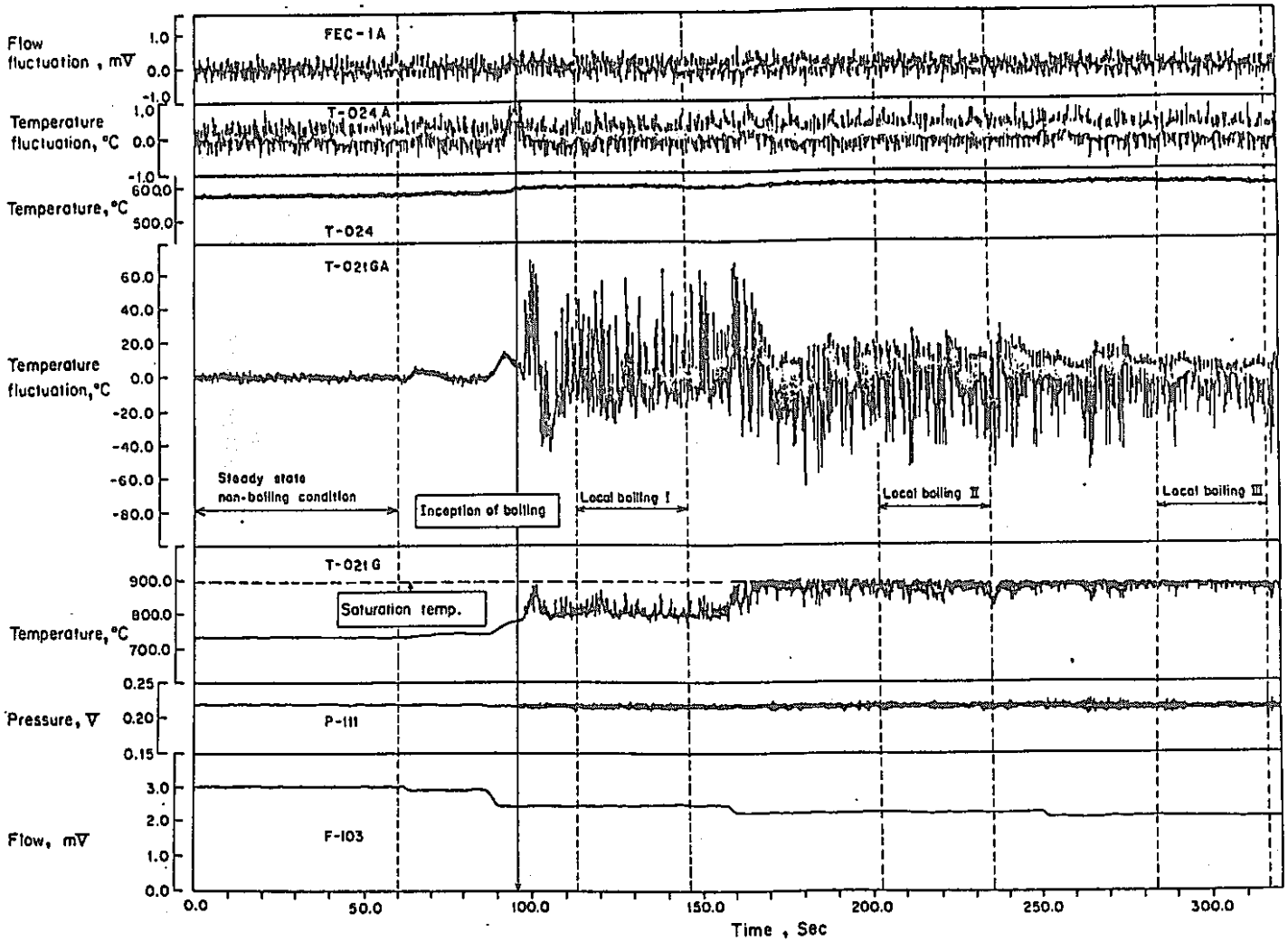

Fig. 3 Signals under local boiling condition

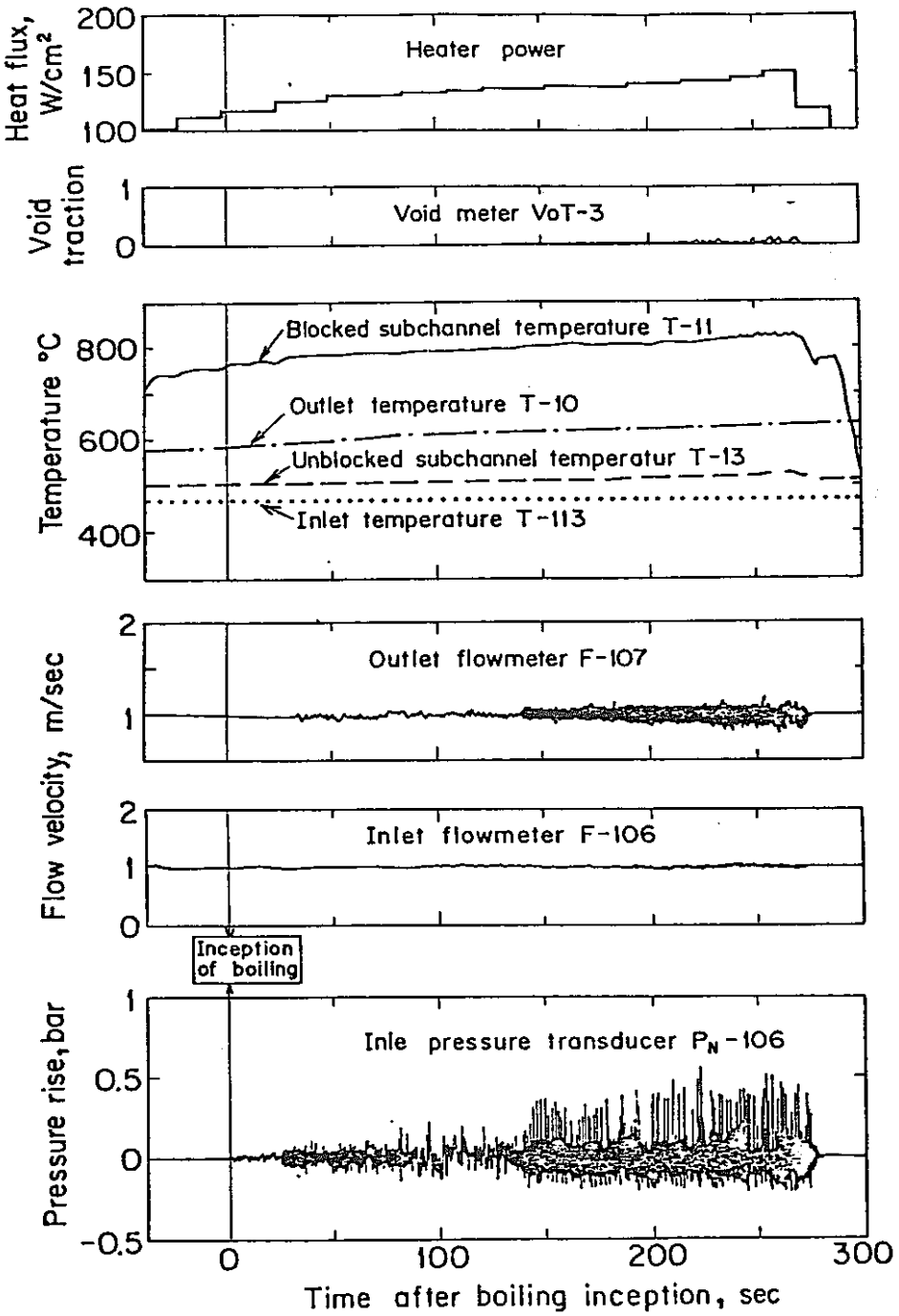

Fig. 4 Records of signals from void meter, thermocouples, flowmeters, pressure transducer during steady-state boiling in locally blocked 37-pin bundle

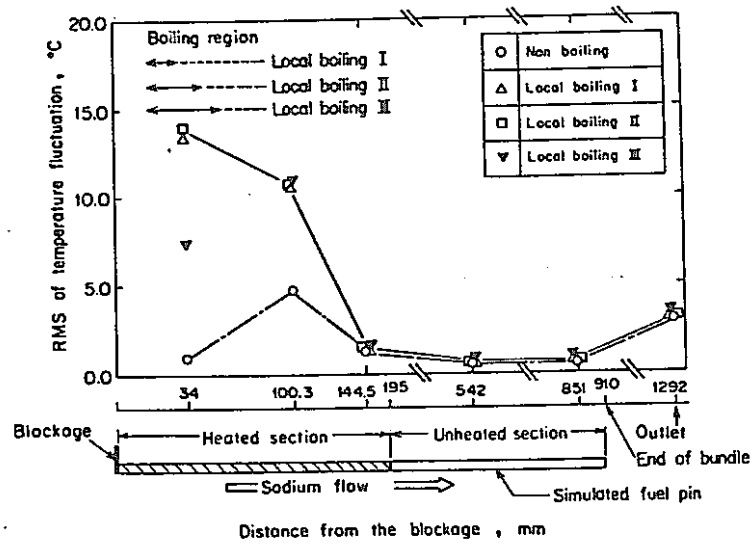

Fig. 5 RMS values of temperature fluctuations measured at several axial positions behind the blockage

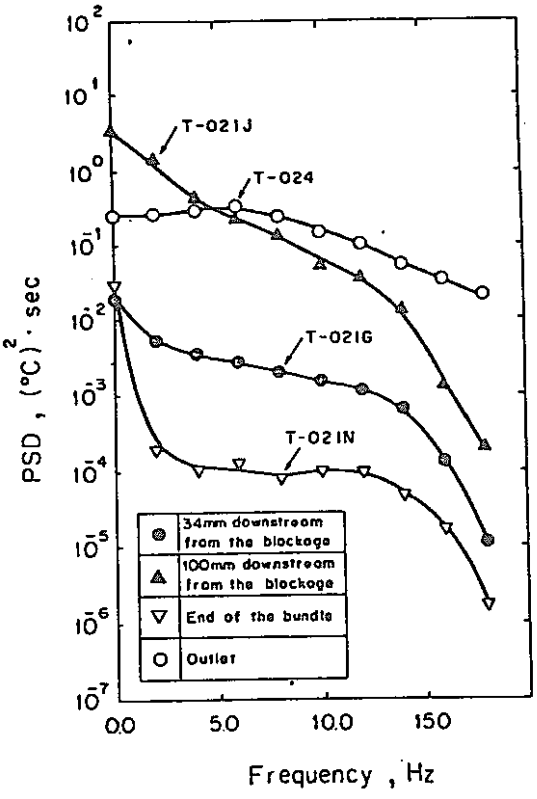

Fig. 6 Power spectral densities of temperature fluctuations measured at several axial positions under non-boiling condition

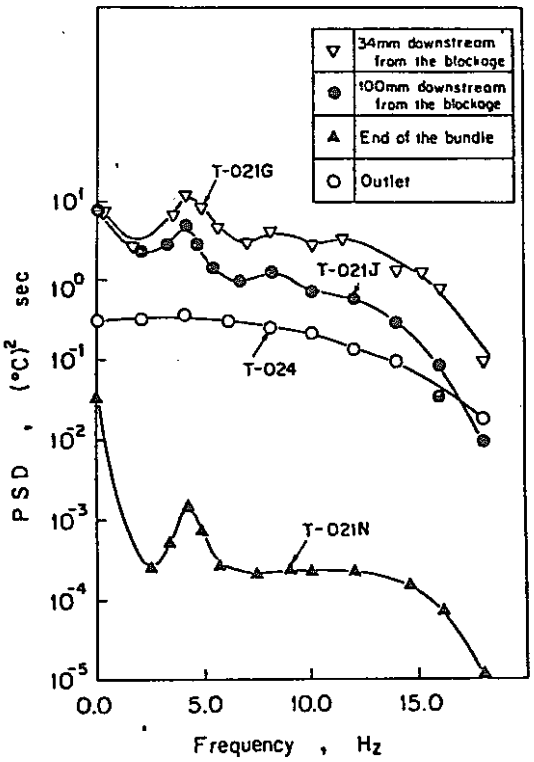

Fig. 7 Power spectral densities of temperature fluctuation measured at several axial positions under boiling III condition

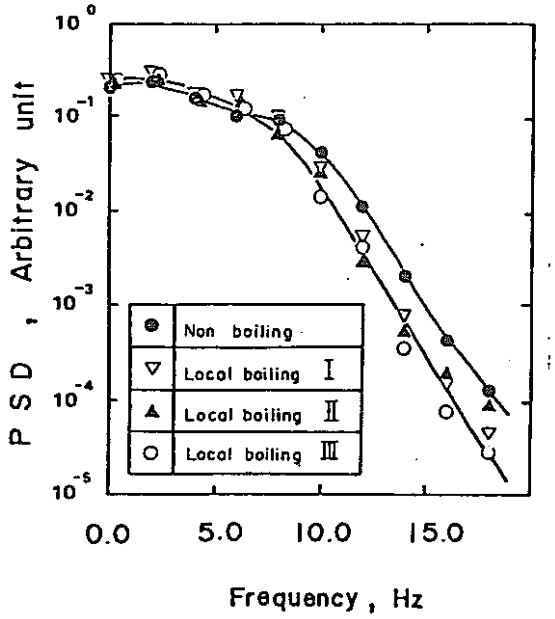

Fig. 8 Power spectral densities of flow fluctuation measured at the outlet

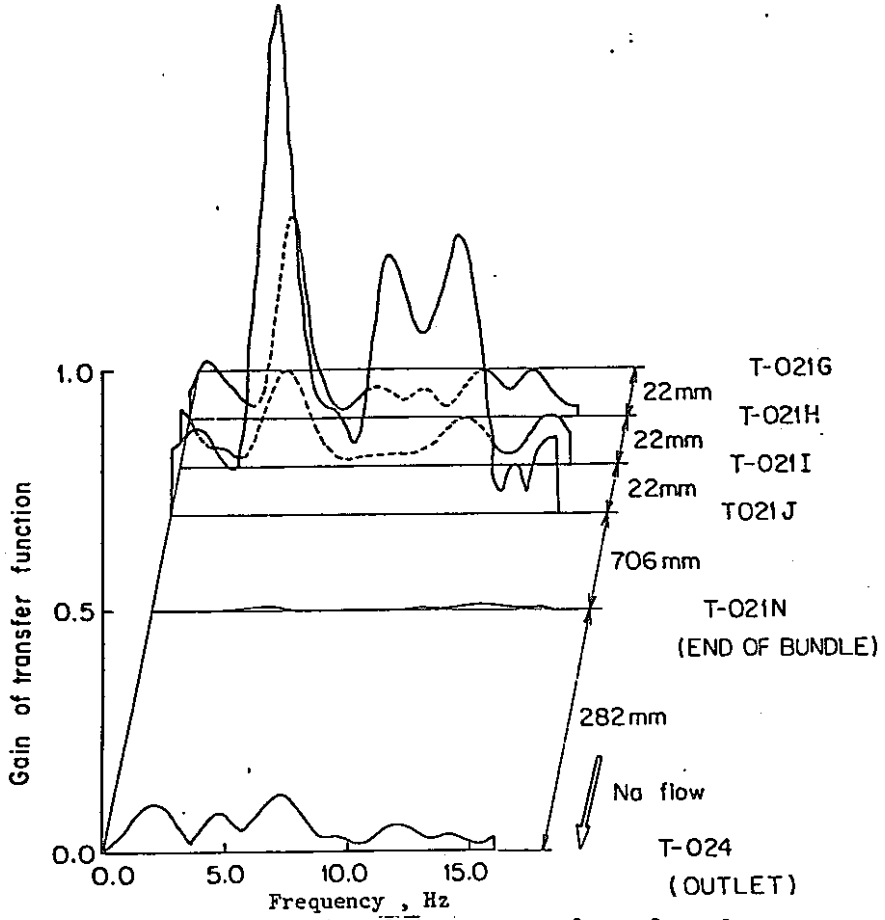

Fig. 9 Transfer functions between several couples of temperature fluctuations

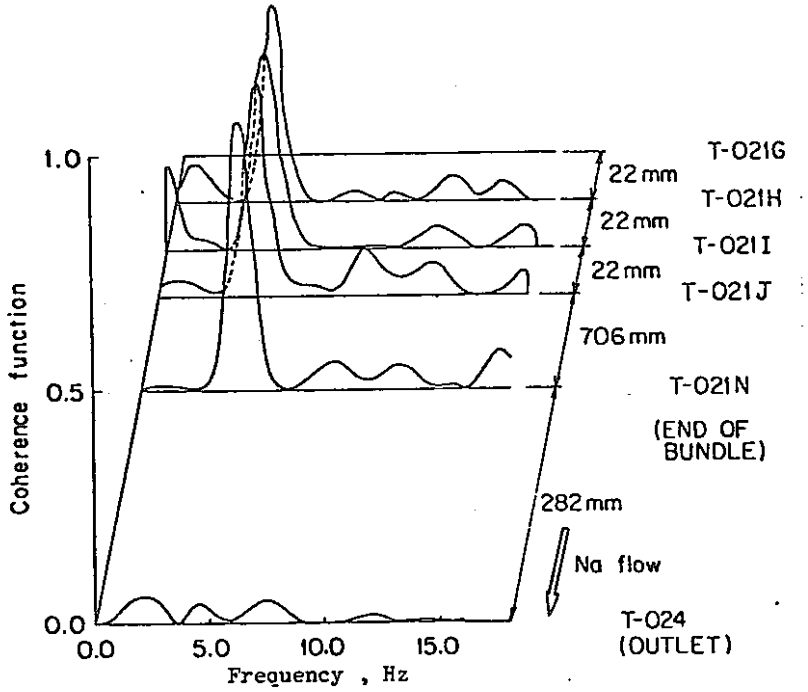

Fig. 10 Coherence functions between several couples of temperature fluctuations

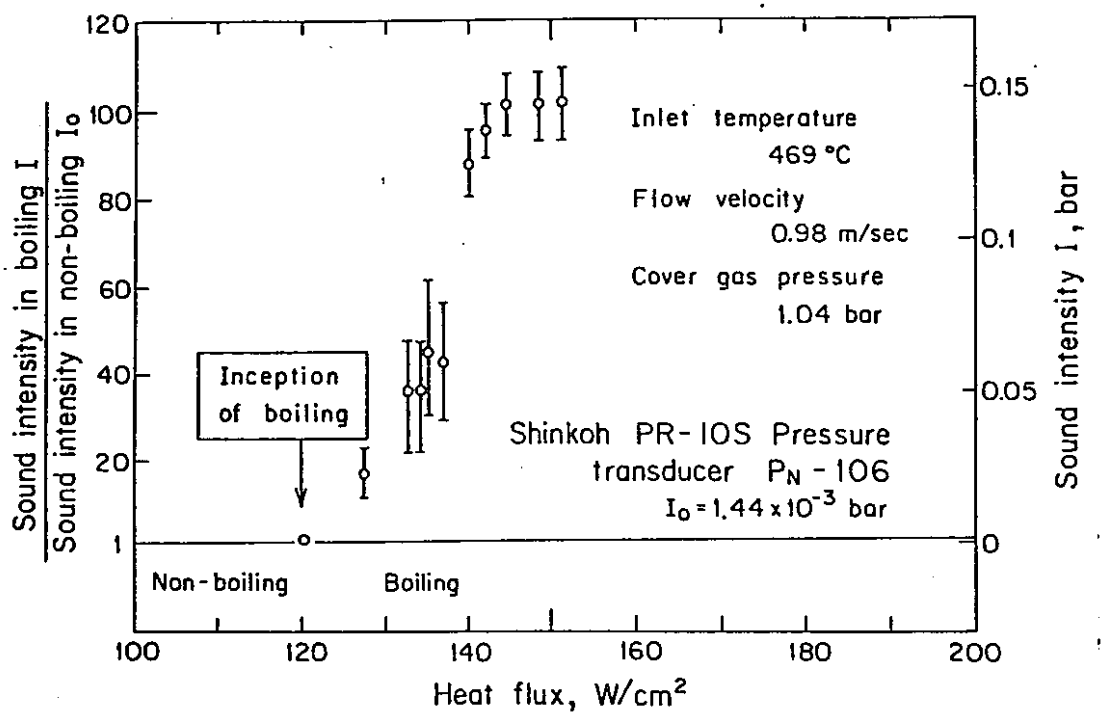

Fig. 11 Effect of heat flux on intensity of acoustic noise measured by pressure transducer P_N-106

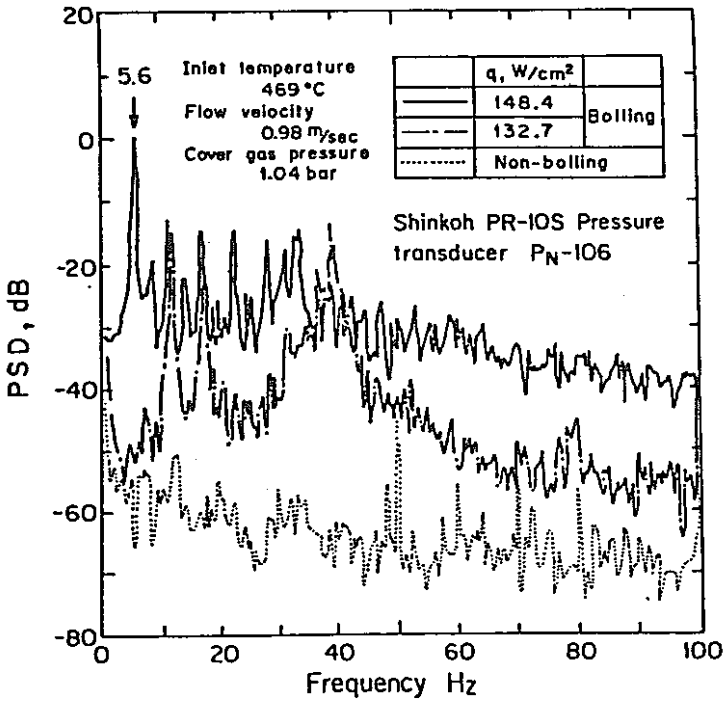

Fig. 12 Frequency spectra of acoustic noise measured by pressure transducer P_N-106

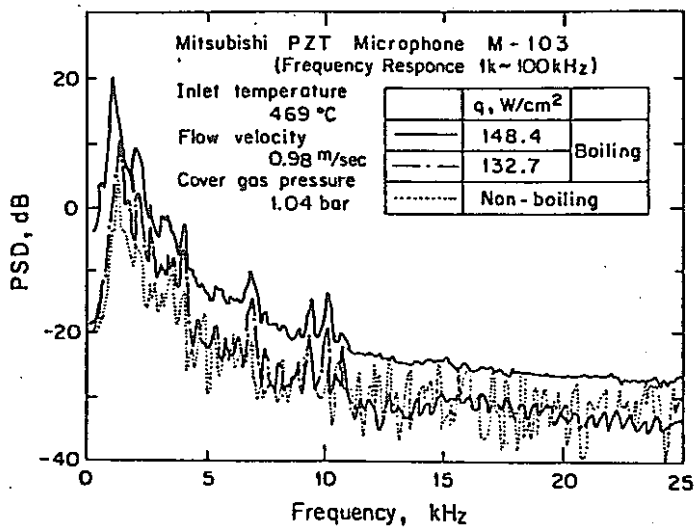

(a) Expansion tank (M-103)

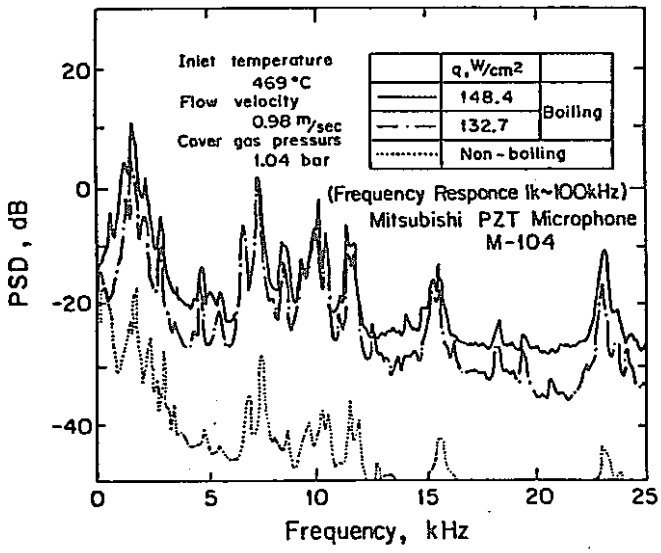

(b) Inlet of test section (M-104)

Fig. 13 Trequency spectra of acoustic noise measured by microphones

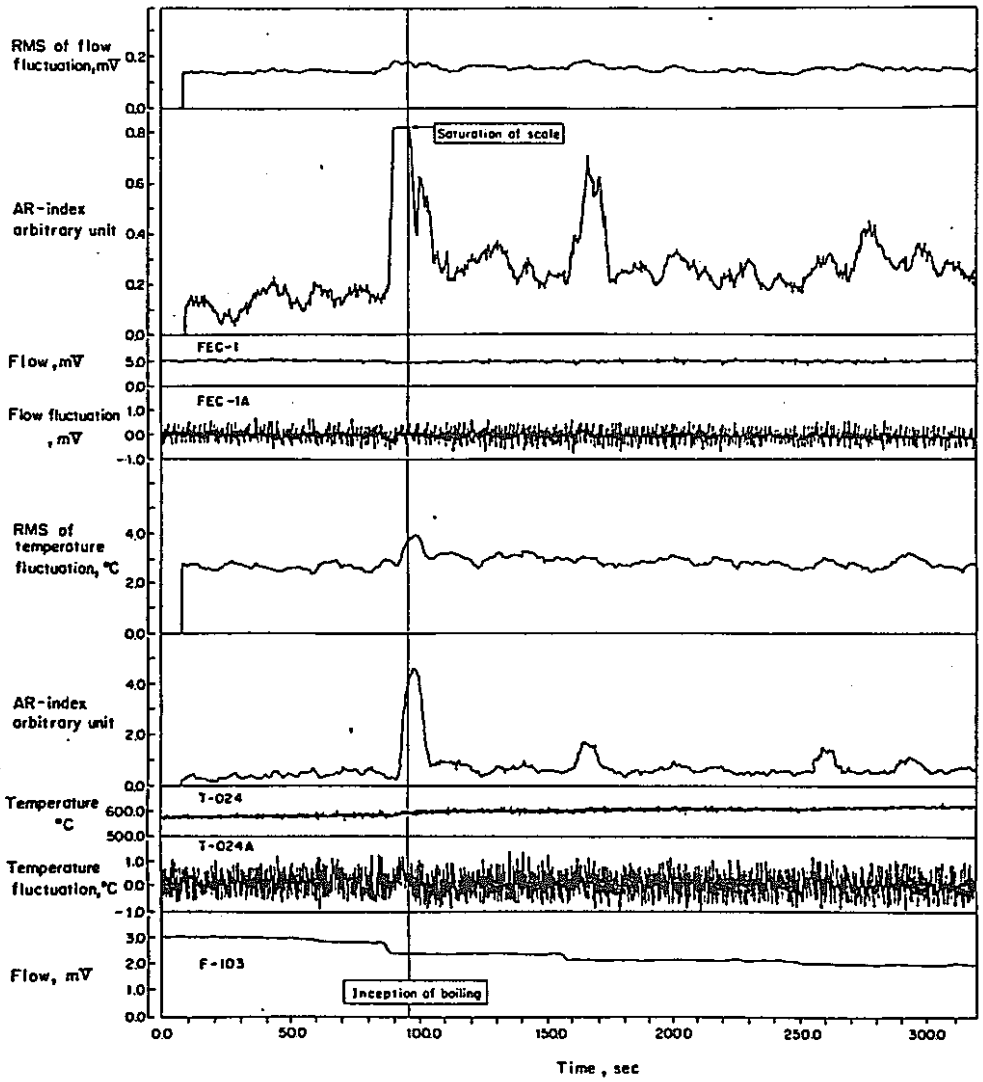

Fig. 14 RMS value and AR index of temperature (T-024) and flow (FEC-1) fluctuations measured at the outlet

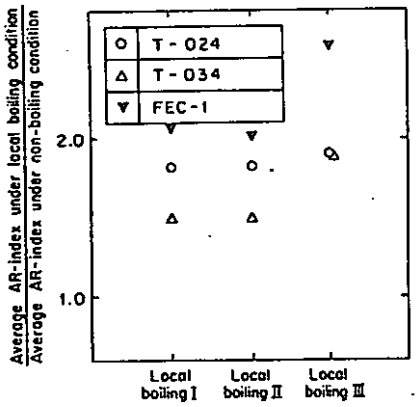

Fig. 15 Ratio of the average AR index under boiling condition to that under non-boiling condition

APPENDIX : SCOPE OF PRESENTATION

Third Specialists' Meeting on Reactor Noise SMORN-III

DETECTION OF LOCAL SODIUM BOILING IN A SIMULATED LMFBR FUEL SUBASSEMBLY

H. INUJIMA*, T. OGINO*, K. HAGA** and Y. KIKUCHI***

* Central Research Laboratory, Mitsubishi Electric Corporation, Japan

** O-arai Engineering Center, Power Reactor and Nuclear Fuel Development Corporation, Japan

*** Department of Nuclear Engineering, Kyoto University Japan

INTRODUCTION

Thank you chairman. My name is Hiroshi Inujima. I belong to the Nuclear Technology Section of Central Research Laboratory, Mitsubishi Electric Corporation.

Today, I would like to present our recent progress on the anomaly detection tests. This work has been conducted by the joint research between PNC and Mitsubishi Electric Corporation, Japan.

In this presentation we deal with a technology on the local core anomaly detection by use of temperature, flow and acoustic noises. This technology aims to detect of local core accidents, such as local sodium boiling, in their initial stages. It will contribute to the safety of Liquid Metal Fast Breeder Reactors, because local core accidents might propagate and finally lead to the whole core accidents.

SUBJECTS OF APPROACH

(1) Statistical properties of temperature and flow fluctuations in the downstream of the blockage under local boiling conditions.

(2) Sensitivity of a newly developed anomaly detection method which uses fluctuation signals.

(3) Statistical properties of acoustic noises under local boiling conditions.

(4) Sensitivity of an anomaly detection method using the statistical index of acoustic noise.

OBJECTIVE AND APPROACHES ..... (First slide, please. SLIDE No. 1)

If the temperature or flow fluctuations are strongly transferred to the down stream, we will be able to detect the local boiling at its early stage using subassembly instrumentations. However, it is not always the case. So, we must, first of all, check the transfer characteristics of boiling information. Using acoustic noise is another method for the detection of local sodium boiling.

The objective of present study is investigate the temperature, flow fluctuations and acoustic noises in a partially blocked subassembly and to reveal the possibility of detecting boiling. For this purpose we have conducted out-of-pile experiments using the Sodium Boiling and Fuel Failure Propagation Test Loop, SIENA, in the O-arai Engineering Center of PNC.

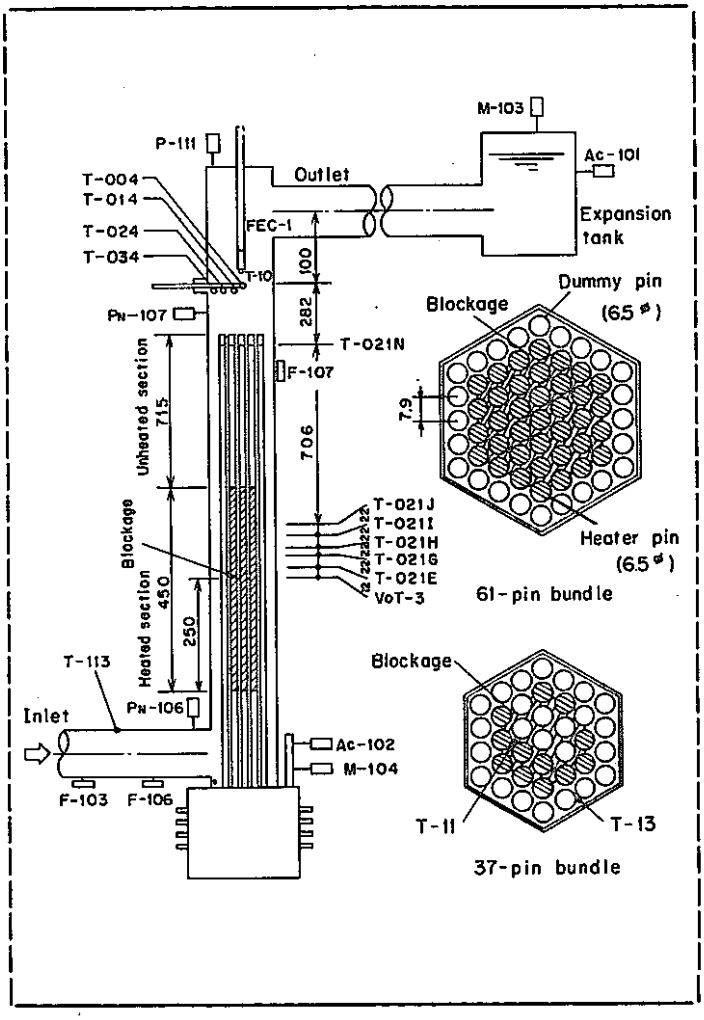

TEST SECTION ..... (Next slide, please. SLIDE No. 2, i.e. Fig. 1)

This slide shows the schematic representation of 61-pin and 37-pin bundles. The 61-pin wire-wrapped bundle is used for the study of temperature and flow fluctuation. Only central 37 pins are electrically heated.

A stainless steel plate is attached at the middle position of the heated section. It blocks the central 36% of total flow area. On the other hand, the 37-pin grid-spaced bundle is used for the study of acoustic noises. In this section only 12 pins are electrically heated. The blocked area is 27%. Many sensors are equipped to these test sections.

1. Chromel-Alumel thermocouples are provided at various points along the test section.

2. An eddy current type flowmeter is installed at the outlet of the bundle.

3. Three types of acoustic transducers are used.

1st. Strain gauge type pressure transducers P_N-106, P_N-107.

2nd. Lead zirconate-tintate microphons M-103, M-104
These are mounted on to the waveguides placed to the expansion tank and the inlet of the test section.

3rd. Quartz accelerometers AC-101, AC-102.

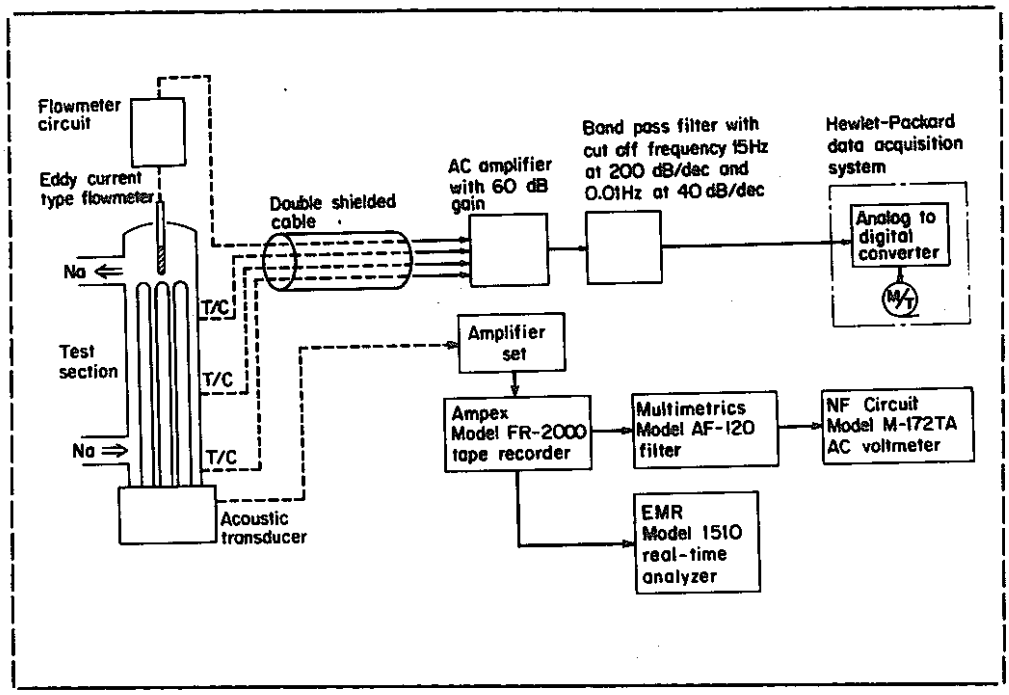

DATA ACQUISITION SYSTEM ..... (Next slide, please. SLIDE No. 3, i.e. Fig. 2)

This slide shows a data acquisition system for noise signals.

1. This is the test section, and the flow meter pre-amp circuit is placed near the test section.

2. Double shielded cables are used for signal transmission.

3. This is the fluctuation measuring circuit. It is composed of a low noise AC amplifier and a band pass filter.

4. Acoustic noises are amplified and recorded on an analog tape recorder. And they are analyzed by this real time analyzer.

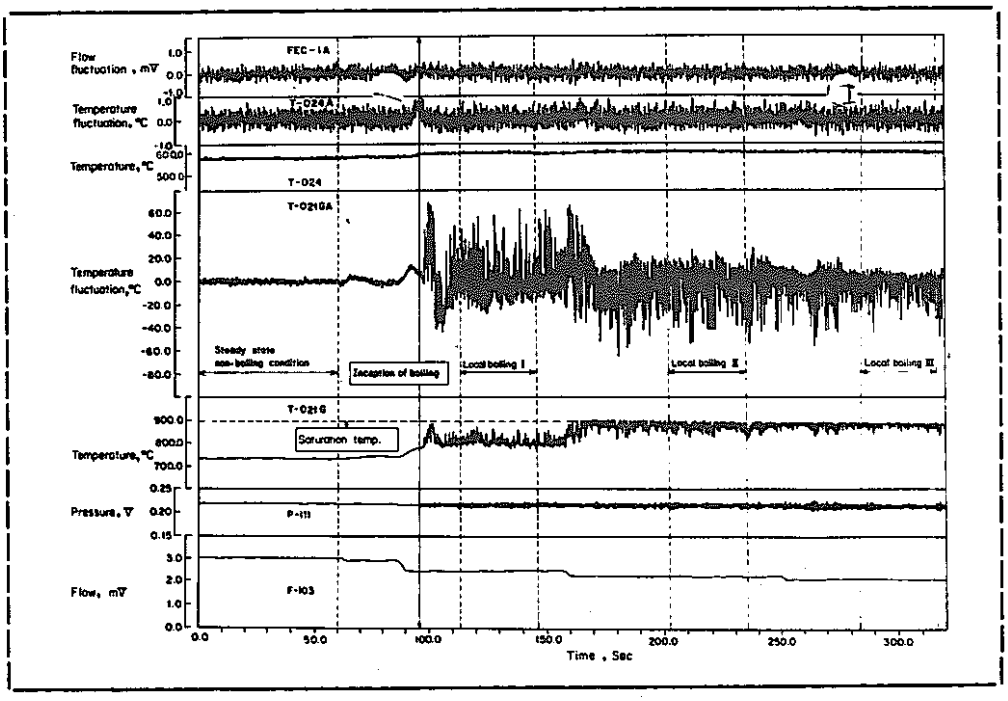

A RECORD OF TYPICAL BOILING RUN ..... (Next slide, please. SLIDE 4, i.e. Fig. 3)

This slide shows a record of a typical local boiling run.

The horisontal axis is a relative time. This (FEC-1A) is the flow fluctuation signal measured by the eddy-current type flow meter. These (T-024 and T-024A) are the subassembly outlet temperature and its fluctuation, respectively. These (T-021G and T-021GA) are the other pair-signals from the thermocouple which is located at 34mm downstream from the blockage. This fluctuation (T-021GA) signal can be considered as the source term of the boiling information. This (p-111) is the subassembly outlet pressure. Boiling inception was indicated by this pressure signal. This (F-103) shows the subassembly inlet flow velocity.

The flow velocity is initially adjusted to the constant value of 1.5m/sec, and the heat flux of each pin was maintained to 61W/cm^2. The flow rate is reduced stepwise.

The boiling is initiated at the second flow reduction step. Three steady state local boiling stages are obtained under different flow velocity conditions. We call them as "Local Boiling I", "Local Boiling II" and "Local Boiling III". During the "Local Boiling II and III stages, the thermocouple located at 34mm downstream of the blockage (T-021G) shows the saturation temperature. On the other hand, the subassembly outlet temperature (T-024) increased only by 3 to 5 degrees at each flow reduction step. It is far below the saturation temperature.

At the moments of the second and the third flow reductions conspicuous increases are found in these signal (both T-021G and its fluctuation T-021GA).

However little changes are found in the subassembly outlet temperature fluctuation (T-024A) except at the second flow reduction. The flow fluctuation (FEC-1A) doesn't show any visible changes not only during the flow reductions but also at the onset of the local boiling.

(PNC-FS-1253)

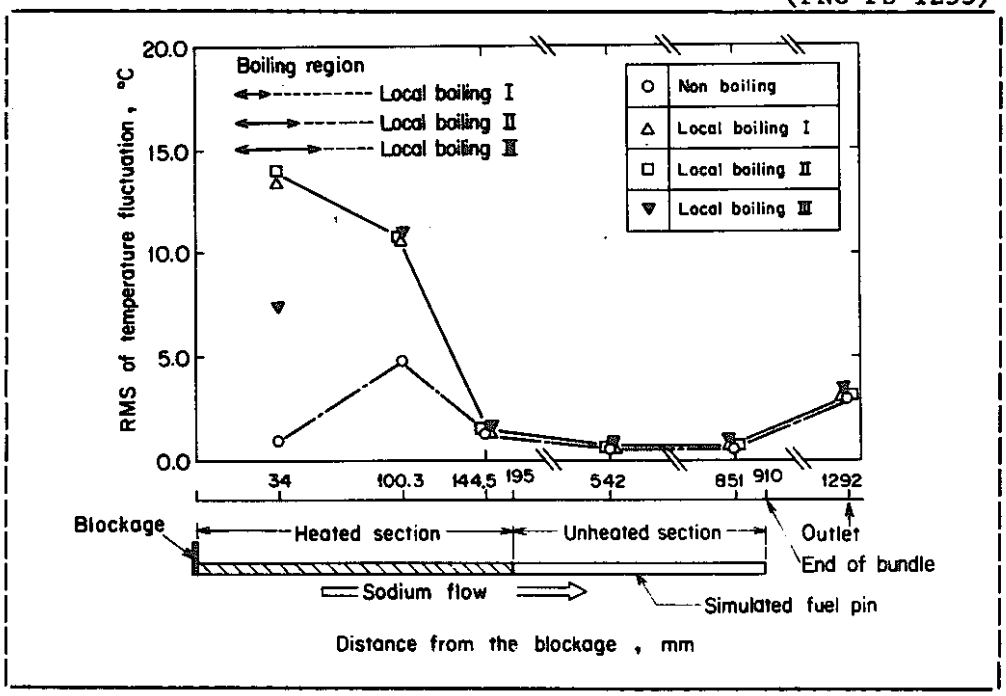

RMS VALUES OF TEMPERATURE FLUCTUATIONS ..... (Next slide, please.

SLIDE No. 5, i.e. Fig. 5)

This slide shows axial RMS value distribution of temperature fluctuations behind the blockage. The boiling length at every stages are noted here.

We can summarize the results of RMS analysis as follows:

1st. At the position immediately behind the blockage, the RMS values of temperature fluctuations under local boiling conditions are about 15 times as large as that under non-boiling condition.

2nd. At the downstream unheated positions, little changes are found in the RMS values of temperature fluctuations during all boiling stages.

3rd. The RMS values of the subassembly outlet temperature fluctuations are about 5 times as large as those observed near the upper end of the pin bundle.

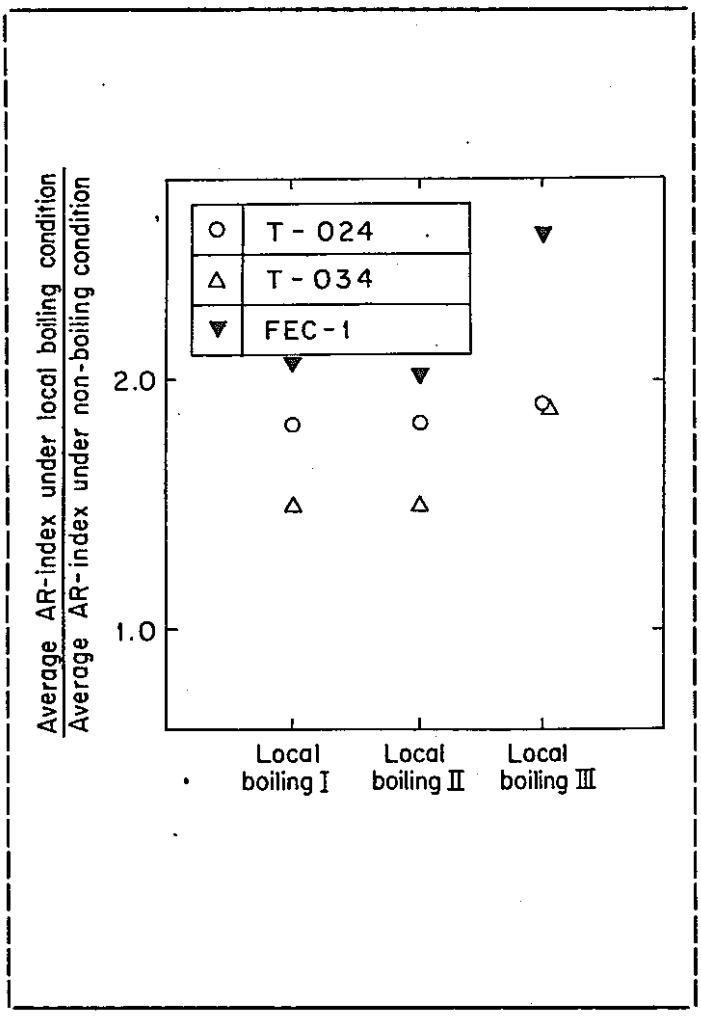

EFFECT OF LOCAL BOILING ON THE AR-INDICIES ..... (Next slide, please. SLIDE No. 6, i.e. Fig. 15)

I'm going to show the detectability of anomaly by use of AR-index. The algorithm of this AR-index described in our paper precisely. Here, I omit to explain it.

This slide shows the ratio of the AR-index levels under steady-state local boiling tests with respect to the non-boiling condition. For the subassembly outlet temperature fluctuation, the ratio was from 1.5 to 1.8, and for the flow fluctuation, it was from 2.0 to 2.5. We can expect from this figure that the ratio will increase with boiling intensity.

We can say that the local boiling may be detected when the boiling region is large enough to change the turbulent mixing at the subassembly outlet, or, in other words, the boiling detection will be possible when the local boiling transits to the oscillatory pattern as is usually observed prior to the occurrence of pin failure.

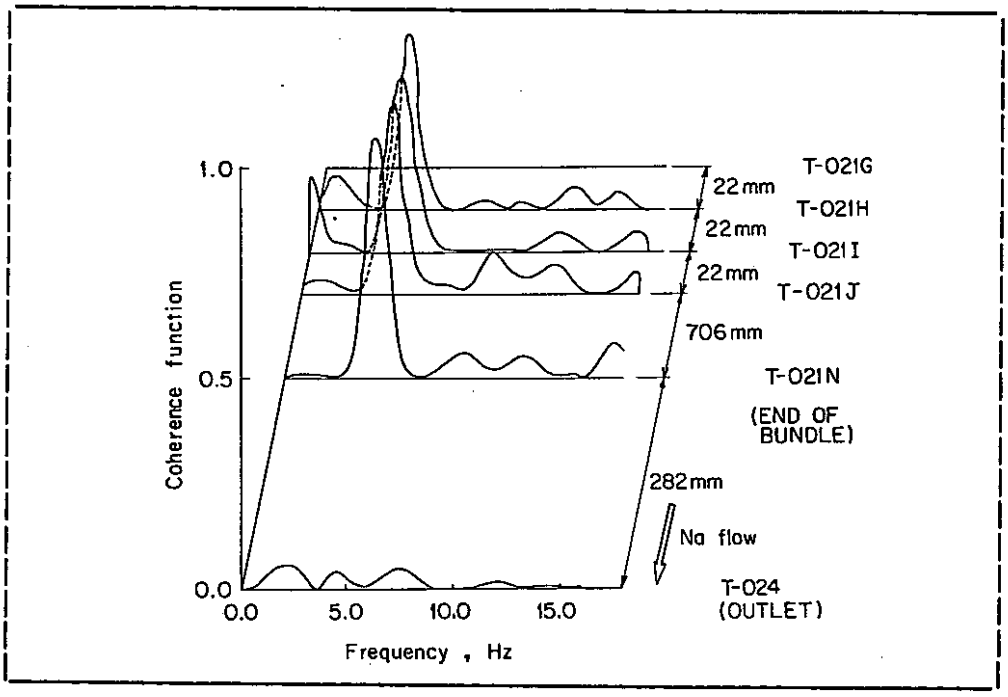

COHERENCE FUNCTIONS ..... (Next slide, please. SLIDE No. 7, i.e. Fig. 10)

This slide shows the Coherence Functions between the temperature fluctuation immediately behind the blockage and at various downstream locations. In this analysis, we can find large peaks in the every location of the bundle section. However, it was hardly found at the subassembly outlet.

From these analysis, we can now make clear the followings.

1st. The coherence functions of the temperature fluctuations show strong attenuation of the fluctuation levels at the unheated downstream region. Yet, the information of the local boiling is surely transferred to the upper end of the pin bundle, even if it is fairly small.

2nd. The subassembly outlet temperature fluctuations are never correlated to that at the boiling position.
It can be considered that the subassembly outlet temperature fluctuation is generated mainly by the turbulent mixing of the coolant flow.

(PNC-FS-872)

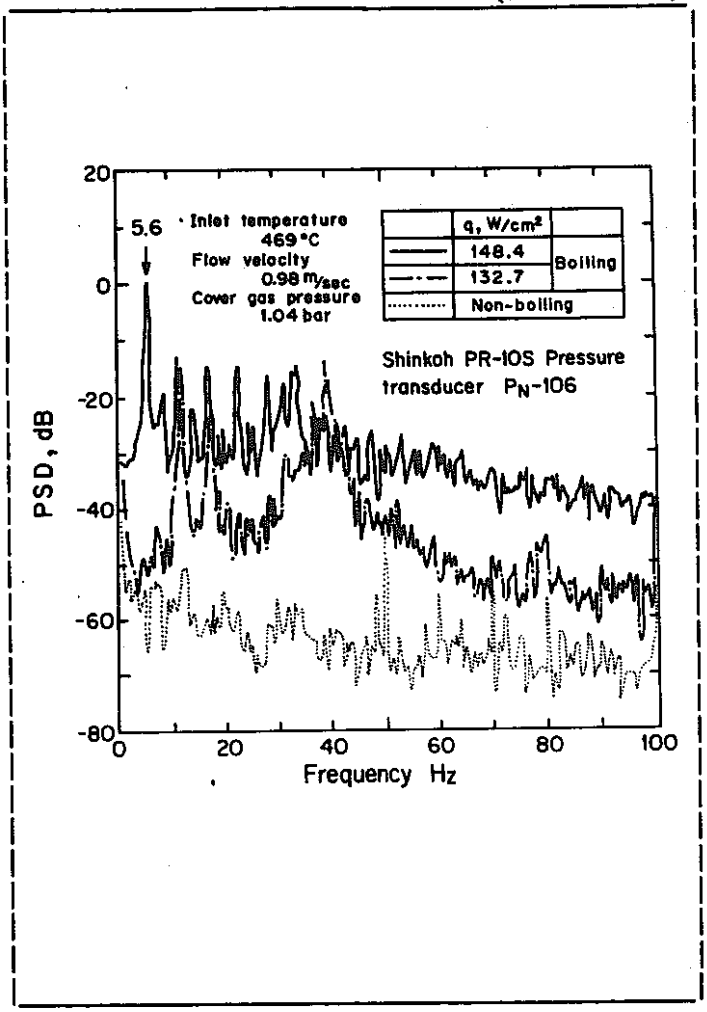

PSDs OF ACOUSTIC NOISE ..... (Next slide, please. SLIDE No. 8, i.e. Fig. 12)

I am going to present about acoustic noises.

This slide shows the PSDs of acoustic noise measured by the inlet pressure transducer (P_N-106) during boiling run. The frequency range is from 0 to 100 Hz. The boiling caused a considerable increase in intensity at all frequencies.

A distinct peak was observed at the frequency of 5.6Hz for the heat flux of 148.4W/cm^2. This was due to the repetition of bubble formation and collapse.

(PNC-FS-866)

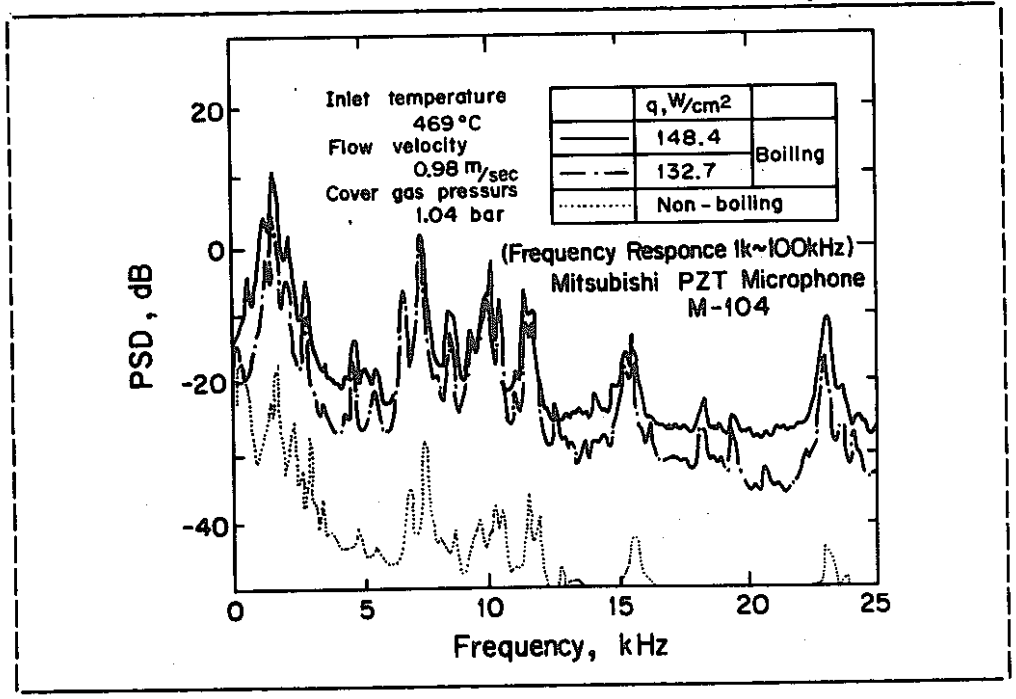

PSDs OF ACOUSTIC NOISE ..... (Next slide, please. SLIDE No. 9, i.e. Fig. 13(b))

This slide shows a comparison of PSD_s of acoustic noises measured at the inlet of the test section (M-104) during the same boiling run.

The boiling caused considerable increase in intensity at all frequency range. But frequency spectra did not show marked change during the boiling.

The wave guide method, which was utilized for the present experiment, is useful for sodium boiling detection because surface waves transmitted with smaller attenuation in intensity.

(PNC-FS-856)

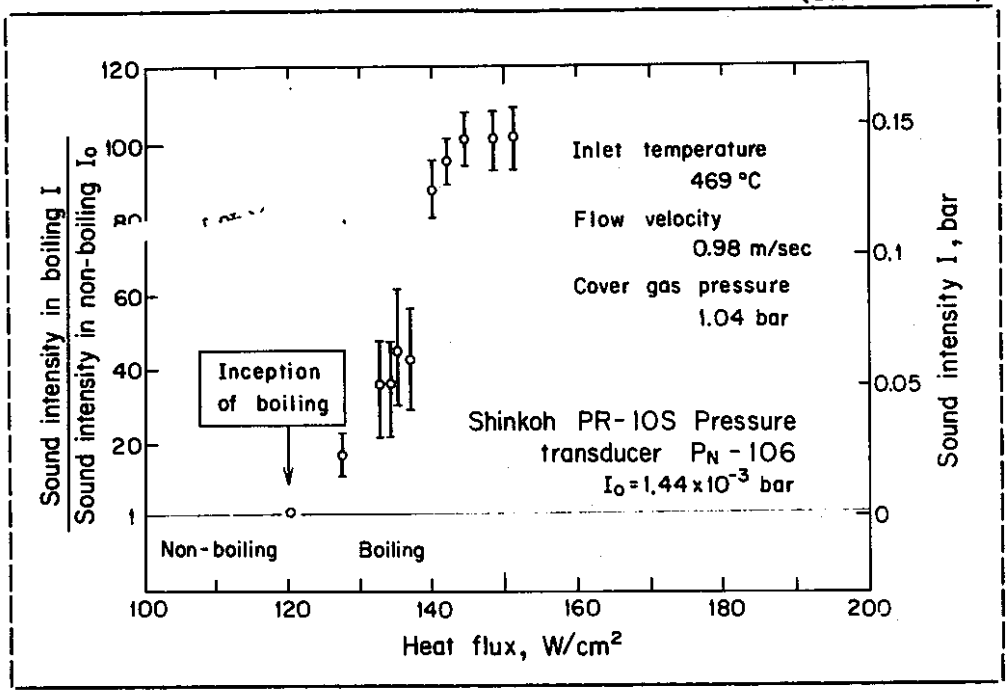

RMS VALUE OF ACOUSTIC NOISE ..... (Next slide, please. SLIDE No. 10, i.e. Fig. 11)

This slide shows the effect of heat flux on the intensity ratio I/Io measured by the inlet pressure transducer (P_N-106) during a typical boiling run.

Here "I" is the noise intensity during boiling and "Io" is the noise intensity in the absence of boiling. Boiling caused a considerable increase in acoustic noise intensity, and it increased with heat flux.

CONCLUSIONS

(1) The strong correlations are found between the temperature fluctuations measured at the boiling position and at the end of the bundle. But the correlation has not been clarified with regard to the fluctuations at the outlet.

(2) It will be promising to detect a local sodium boiling accident by temperature and flow fluctuations when the boiling intensity becomes fairly large.

(3) The whitheness test method (WTM) of fluctuation signals is sensitive and reliable for detecting local accidents in a subassembly.

(4) The intensity of boiling acoustic noise (approximately 10 and 100 mbar in RMS value) is much higher than the background noises such as mechanical and flow noises.

(5) The peak observed at the low-frequency hertz ranges is due to the repetition of bubble formation and collapse. In the high-frequenay kilohertz ranges, however, the spectra have several resonance peaks and do not change during boiling. The above observations confirm that the measurement of acoustic noise signals by using waveguides is promising for early detection of local sodium boiling in LMFBR fuel subassemblies.

CONCLUSIONS ..... (Last slide, please. SLIDE No. 11)

Analyses of temperature, flow and acoustic noises under local sodium boiling conditions yielded the following conclusions;

(1) The strong correlations are found between the temperature fluctuations measured at the boiling position and at the end of the bundle. But the correlation has not been clarified with regard to the fluctuations at the outlet.

(2) It will be promising to detect a local sodium boiling accident by temperature and flow fluctuations when the boiling intensity becomes fairly large.

(3) The whiteness test method (WTM) of fluctuation signals is sensitive and reliable for detecting local accidents in a subassembly.

(4) The intensity of boiling acoustic noise (approximately 10 and 100mbar in RMS value) is much higher than the background noises such as mechanical and flow noises.

(5) The peak observed at the low-frequency hertz ranges is due to the repetition of bubble formation and collapse. In the high-frequency kiloherts ranges, however, the spectra have several resonance peaks and do not change during boiling. The above observations confirm that the measurements of acoustic noise signals by using waveguides are promising for early detection of local sodium boiling in LMFBR fuel subassemblies.

2. 1981 ASME WINTER ANNUAL MEETING

2 Experimental Investigation of Local Cooling Disturbances in LMFBR Fuel Subassemblies*
(Paper No. 81-WA/HT-40)

K. Yamaguchi, M. Uotani, K. Haga and F. Namekawa

Edited by K. Yamaguchi

3 Out-of-Pile Experiments for Fission Gas Release in LMFBR Fuel Subassemblies
----- Gas Release into Blockage in a Simulated LMFBR Fuel Bundle
(Paper No. 81-WA/HT-62)

F. Namekawa, K. Yamaguchi and K. Haga

Edited by F. Namekawa

---

* Present work was conducted by the collaborative research between PNC and Toshiba Corp. (Contract number 560F001)

Experimental Investigation of Local Cooling Disturbances in LMFBR Fuel Subassemblies

K. Yamaguchi, M. Uotani*, K. Haga

FBR Safety Section, SG Division, Oarai Engineering Center, PNC

F. Namekawa

Nuclear Engineering Laboratory, Toshiba Corporation

ABSTRACT

Temperature increases due to central-type planar blockages were examined with a series of out-of-pile pin bundle experiments. The heat exchange layer model introduced here to analyze the observed thermohydraulic fields behind different size blockages successfully interpreted almost all test results of PNC, ORNL and KfK. These results were correlated to yield an empirical formula available for estimating maximum temperature increases in various subassemblies, including spacer wire type, grid type, loosely assembled and tightly assembled ones.

NOMENCLATURE

A	:	flow area
C_B	:	bare bundle peaking factor, $\Delta T_{bare}/\Delta T_{wake}$
C_W	:	spacer wire distortion factor, $\Delta T_{wire}/\Delta T_{bare}$
c_p	:	specific heat
D_B	:	characteristic length of the blockage, $\sqrt{l_a \cdot l_w}$
d_h	:	equivalent diameter
F	:	fraction of blocked flow area
l_a	:	corner-to-corner distance of the blockage
l_w	:	flat-to-flat distance of the blockage
N_R	:	Ring Parameter, D_B/p
p	:	pin pitch
q"	:	heat flux
T	:	temperature
U_o	:	inlet velocity
U_B	:	velocity at the blocked plane, $U_o/(1-F)$
z	:	axial distance from the blockage
γ	:	specific gravity
θ_M	:	measurement angle
θ_W	:	spacer wire angle
τ	:	residence time of the recirculating flow, $d_h \cdot c_p \gamma \cdot (T_{wake}-T_{core})/4q"$
τ_B*	:	dimensionless residence time, $\tau U_o/D_B$
τ_∞*	:	modified dimensionless residence time, $\tau U_o/d_h$

Subscripts

bare	:	bare bundle (no spacers)
wire	:	wire wrapped bundle
core	:	core flow region (outside blockage)
wake	:	wake region
in	:	inlet
out	:	outlet
max	:	maximum

*Present address: Central Research Institute of Electric Power Industry,

INTRODUCTION

In the Liquid Metal Fast Breeder Reactor (LMFBR) core safety research and development (R&D) program, it is of great importance to develop a detailed understanding of the accident progression resulting from local faults and to assure the termination of this accident without serious core damage. The hypothetical planar blockage in a fuel subassembly is a possible initiator of the propagation of cooling disturbance under certain circumstances. Investigations of the critical conditions which could lead to sodium boiling, dryout, cladding melting and movement, fuel migration, and so on have resulted in formulation of an accident scenario.

As a first step of clarifying the accident scenario induced by the blockage formation, the quantitative representations of local temperature rise and the critical condition of the onset of local boiling are needed. There are many experimental investigations, such as in-sodium experiments at Power Reactor and Nuclear Fuel Development Corporation (PNC) (1),(2), at Oak Ridge National Laboratory (ORNL) (3) and at Kernforschungzentrum Karlsruhe (KfK) (4), and water mockup tests at PNC (5), ORNL (6) and KfK (7). The results are, however, obtained under differing test conditions and philosophies which prevent their mutual utilization to a specific reactor design case. The effects of the key factors listed in Table 1 should be separately treated to overcome the difficulties in question.

Table 1 Summary of the effective factors in the assessment of local blockage accident.

Factor	variable
spacer type	wire/grid
tightness of assembling	d_h
location of the blockage	central/edge/corner
blockage size	D_B
blocked flow area	F
porosity	leak flow rate
heat generating blockage	q"

The objective of this paper is to review previous test results and to develop a universal heat transfer model through which one can combine particular test results with those measured under quite different test configurations. In this study, permeability of flow blockage is not considered since it is not an inherent matter of safety assurance. Also the edge and corner blockages and the heat generating blockages are not considered here, but will be the subject of future investigations.

EXPERIMENTAL FACILITY

Loop

A series of central-type fuel bundle blockage experiments was performed with the Sodium Boiling and Fuel Failure Propagation Test Facility, SIENA, in the FBR Safety Section of O-arai Engineering Center (OEC/PNC).

Figure 1 shows the schematic diagram of the loop. Two test sections could be installed simultaneously when required, with either of them being used for each experiment while the other was used as a bypass line. The attachment ports of the T-2 test section are designed to have a capability of receiving a pin bundle of size up to a 7-pin bundle. A large bundle, such as a 37 or 61-pin bundle, is mounted on the ports of the T-3 test section. The sodium driven by the main pump partly enters the test section, flows up through the

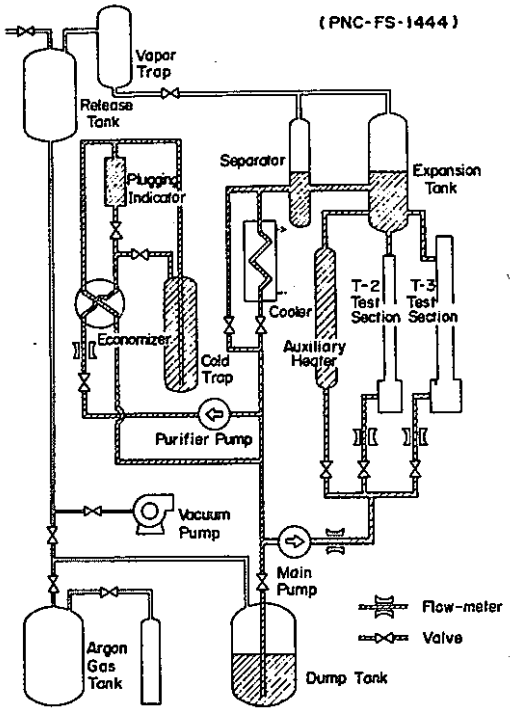

Fig. 1 Schematic diagram of sodium boiling and fuel failure propagation test facility, SIENA.

pin bundle being heated, reaches the expansion tank where it mixes with the bypassed sodium and moves to the subsequent separator tank. After leaving these tanks, the sodium enthalpy is ultimately lowered by the air cooler to maintain the cold-leg sodium temperature constant. The loop has another circuit parallel to the test sections. The auxiliary heater is there so that the loop sodium temperature condition can be regulated. During the tests, flow conditions through three parallel passages from main pump to expansion tank are independently controlled by throttling the inlet valves or by changing the main pump power.

A purification system and gas, vacuum and vapor trapping lines are equipped as back up of the loop operation.

Pin Bundles

In order to simulate an LMFBR fuel subassembly, four bundles (7 and 37-pin grid, 37 and 61-pin wire-wrapped) were used in turn. Details are illustrated in Fig. 2 and are summarized in Table 2. Except for

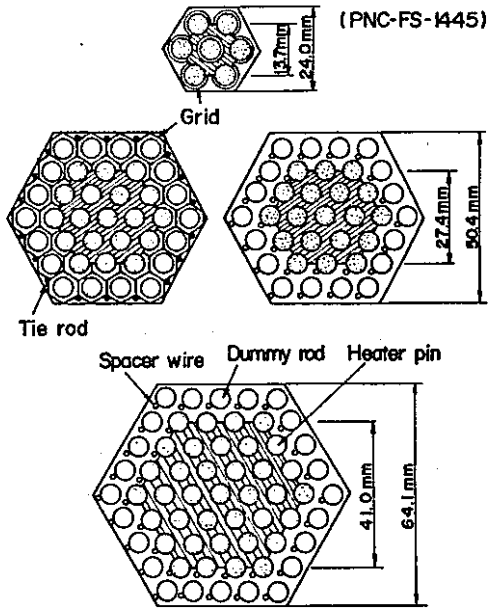

Fig. 2 Cross sections of 7, 37, 37 and 61-pin bundles with central blockages.

Table 2 Summary of the pin bundle geometries.

Pin bundle		7GC**	37GC	37WC**	61WC	MONJU
Pins (Heater)		7 (7)	37 (19)	37 (19)	61 (37)	169 -
Tie rods		0	18 *	-	-	-
Heated section length	(mm)	450	456	455	450	930
Location of blockage	(mm)	350.5	304	300	255	-
Thickness of blockage	(mm)	0.5	5	5	5	-
Width of wrapper tube	(mm)	24.0	50.4	50.4	64.1	104.6
Thickness of wrapper tube	(mm)	4	10	10	12	3
Pin diameter	(mm)	6.5	6.5	6.5	6.5	6.5
Pin pitch	(mm)	7.9	7.9	7.9	7.9	7.87
Flow area	(mm^2)	266.6	915.5	924.3	1456.5	3636.1
d_h	(mm)	4.72	3.51	3.43	3.40	3.22
D_B	(mm)	14.7	29.4	29.4	44.1	-
F	(-)	0.44	0.39	0.26	0.36	-
H_B	(-)	1.86	3.72	3.72	5.58	-
Height of grid spacer	(mm)	5	15	-	-	-
Diameter of spacer wire	(mm)	-	-	1.3	1.3	1.32
Axial pitch of spacer	(mm)	-	200	265	265	307

* Diameter of each tie rod is 2.0 mm.
** GC = grid spacer, central blockage; WC = wire spacer, central blockage.

the first one, the bundles consisted of central heater pins and surrounding dummy pins. The dummy pins were used because the sodium temperature field in the unblocked core flow region could be adjusted to be almost identical to the desired one by regulating the inlet sodium temperature instead of heating the outermost pins. The diameter of each pin was 6.5 mm and

the pin pitch was 7.9 mm. The axial heated length of the heater pin was about 450 mm and the heat flux was uniform. A spacer wire of 1.3 mm diameter was wrapped around each pin with a helical pitch of 265 mm for the last two bundles, while the first two were grid-spacer type bundles. Near the middle position of the heated section, a centrally located stainless steel blockage of 0.5 or 5 mm thickness was attached. The blockages covered 25 to 45 % of the total flow areas.

Instrumentation

The temperature increases behind the blockages were measured by many 0.3 mm diameter thermocouples embedded into pin claddings for pin surface temperature measurement and immersed in the subchannel centers for sodium temperature measurement. Some of the spacer wires of 1.3 mm diameters served as the thermocouples. All thermocouples were calibrated prior to the experiments by checking their outputs at some typical isothermal conditions in the range of expected sodium temperatures. The reliable thermocouple of large diameter was inserted in the inlet piping to measure the inlet temperature. Each temperature rise in the bundle is defined as the temperature at a measurement point minus the inlet temperature.

The inlet sodium flow rate was measured by an electromagnetic flow-meter attached to the inlet piping. The inlet flow velocity is calculated by multiplying the flow-meter reading by the conversion factor predetermined to satisfy the heat balance around the loop.

These output signals were recorded on a digital data acquisition system after the steady-state single-phase conditions were attained with sodium velocity and pin power level adjusted within the respective ranges: 0.2 to 4.7 m/s and 2.4 to 94.3 W/cm^2 (see Table 3).

Table 3 Experimental conditions.

Pin bundle	Operation No.	U_o (m/s)		q'' (W/cm^2)		T_{in} (K)		$T_{out}-T_{in}$ (K)	
		min.	max.	min.	max.	min.	max.	min.	max.
7GC	Part 1	0.2	4.4	3.9	55.2	569	648	15	63
	2	0.5	4.4	4.2	63.1	535	570	19	57
37GC	Part 1	0.5	4.2	2.4	18.0	537	570	5	15
	2	0.5	4.2	2.4	65.0	526	560	7	39
37WC	Part 1	0.5	4.7	2.5	19.1	532	557	8	38
	2	0.5	4.7	7.1	64.0	526	563	5	23
61WC	Part 1	0.5	4.0	4.6	47.3	533	561	8	32
	2	0.5	4.1	4.6	55.7	536	565	14	55
	3	0.6	4.0	4.6	94.3	529	650	8	49

EXPERIMENTAL RESULTS AND DISCUSSIONS

Swirl Flow

In general, a complex swirl flow in a wire-wrapped pin bundle with a blockage can cause a three-dimensional distortion of the temperature field. To obtain a precise knowledge on this temperature field is, however, impractical when the bundle is large. The thermocouple location scheme adopted in designing the 61-pin bundle was selected to be capable of obtaining separately the general two-dimensional isotherms of sodium temperature increases along the global swirl flow and the circumferential temperature profiles distorted due to swirl flow. It is illustrated in Fig. 3.

More than half of the total thermocouples used in the test bundle were immersed in the innet six and the eighth subchannel centers along a certain angular direction on each horizontal plane. The direction was shifted rotationally with the same helical pitch as the spacer wires. This main measurement angle at an arbitrary axial plane ranged from $\theta_W + \pi/4$ to $\theta_W + \pi/2$, except for the one at the plane 22 mm downstream from

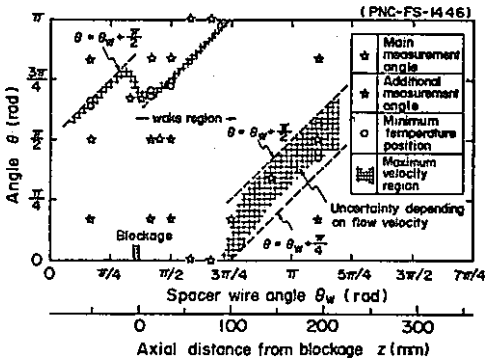

Fig. 3 Relation between thermocouple location and estimated maximum velocity region in 61-pin bundle test section.

the blockage. In addition, nearly a quarter of the total thermocouples were attached $\pi/3$ rotationally in the second and third subchannel centers at four planes. The circumferential temperature profile measured by these additional thermocouples can give a rough idea of the shape of the swirl flow, i.e. a line drawn through maximum velocity points on several planes, where the maximum velocity points can be represented by the minimum temperature points derived from the circumferential temperature profiles.

The shaded zone in Fig. 3 is the estimated shape of the swirl flow thus derived. This figure shows that the shape of the swirl flow around the blockage is a specified one without regard to the flow velocity. It seems to be given by the geometrical conditions of spacer wires and blockage. In addition, we can confirm that the main measurement thermocouples are located near the path of the global swirl flow. These considerations reveal that almost all of the main measurement thermocouples would give consistent data for mapping the two-dimensional isotherms. Otherwise, the measured data would have little coherency among each other and would cause the two-dimensional isotherms to result in misleading patterns depending on the flow velocity.

Two-Dimensional Isotherms

Figure 4 shows a typical two-dimensional isothermal map of sodium temperature increases observed in the 61-pin bundle experiment by a total of 59 thermocouples. The horizontal axis is the "triangular" subchannel number counting from the bundle center. All isotherms such as those shown in Fig. 4 were analyzed to draw the envelope of the two-dimensional recirculating sodium flow, i.e. the wake region. The result is traced by the broken line in Fig. 4, where the dotted points in each subchannel are the positions at which individual axial temperature distribution curves take their minimum values. The broken line is, therefore, the envelope of the wake region. It was concluded for a given bundle configuration that the shape and size of the wake region were not unique to each run but were very similar to other runs, even if the flow velocity was very slow. The isotherms disagreed with recirculating flow patterns.

The maximum temperature position appeared at the immediate vicinity of the blockage center. This feature differs much from the findings by Huber and Peppler in KfK (4). However, there is evidence to believe that the cause of the difference lies in the geometrical difference around the peripheral edges of the blockages. KfK's bundle has latticed hexagonal

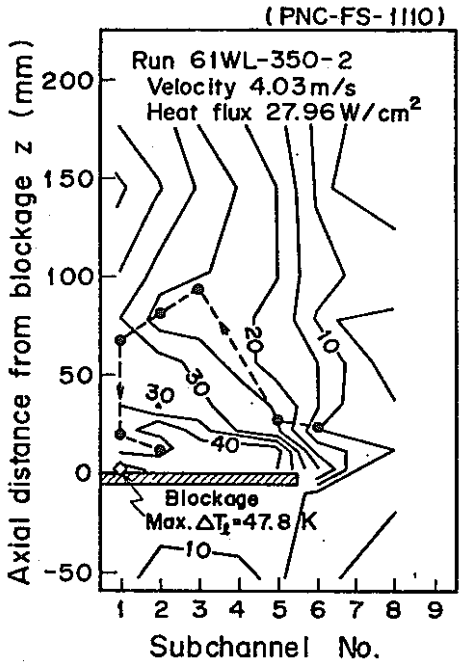

Fig. 4 Typical isotherms of sodium behind the blockage of 61-pin bundle test section.

cells of the grid spacer in the unblocked section of the blocked plane, which force the core flow through the unblocked section to be directed vertically. The recirculation flow pattern will become an axially extended ring-like shape, where the flow velocity near the bundle center will be sufficiently high. On the other hand, PNC's bundle has different flow regulating matters, i.e. the spacer wires. They permit the core flow to move obliquely toward the wake region at the position near the blocked plane. The promoted cooling capability of the wake center yields, therefore, the maximum temperature point not at the wake center but at the vicinity of the blockage center.

Residence Time

Only at the high flow rate range were the inside-wake temperature increases directly proportional to the simple parameter, "heat flux/flow velocity". From water mockup tests in PNC (5) and KfK (7), it was shown that the global recirculating flow velocities within the wakes were proportional to the core flow velocities for all flow rate cases. Also confirmed in the present study was the proportionality of the complex temperature field to the heat flux. The lack of proportionality between temperature increases and (1/flow velocity) at low flows is ascribed to the partial contribution of molecular heat conduction in sodium.

Based on the familiar definition of residence time,

$$\tau = \frac{d_h}{4} c_p \gamma \frac{T_{wake}-T_{core}}{q''} , \qquad (1)$$

τ was calculated for various core flow velocities, U_B, and measured temperatures. In this calculation, all thermocouples included in the wake yield the mixed mean sodium temperature under the assumption of uniform local velocity within the wake:

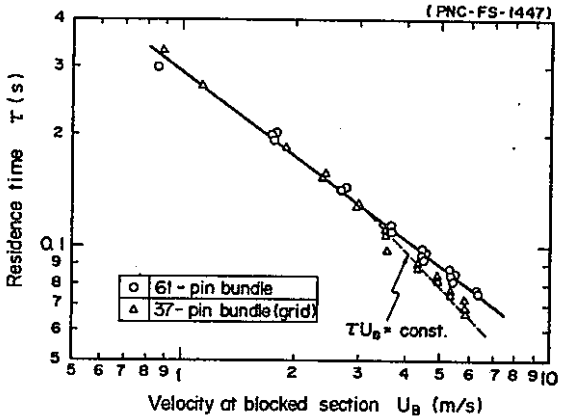

Fig. 5 Relation between residence time and flow velocity.

$$T_{wake}-T_{core} \approx \int_A (T-T_{core})dA/A . \qquad (2)$$

The results for 37 and 61-pin bundle configurations are shown in Fig. 5. From the above discussion on the proportionality between temperature increases and (1/flow velocity), τU_B should asymptotically approach the constant value at high flows which would be determined by the enthalpy balance between the wake region and the core flow region. For the 61-pin bundle case, this tendency was not clearly found within the tested velocity range, since the pumping head capacity was insufficient to raise the flow rate high enough to treat the heat transfer as convection controlled. However, the asymptotic values for different blockages would not be expected to converge to the same value.

Heat Exchange Layer Model

If the high enthalpy liquid within the wake is cooled mainly by the lateral cross flow through the small gaps between pins, the inside-wake temperature rise and the residence time should also be controlled by cross flow. From the insight of the isotherms, a key factor is that the pins which are standing around the interface area between the wake region and the core flow region obstruct the lateral cross flow through the interface region. Since the pins are arranged triangularly, the influence of the cross flow can be considered to extend only one or two subchannels. The similarity of radial temperature gradient may hold, therefore, only within the interface region. This idea is modeled in Fig. 6, where two radial temperature gradient guesses for the large blockage case

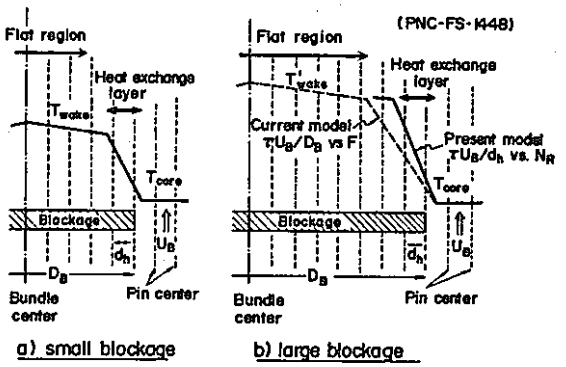

Fig. 6 Heat exchange model from wake region behind blockage to core flow region.

are illustrated based on the finding behind the small blockage. The previous method of normalizing the asymptotic value of τU_B (or τU_o) by the blockage size D_B (8) is based on the assumption that the radial temperature field expected in the case of a large blockage is similar, over the wide region equal to the blockage size, to that observed behind a small blockage. On the contrary, the present model, which (as a natural result of the assumption of the unchangeable width of the interface region) normalizes τU_B by d_h, assumes a horizontally steepened temperature gradient within the limited interface region. This interface region can be identified as a universal heat exchange layer for convective heat transfer.

The heat exchange layer model suggests that the total lateral heat exchange rate may be given by the geometrical condition. If the capacity of heat removal through a pin gap is well fixed under a given hydraulic condition, then the total lateral heat exchange rate is no more than a specified value depending on the number of gaps contributing to the heat exchange. Here, a new variable named "Ring Parameter", N_R, is introduced:

$$N_R = D_B/p \quad . \qquad (3)$$

The Ring Parameter is proportional to the number of pins or pin gaps around the contour line of the blockage for central-type blockages.

The modified dimensionless residence time, $\tau U_B/d_h$, was correlated with the Ring Parameter in Fig. 7, together with the previous correlation of $\tau U_o/D_B$ versus fraction of blocked flow area (8). Almost all data available fall on the line as expressed by the following empirical formula:

$$\tau U_B/d_h = 35.3\ N_R^{0.85} \quad . \qquad (4)$$

On the other hand, the dimensionless residence time for the 61-pin bundle by the previous definition is too low to be correlated by the previous intuitive method.

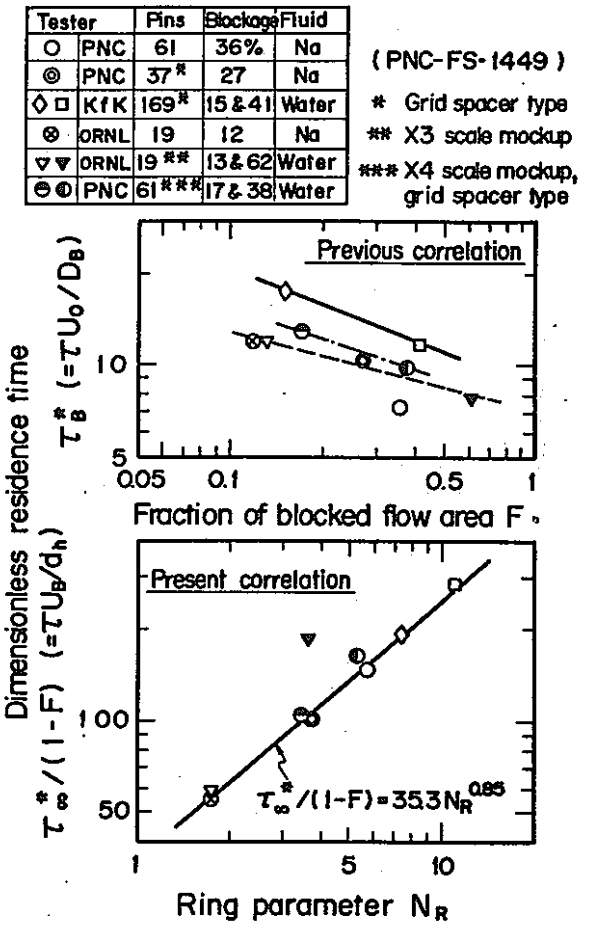

Fig. 7 Correlation of the residence time of sodium flow within the wake.

Restriction on Applicability

In Fig. 7, the ORNL data point for a mockup 19-pin bundle in water with extremely large blockage (F = 62 %) looks appropriate in the previous correlation ($\tau U_o/D_B$ vs. F); however it is about twice as large as that of PNC's 37-pin bundle with 27 % blockage in the present correlation ($\tau U_B/d_h$ vs. N_R) although both of them have the same value of Ring Parameter. This result implies that the wake behind the 62 % blockage was not as effectively cooled or that the recirculating flow velocity was about half that of other cases if the core flow velocity is equal to those in other large bundles. Consequently, it may be concluded that the similarity of the hydraulic fields on which the heat exchange layer model is based is not guaranteed when the blockage is large enough to occupy the outermost pin-ring. The coupling manner of the recirculating flow to the core flow seems to differ as the blockage becomes too large, where the effect of the wrapper tube wall cannot be ignored. Then, the previous correlation method rather than the present model would be attractive.

The model may not necessarily apply for very small blockage cases such as a one-subchannel blockage. A rough insight would imply that the model requires at least two rows of blocked pin arrays which can shear the lateral cross flow through succeeding small pin gaps. However, there are no data to verify this conjecture. A similar discussion can be applied to the tightness of the pin bundle assemblies, i.e. the pin spacing and the pitch-to-diameter ratio. Figure 7 reveals that the model is effective within the range up to pin diameters and spacings four times as large as in ordinary fuel subassemblies. Although all data are for nearly the same pitch-to-diameter ratio, the effect of differing pitch-to-diameter ratios would be identical to that of differing hydraulic diameters.

These considerations imply the applicability ranges of the heat exchange layer model and Eq. (4) as follows:

$$1\ \% < F < 60\ \% \quad \text{of 169-pin bundle} \qquad (5)$$

$$3\ \text{mm} < d_h < 16\ \text{mm} \qquad (6)$$

Besides these restrictions, the flow reduction effect due to the increased pressure drop by the blockage should be accounted for. This effect can be taken into account simply by reducing the value of U_B in Eq. (4) by the amount which may be expected from an appropriate correlation between blockage size and flow velocity.

Peaking Factors

Two peaking factors are needed for the practical utilization of Eq. (4): one is the bare bundle peaking factor, C_B, and the other is the spacer wire distortion factor, C_W. These variables are defined as follows:

$$C_B = (T_{max,bare}-T_{core})/(T_{wake}-T_{core}) , \quad (7)$$

$$C_W = (T_{max,wire}-T_{core})/(T_{max,bare}-T_{core}) . \quad (8)$$

Figure 8 shows the data of the bare bundle peaking factor measured in the 37-pin grid and 61-pin wire-wrapped bundle blockage experiments, where this peaking factor in the wire-wrapped bundle is represented by the ratio of the maximum temperature increases measured by the main measurement thermocouples over the inside-wake temperature increase defined by Eq. (2). Figure 9 draws the examples of the original data which yield the spacer wire distortion factor.

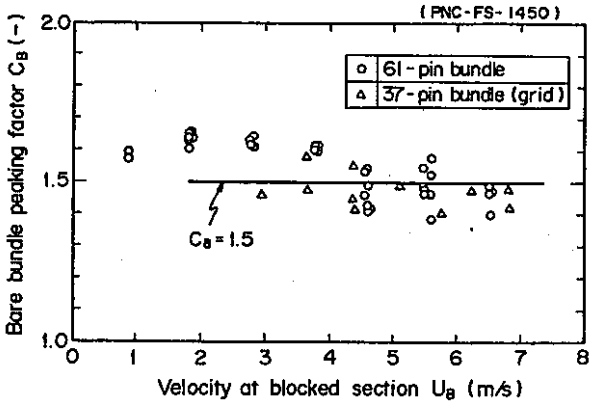

Fig. 8 Relation between bare bundle peaking factor and flow velocity.

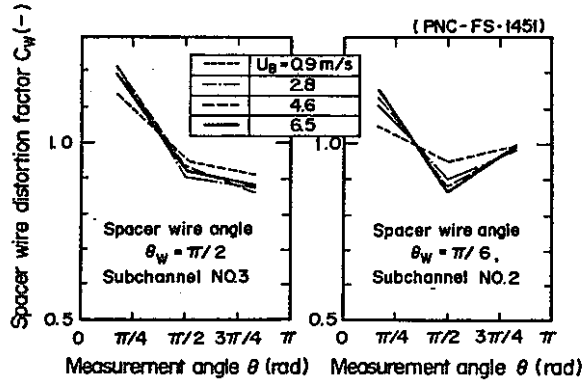

Fig. 9 Relation between spacer wire distortion factor and flow velocity (61-pin bundle experiment).

As are seen in Figs. 8 and 9 for high velocity cases where molecular heat conduction becomes negligible, these two factors appear to approach constant values:

$$C_B = 1.5 , \quad (9)$$

$$C_W = 1.2 . \quad (10)$$

Concerning the bare bundle peaking factor, Gregory and Lord (9) show the value of 1.6. It is apparent from Fig. 8 that there is little difference between their value and Eq. (9). Hence, it appears that Eq. (9) covers a wide range of blockage sizes sufficient for practical utilization with Eq. (4). On the other hand, the spacer wire distortion factor is not perfectly analyzed anywhere. It would be better to treat this value as a function of blockage size. For instance, a similar distortion effect could not be identified in the case of a 37-pin wire-wrapped bundle, where there were few thermocouples by which the effect of spacer wire could be examined in detail. Nevertheless, we recommend that Eq. (10) be used for all geometrical conditions until further study is completed.

Estimation of Temperature Increases

Equations (4), (9) and (10) lead to the empirical formula for estimating the maximum temperature in the wake:

$$T_{max}-T_{core} = C_B \cdot C_W \cdot 35.3(D_B/p)^{0.85}/[\frac{c_p \gamma U_o}{4q''(1-F)}] . \quad (11)$$

A typical result of applying Eq. (11) to an operating condition of MONJU is illustrated in Fig. 10, in which the fraction of assumed blocked flow area is taken as the horizontal axis. As pointed out by Basmer et al. (10) with the Kirsch model of hydraulic field (7), the inside-wake temperature first increases with the blockage size, attains the maximum value at 30 % blockage, and then decreases monotonically if the flow reduction caused by the increased pressure drop is not so dominant. When the blockage becomes extremely large, the inside-wake temperature will increase again. The decreasing tendency is ascribed to the increases of core flow and recirculating flow velocities by the increase of blocked flow area with the assumed constant inlet flow rate. The subsequent increasing tendency is caused by the reduction of inlet flow rate and also by the deterioration of the heat removal through the heat exchange layer.

It is seen from Fig. 10 that the central-type blockage in the MONJU fuel subassembly will not cause local boiling unless the flow reduction is so large that it can be detected by a core exit flow-meter (or

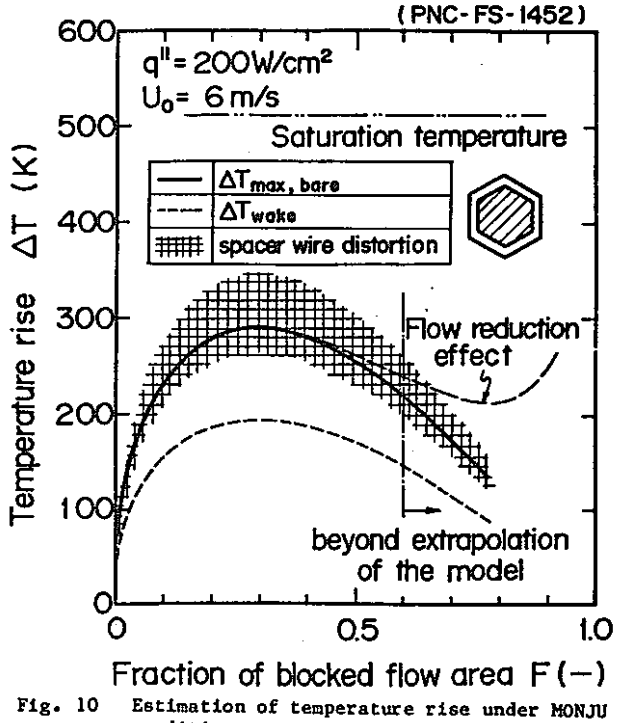

Fig. 10 Estimation of temperature rise under MONJU condition.

thermocouple) whose threshold for the detection of blockage formation corresponds to the 60 % blockage condition. It may be mentioned that one of the most restrictive conditions of MONJU relative to boiling inception is the combination of 30 % blockage formation and operation at a power-to-flow ratio of 125 % of the design value. Even under these severe conditions, sodium should not reach the boiling point.

CONCLUSIONS

A series of central-type fuel bundle blockage experiments was performed. The results were summarized referring to the similar test results by others, and the following conclusions have been drawn concerning the single-phase heat transfer.

(1) The heat exchange layer model presented in this paper successfully correlated almost all temperature rise data available. The Ring Parameter introduced here assisted the interpretation of the lateral cross flow controlled nature of global heat transfer within the heat exchange layer. The restriction for the applicability of the model was also clarified.

(2) An empirical formula was derived to estimate local temperature increases behind various central-type blockages. Two peaking factors, bare bundle peaking factor and spacer wire distortion factor, were estimated separately for convenience.

(3) The central-type blockage will not cause local boiling for MONJU's design conditions unless the flow reduction is so large that it can be detected by a core exit flow-meter (or thermocouple).

Intermediate sizes of edge and corner-type blockages produce higher temperature fields, leading to undetected local sodium boiling in the worst case. This case will be investigated in the future. The additional cooling and heating by the porosity of the blockage and by the heat generating blockage, respectively, will require further study.

ACKNOWLEDGMENTS

The authors are indebted to Messrs. K. Mochizuki, A. Ohtsubo, and M. Hori for their sponsorship, and to Messrs. Y. Kikuchi, Y. Daigo, K. Sahashi, T. Isozaki and T. Komaba for their engineering and technical contributions throughout the performance of individual experiments. The authors particularly wish to express their thanks to Messrs. C. L. Larson and D. H. Jones and Miss S. Onose for their efforts on manuscript preparation.

REFERENCES

1 Uotani, M. et al., "Local Flow Blockage Experiments in 37-Pin Sodium Cooled Bundles with Grid Spacers," Proceedings of the 8th Liquid Metal Boiling Working Group Meeting, Mol, Oct. 1978.

2 Yamaguchi, K. et al., "Local Temperature Rise and Boiling Behavior behind a Central Blockage in a Wire-Wrapped Pin bundle," Proceedings of the 9th Liquid Metal Boiling Working Group Meeting, Rome, June 1980.

3 Han, J. T. and Fontana, M. H., "Blockage in LMFBR Fuel Assemblies," Thermal and Hydraulic Aspects of Nuclear Reactor Safety, Vol. 2, Liquid Metal Fast Breeder Reactors, ASME, 1977, pp. 51-121.

4 Huber, F., Peppler, W., "Form and Development of Boiling behind a 49 % Central Blockage in a 169 Pin Bundle," Proceedings of the 7th Liquid Metal Boiling Working Group Meeting, Petten, June 1977.

5 Nakamura, H., Miyaguchi, K., and Takahashi, J., "Hydraulic Simulation of Local Blockage in a LMFBR Fuel Subassembly," Nuclear Engineering and Design, Vol. 62, Dec. 1980, pp. 323-333.

6 Fontana, M. H. et al., "Thermal-Hydraulic Effects of Partial Blockages in Simulated LMFBR Fuel Assemblies with Application to the CRBR," ORNL-TM-4779, 1975.

7 Kirsch, D., "Investigations on the Flow and Temperature Distribution Downstream of Local Coolant Blockages in Rod Bundle Subassemblies," Nuclear Engineering and Design, Vol. 31, 1974, pp. 226-279.

8 Bishop, A. A., Engel, F. C., and Markley, R. A., "Partial Flow Blockage Effects within a LMFBR Fuel Assembly," Proceedings of the 1975 National Heat Transfer Conference (CONF-750804-5), San Francisco, California, Aug. 1975.

9 Gregory, C. V., and Lord, D. J., "The Study of Local Blockages in Fast Reactor Subassemblies," Journal of the British Nuclear Energy Society, Vol. 13, No. 3, 1974, pp. 251-260.

10 Basmer, P. et al., "Experiments on Local Blockages," Proceedings of the 6th Liquid Metal Boiling Working Group Meeting, Riseley, Oct. 1975.

APPENDIX: SCOPE OF PRESENTATION

1981 ASME WINTER ANNUAL MEETING

Experimental Investigation of Local Cooling Disturbances in LMFBR Fuel Subassemblies

K. Yamaguchi, M. Uotani, K. Haga,

O-arai Engineering Center, Power Reactor and Nuclear Fuel Development Corporation (OEC/PNC), Japan

and

F. Namekawa

Nuclear Engineering Laboratory, Toshiba Corporation, Japan

INTRODUCTION

Thank you, chairman. Next, I would like to present our summary study on the local cooling disturbance caused by the local flow blockage.

1981 ASME WINTER ANNUAL MEETING,
WASINGTON, D.C., NOV. 15-20, 1981

EXPERIMENTAL INVESTIGATION OF LOCAL COOLING DISTURBANCES IN LMFBR FUEL SUBASSEMBLIES

K. YAMAGUCHI*, M. UOTANI*, K. HAGA* AND F. NAMEKAWA**
* OEC/PNC, JAPAN, ** TOSHIBA CORP., JAPAN

OBJECTIVES

(1) INTERPRET THE RESULTS OF OUT-OF-PILE LOCAL BLOCKAGE EXPERIMENTS CONDUCTED AT VARIOUS LABORATORIES UNDER QUITE DIFFERENT TEST CONFIGURATIONS.

(2) OBTAIN AN EMPIRICAL FORMULA AVAILABLE FOR ESTIMATING MAXIMUM TEMPERATURE INCREASES IN VARIOUS ASSEMBLIES.

(3) FIND THE CRITICAL CONDITION OF THE ONSET OF LOCAL BOILING.

OBJECTIVES ..... (First slide, please. SLIDE No. 1)

The hypothetical planar blockage in a FBR fuel subassembly is a possible initiator of the propagation of cooling disturbance. Therefore, it is very important to develop a detailed understanding of the accident progression resulting from the blockage formation.

There are many experimental investigations. The results are, however, obtained under differing test conditions and philosophies. They often prevent the mutual utilization of the results to a specific reactor design case. We must overcome this difficulty to develop a safety assessment work of the local blockage accident.

First of all, we should interpret by a universal heat transfer model the results of out-of-pile local blockage experiments conducted at various laboratories under quite different test configurations. When we obtain an empirical formula available for estimating maximum temperature increases in various assemblies, we can find the critical condition of the onset of local boiling.

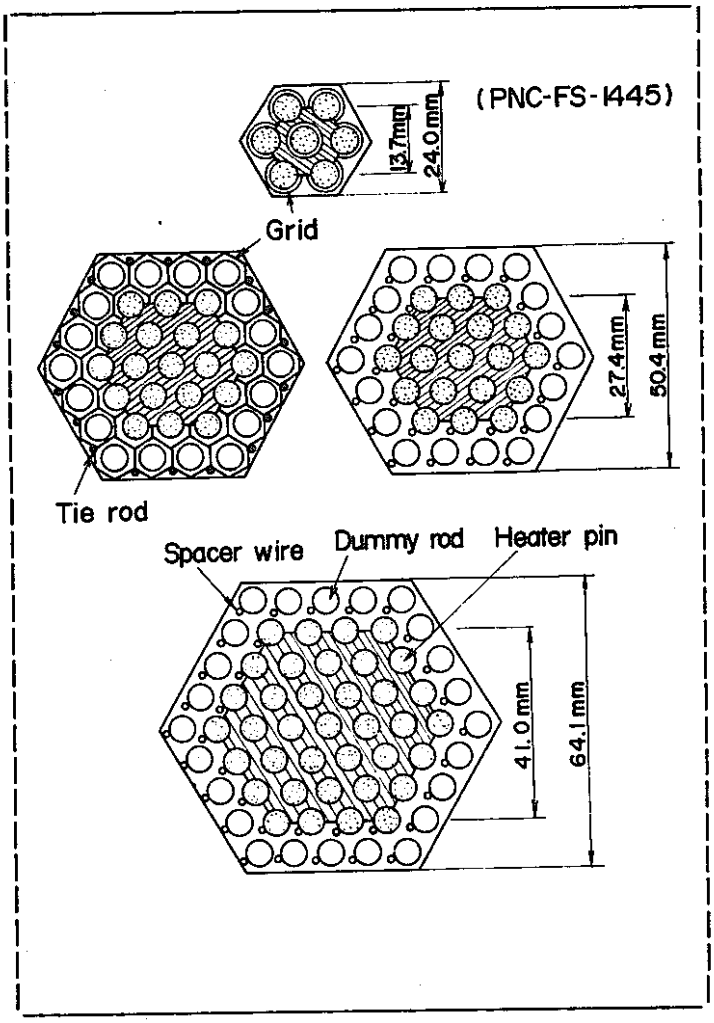

TEST SECTION ..... (Next slide, please. SLIDE No. 2, i.e. Fig. 2)

For this study, we have conducted four series of central-type blockage experiments. The first series used a 7-pin grid type bundle, the second and the third series used 37-pin grid and wire-wrapped bundles, and the last series used a 61-pin wire-wrapped bundle. These bundles were installed in the out-of-pile test facility, SIENA.

Besides these in-sodium experiments at PNC, our summary work referred the similar studies, such as in-sodium experiments at ORNL and KfK, and water mockup tests at PNC, ORNL and KfK.

SUMMARY OF THE EFFECTIVE FACTORS

FACTORS	VARIABLES
SPACER TYPE	WIRE AND GRID
TIGHTNESS OF ASSEMBLING	D_H
LOCATION OF THE BLOCKAGE	CENTRAL
BLOCKAGE SIZE	D_B
BLOCKED FLOW AREA	F

EXAMINED SCOPE ..... (Next slide, please. SLIDE No. 3, i.e. Table 1)

This slide shows the key factors which were separately treated in this study. An application of the present study to the edge or corner blockages are possible. However, I would like to show only the result for central-type blockages to focus our minds on the basic concept of the heat transfer model we want to propose today.

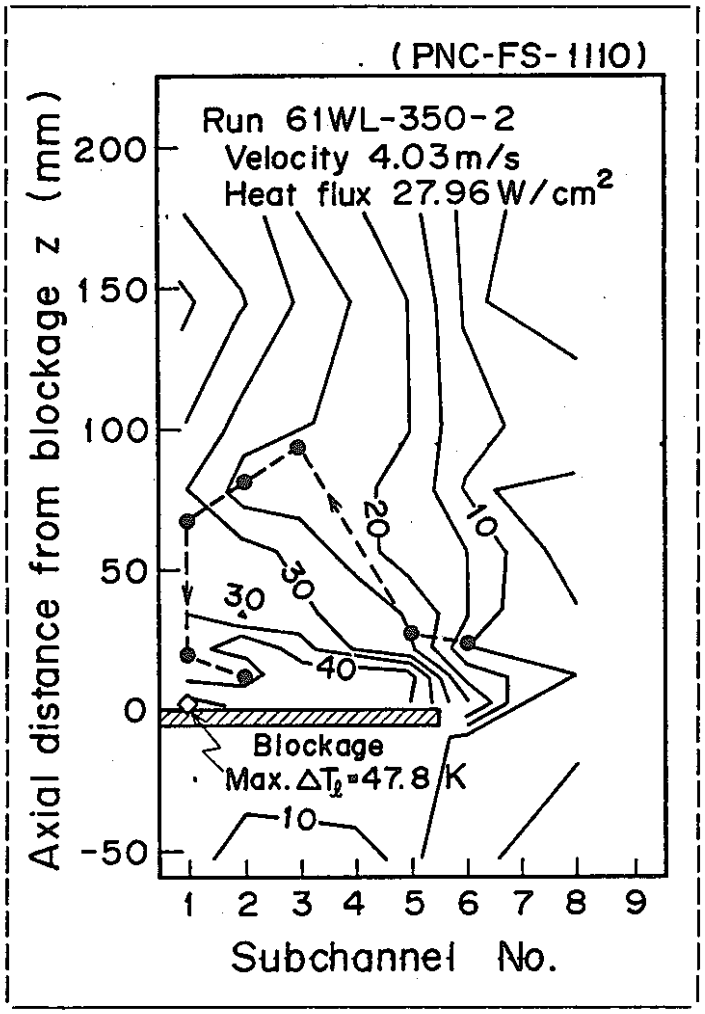

ISOTHERMS ..... (Next slide, please. SLIDE No. 4, i.e. Fig. 4)

Now, I would like to examine the fundamental properties of the thermal and hydraulic fields behind the blockage.

This slide shows a typical two-dimensional isotherms of sodium temperature increases observed in the 61-pin bundle. The horizontal axis is the "triangular" subchannel number counting from the bundle center. The vertical axis is the distance from the blockage. All isothermal maps like this were analyzed to draw the envelope of the two-dimensional recircurating sodium flow, i.e. the wake region. A typical result is traced here by the broken lines.

It was concluded for a given bundle configuration that the shape and size of the wake region were not unique to each run but were very similar to other runs, even if the flow velocity was very slow. In the water mockup tests at PNC and KfK, it was shown that the global recirculating flow velocities within the wakes were proportional to the core flow velocities for all flow rate cases. In addition, the

proportionality of the complex temperature field to the heat flux was confirmed in our study.

These findings reveal that the heat transfer from the wake region to the core flow region can be treated as convection controlled, for the general cases.

HEAT EXCHANGE LAYER MODEL

These isotherms indicate us another important information that a large amount of heat is transported through the narrow region at the edge of the blockage. If the high enthalpy liquid within the wake is cooled mainly by the lateral cross flow through this region, the inside-wake temperature rise should also be controlled by the cross flow.

Since the pins standing around the interface area between wake region and core flow region obstruct the cross flow, the influence of the cross flow can be considered to extend only one or two subchannels. The similarity of radial temperature gradient may hold, therefore, only within this interface region. This idea is modeled in the next slide.

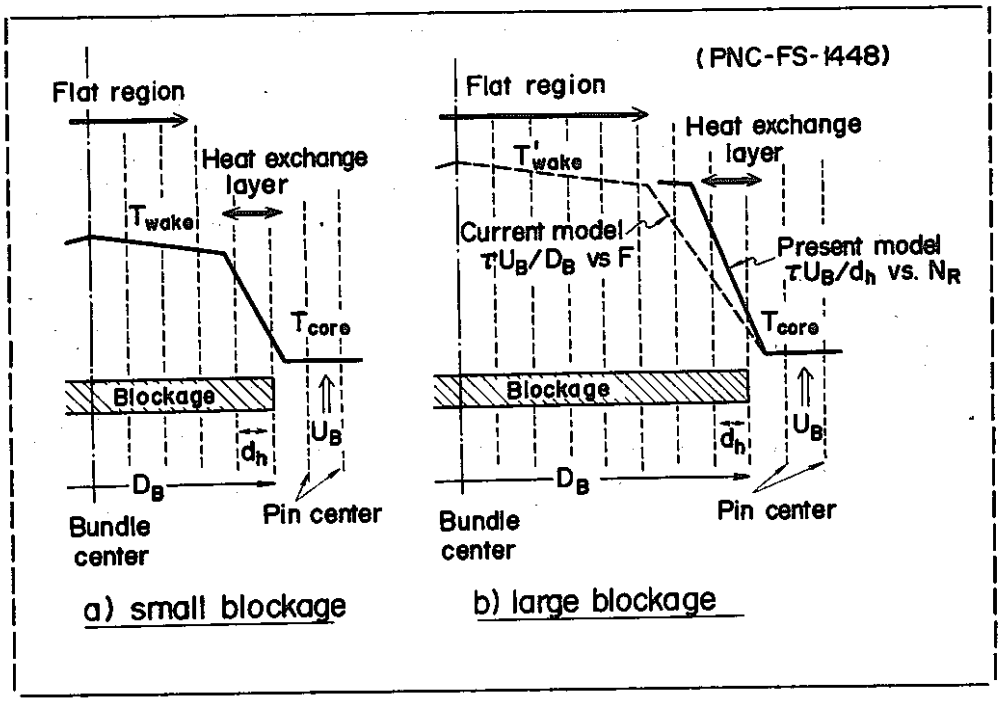

..... (Next slide, please. SLIDE No. 5, i.e. Fig. 6)

Please suppose that the left illustration is a measured radial temperature profile at a certain plane behind a small blockage. The solid arrow means the dominant heat exchange region.

The right illustration shows two radial temperature gradient guesses for the large blockage case.

The previous model is based on the assumption that the dominant heat exchange region would expand by the geometrical scale factor between two blockages. However, our model assumes a horizontally steepened temperature gradient within the same width interface region. This interface region can be identified as a universal heat exchange layer for convective heat transfer.

EMPIRICAL CORRELATIONS

In order to intercompare the various temperature rise data measured behind different blockages, we usually use the concept of sodium residence time τ within the wake region. τ is proportional to the inside-wake temperature increases. As already mentioned, it is inversely proportional to the core flow velocity. Therefore, τU_B is always constant if the bundle configuration is unchanged.

For different size blockages, the previous model used blockage diameters D_B for the geometrical normalization constant of τU_B. And

the fraction of blocked flow area F was used to correlate the normalized data.

On the contrary, the present model normalizes τU_B by the hydraulic diameter of one subchannel, i.e. a scale of the universal heat exchange layer. Next, we must find an answer to the question "what is the most reasonable variable to correlate the normalized data?"

The universal heat exchange layer model suggests that the total lateral heat exchange rate may be given by a geometrical condition. If the capacity of the heat removal through a pin gap is well fixed under a given hydraulic condition, then the total lateral heat exchange rate is no more than a specified value depending on the number of gaps contributing to the heat exchange. In order to verify this hypothesis, we have introduced a new variable named "Ring Parameter". The Ring Parameter is proportional to the number of pins or pin gaps around the contour line of the blockage, for cnetral-type blockages.

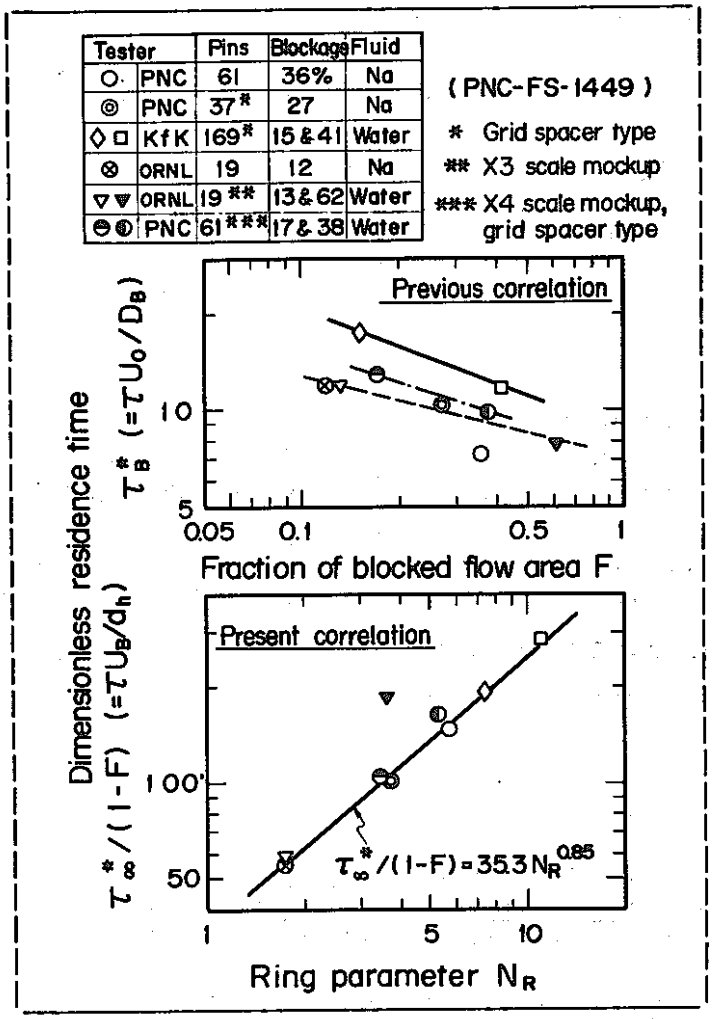

..... (Next slide, please. SLIDE No. 6, i.e. Fig. 7)

The intercomparison of all data by these two approaches resulted in quite different correlations. They are shown in this slide. The upper figure is the result of the previous model, and the lower figure is that of the present model.

In the lower figure, almost all data available fall on the line as expressed by this formula. Therefore, we can conclude that the temperature increases behind various blockages are well predictable by this empirical formula.

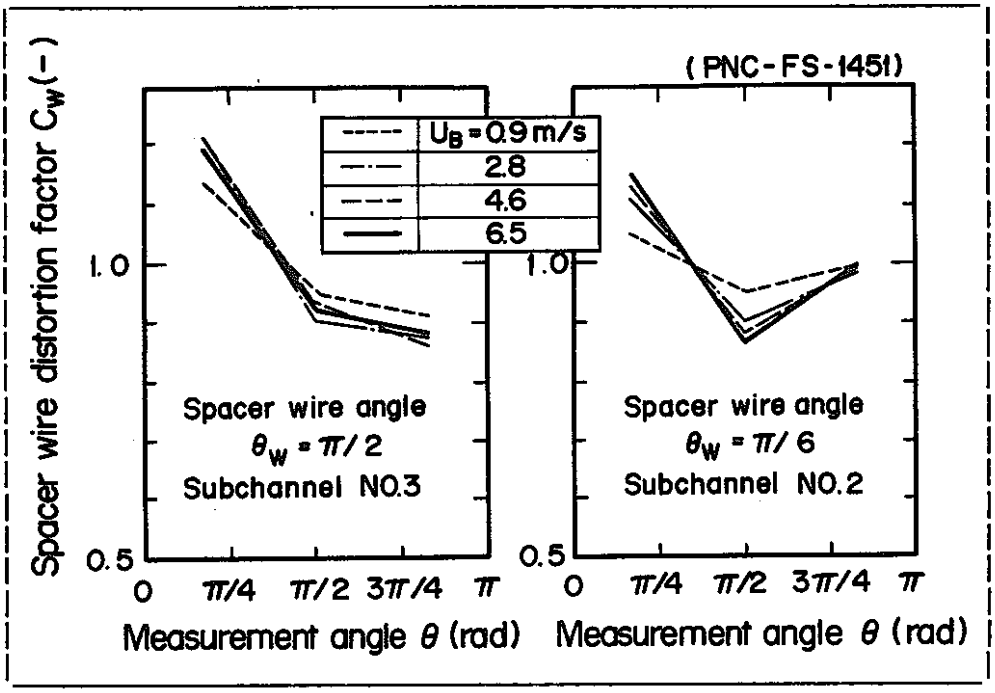

LOCALITY ..... (Next slide, please. SLIDE No. 7, i.e. Fig. 9)

Now, I would like to show the back-data to give additional information of the local temperature peaking and the spacer wire effect required for the practical utilization of the empirical formula.

Here, the temperature distortions against the mean values are traced at typical two horizontal planes. The high temperature positon means that the sodium tends to stagnate at this angular location, and the low temperature position means that the sodium flow is concentrated there.

The angular locations of minimum temperature positions are rearranged in the next slide.

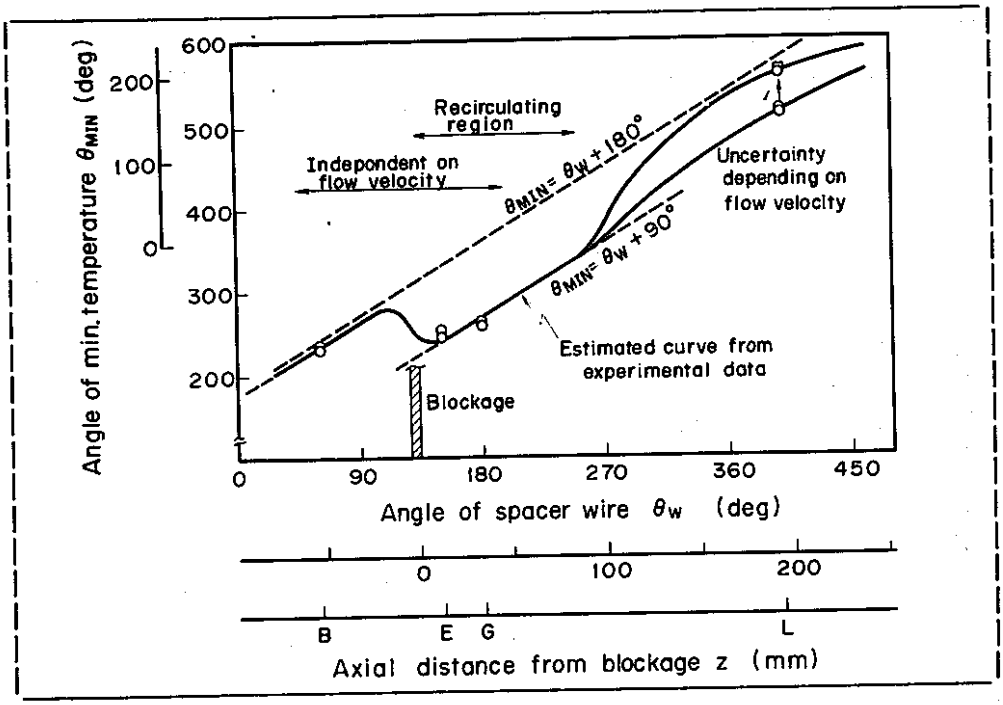

..... (Next slide, please. SLIDE No. 8, i.e. Fig. 3)

Here, the horizontal axis is the axial location of the measured plane, and the vertical axis is the angular location of the minimum temperature position on each plane. The shaded zone is the most flow concentrated path derived by connecting minimum temperature positions. From this figure, we can easily identify the global shape of swirl flow. The restriction to the freedom of sodium flow by the spacer wire and the blocakge causes very regular three-dimensional distortion of the local temperatures.

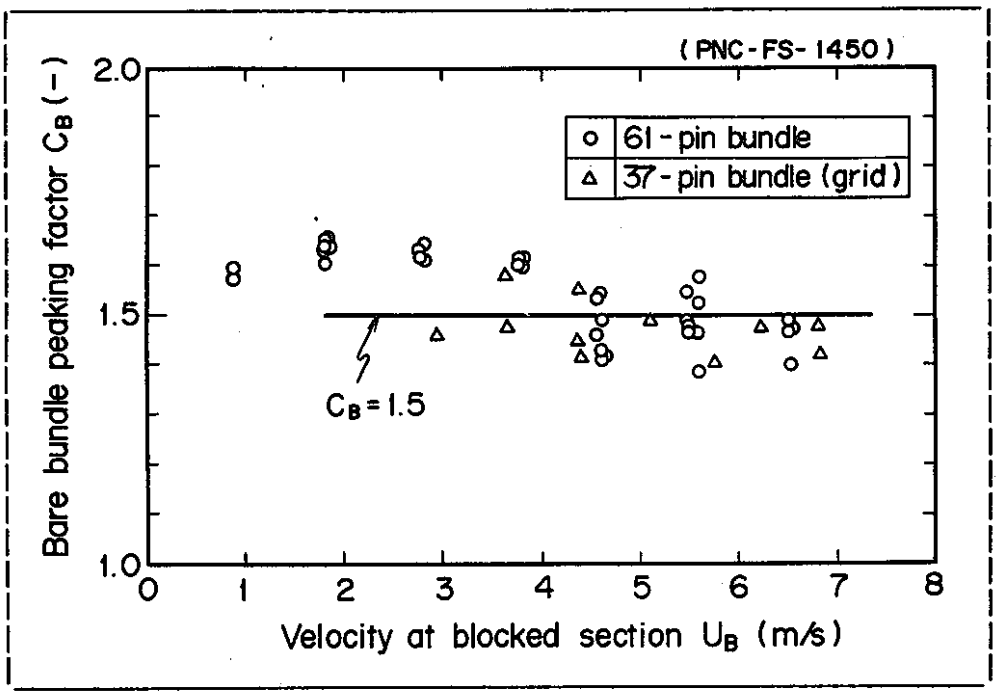

..... (Next slide, please. SLIDE No. 9, i.e. Fig. 8)

Even if the wire effect is canceled by picking up the temperatures along the swirl flow at every measurement planes, there still exists a large temperature peaking in the wake region. We can treat it as a bare bundle peaking factor. This slide shows that the peaking is about 1.5 for the examined cases.

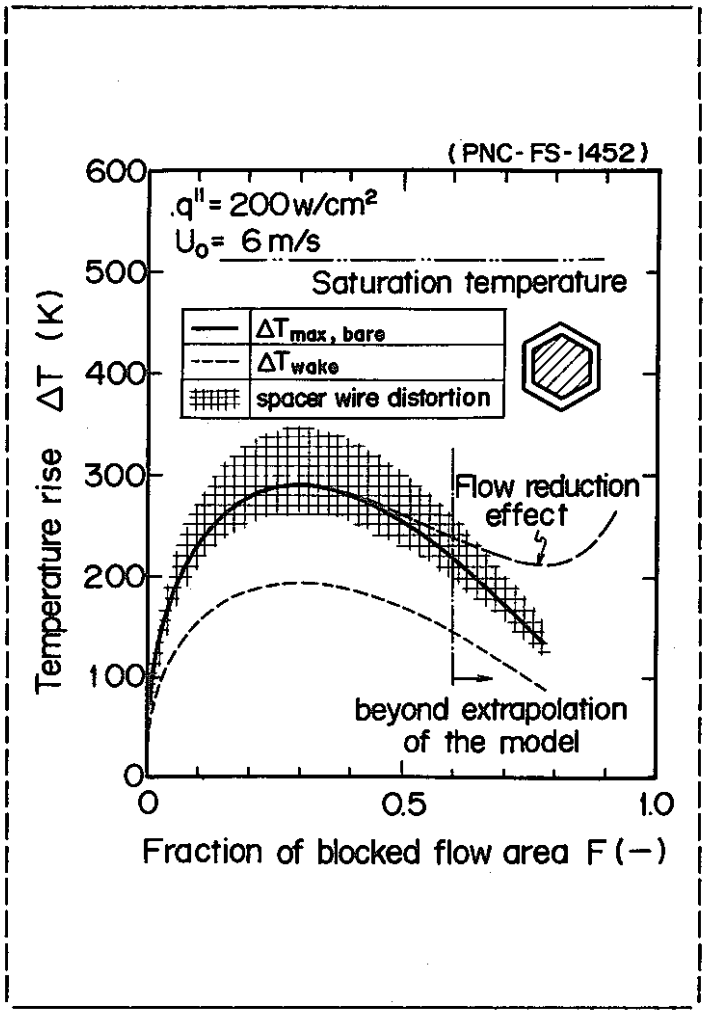

..... (Next slide, please. SLIDE No. 10, i.e. Fig. 10)

This slide shows the estimated temperatures behind various sizes of central-type blockages. The Japanese prototype reactor "MONJU" operating conditions were used as calculation parameters. Here, this line represents average sodium temperatures and this yellow band represents maximum temperatures behind blockages.

The temperature rise in the wake region increases with blockage size when the Ring Parameter is less than 8, that is the 30% blockage ratio. However, when the Ring Parameter is greater than 8, the temperature rise gradually decrease with increasing blockage size due to the increased coolant velocity at the blocked section.

Therefore, we can conclude that the central-type local blockage would not cause local boiling under normal operating conditions. One of the critical conditions for the boiling onset is the overlapped condition of the 30% blockage and 25% over-mismatch of power-to-flow ratio.

CONCLUSION

(1) THE UNIVERSAL HEAT EXCHANGE LAYER MODEL SUCCESSFULLY CORRELATED ALMOST ALL TEMPERATURE RISE DATA AVAILABLE.

(2) AN EMPIRICAL FORMULA WAS DERIVED TO ESTIMATE LOCAL TEMPERATURE INCREASES BEHIND VARIOUS CENTRAL-TYPE BLOCKAGES.

$$T_{MAX}-T_{CORE} = C_B \cdot C_W \; 35.3 \; N_R^{0.85} / \left[\frac{c_p \gamma U_0}{4q''(1-F)}\right]$$

$$N_R = D_B/P$$

(3) THE CENTRAL-TYPE BLOCKAGE WILL NOT CAUSE UNDETECTED LOCAL BOILING FOR THE "MONJU" DESIGN CONDITIONS.

CONCLUSION ..... (Next slide, please. SLIDE No. 11)

I would like to summarize my presentation.

I have proposed the universal heat exchange layer model. Based on this model, an empirical formula was derived to estimate local temperature increases behind various central-type blockages. Two peaking factors, i.e. the bare bundle peaking factor and the spacer wire distortion factor, were estimated experimentally. The maximum temperature within the wake region can be estimated by this equation.

In addition, it was shown that the central-type blockage would not cause undetected local boiling for the "MONJU" design conditions.

That is all. Thank you.

Out-of-Pile Experiments for Fission Gas Release in LMFBR Fuel Subassemblies—Gas Release into Blockage Wake Region with a Wire-Wrapped 37-Pin Bundle

F. Namekawa*, K. Yamaguchi, K. Haga

FBR Safety Section, SG Development Division, Oarai Engineering Center, PNC

ABSTRACT

This paper deals with fuel pin cooling capability under fission gas release into a wake region of local blockage in a fuel subassembly of an LMFBR, as a consequence of pin failure caused by a local blockage. Experiments for fission gas release into a locally blocked 37-pin bundle are described and results are given regarding various fission gas release modes. Data revealed that only at the gas accumulation zone in the wake region did temperature behind blockage increase significantly. The temperature field strongly depends on both coolant velocity and gas release rate. Present results indicat that no significant pin failure propagation would occur, under reactor conditions, even if local dryout occurred due to fission gas release.

NOMENCLATURE

C_p = specific heat capacity for sodium, J/kgK
D = gas release nozzle diameter, m
D_h = subchannel hydraulic equivalent diameter, m
G_g = gas release rate, g/s
G_{go} = initial gas release rate, g/s
g = gravity acceleration, m/s^2
L = distance from blockage, m
m = gas release exponent
P_a = sodium pressure at gas injection nozzle location, Pa
P_g = gas plenum pressure, Pa
P_{go} = initial gas plenum pressure, Pa
q = heat flux, W/m^2
T = temperature, °C
T_{in} = inlet sodium temperature, °C
T_g = gas plenum temperature, °C
U = sodium velocity, m/s
U_b = sodium velocity at blocked section, m/s
U_o = sodium velocity in normal bundle, m/s
V = gas plenum volume, m^3
α = void fraction
δ = factor, Eq. (3)
η = blocked area ratio
Ξ = normalized temperature, Eq. (1)
κ = ratio of specific heat capacity for released gas
ρ = sodium density, kg/m^3
ρ_g = gas density at gas plenum, kg/m^3
τ = time after gas injection, s
ϕ = heat input per subchannel volume, W/m^3

* Consulting Staff from Nuclear Engineering Laboratory, Toshiba Corporation

INTRODUCTION

In designing a Liquid Metal Cooled Fast Breeder Reactor (LMFBR), it is of great importance to evaluate the potential for pin-to-pin failure propagation within fuel subassemblies. Considerable research on failure propagation has been performed in many countries involved in LMFBR development.

The pin-to-pin failure propagation is initiated by small local faults within a subassembly. It is generally believed that local blockage in a pin bundle is one of the most likely initiators of local faults, since pins are closely arrayed in the subassembly. It is, however, difficult for in-core flow-meters and/or thermocouples to detect the local blockage until the blocked area exceeds about half of the total flow area (1). The consequence of cooling disturbance due to local blockage within a fuel subassembly is an increase in the temperature of sodium, cladding and fuel. Experimental and analytical studies recently reported by Yamaguchi et al.(2), Huber and Peppler(3) and Ishimaru et al.(4) have indicated that a wide flow area blockage or power-to-flow mismatch is needed to the occurrence of boiling, but increase in the cladding temperature above the normal operation temperature will lead to a reduction in its mechanical strength. The fission gas pressure, increasing with the fuel pin burn up, may reach a sufficiently high value at the end of life of the equilibrium core to result in cladding rupture in the blockage affected region. The fission gas release due to the cladding rupture will further disturb the coolability in the neighborhood of the ruptured pin and lead to potential pin-to-pin failure propagation.

Since most of the experimental studies on fission gas release, reported by Haga et al.(5), Bell et al.(6), Wilson et al.(7) and Van Erp et al.(8), have been conducted without the blockage, they would not be adequate for an evaluation of fission gas release, as a consequence of the local blockage within fuel subassemblies.

This paper describes fuel pin cooling performance under fission gas release caused by the local blockage

within fuel subassemblies in LMFBRs. The objectives of the present experimental study are to determine the temperature rise due to fission gas release in the blockage wake region and to evaluate the potential for pin-to-pin failure propagation under reactor conditions.

EXPERIMENTAL EQUIPMENT AND PROCEDURES

Test Section

A series of out-of-pile experiments were carried out in SIENA (Sodium Installation for Experiment on Nuclear Reactor Safety Analysis) loop at O-arai Engineering Center of PNC.

A test assembly layout view is shown in Fig. 1. The simulated fuel pins 6.5 mm in diameter are wound with wire-spacers 1.3 mm in diameter and contained within a hexagonal can which has a 50.4 mm flat to flat dimension. This subassembly designated 37D T.S., consisted of 37 pins, 18 of which were electrically heated. The heated length and maximum heat flux capability at the surface was 455 mm and 200W/cm^2, respectively. The local blockage model, made of stainless steel without permeability, was located 300 mm downstream from the lower end of the heated section and blocked central 24 subchannels (26 % of total flow area). The gas injector pin was mounted at the center of the pin bundle. As was noted earlier, pin failure would be likely to occur in the blockage wake region. Gas injector pin is, therefore, located 12 mm downstream from the blockage. There are various manners of pin failure or rupture (e.g., pin hole or crack, single or mutiple failure). In these experiments, pin failure was simulated by a small nozzle such a pin hole. As a single nozzle pin, three kinds of gas injector pins were used whose nozzle diameter were 0.3 mm, 0.5 mm and 0.8 mm, respectively. In addition to them, a multi-nozzle pin (12 holes at equal circumferential distances), whose individual nozzle diameters were 0.3 mm, was also used.

The gas injector pin and its gas supply system are shown in Fig. 2. The gas injector pin has 6.5 mm outside diameter, the same diameter as other simulated fuel pins, and 3.5 mm inside diameter, which contains a rod 3.0 mm in diameter. This rod is designed to break the rupture disc and cause gas release into flowing sodium. Argon gas was used, as the simulated fission gas.

Pin surface temperature were measured with 0.3 mm diameter thermocouples which were embedded in the heated pin surface. Void fractions within pin bundles were measured with potential tap voidmeters, which were set on the hex can surface. The sodium flow rate through the test bundle was measured at both subassembly inlet and outlet. The released gas pressure was measured at the gas plenum in the gas injector pin. These output signals from the above sensors were recorded on a digital data acquisition system.

Test Procedures

Prior to the gas release experiments, the thermocouples were calibrated by flowing sodium through the test subassembly.

At first, transient gas release experiments were carried out. The transient gas release was initiated by breaking the rupture disc in the gas injector pin. After the transient gas release experiments were performed, V-601, the isolation valve between the gas injector pin and the gas heater, was opened to conduct the steady gas release experiments. Gas temperature before the onset of gas release was adjusted to about the same temperature as sodium at the gas injection

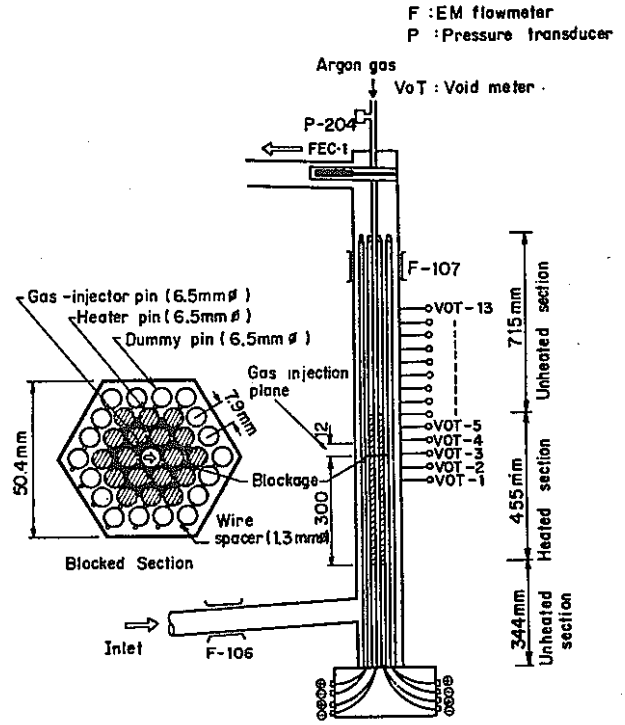

Fig. 1 37-pin bundle test section (37D T.S)

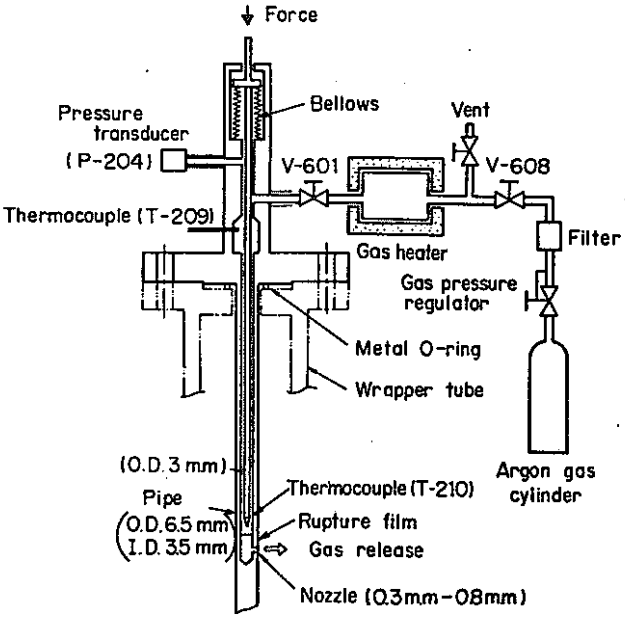

Fig. 2 Gas injector pin and gas supply system

nozzle location.

In the present experiments, heat flux at the pin surface was controlled to prevent it exceeding about 30W/cm^2 to avoid sodium boiling and pin deformation. As shown in Fig. 3 the proportional correlation between

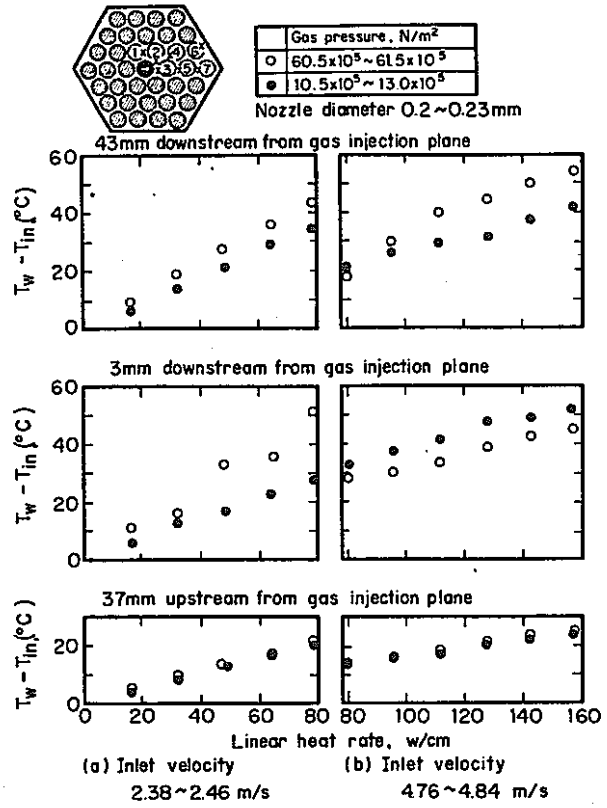

Fig. 3. Effect of linear heat rate on wall temperature rise for steady gas release tests (9)

temperature rise due to gas release and heat flux has been confirmed in the previous experiments (9). Though these results in Fig. 3 was obtained without blockage, the proportional correlation can be applied to a series of the present results. Thus, the present results which were obtained under low-heat flux condition is extrapolated to reactor condition (i.e., high heat flux condition) on the assumption that the proportional correlation is kept.

A summary of test conditions is presented in Table 1.

RESULTS AND DISCUSSION

Temperature Distribution behind the Blockage

A typical temperature profile behind the blockage is shown in Fig. 4, when gas was released into the blockage wake region under steady state. The temperature rise behind the blockage increases significantly, compared with single phase flow (i.e., no gas release). The experimental result with normal bundle (i.e., without blockage) reported by Haga et al.(5) has pointed to the fact that, except for the gas impinging surface, no significant temperature rise was measured. In the present result, however, significant temperature rise appears not only at the gas impinging surface but also in most of the wake region. In the wake region, the temperature rise due to gas release is about one order of magnitude higher, than that for the gas impinging surface in a normal bundle (5). In flow visualization experiments using the same geometrical 37-pin bundle, Nakamura et al.(10) observed that released gas stays a long time in the

Table 1 A summary of test conditions

Item	Steady gas release	Transient gas release
Gas plenum pressure Pg, MPa	0.294 ~ 5.88	2.94 ~ 7.84
Gas release rate Gg, g/s	0.05 ~ 3.46	——
Gas plenum volume V, cm³	——	70
Gas temperature in gas plenum, Tg, °C	245 ~ 350	245 ~ 316
Sodium velocity in normal bundle, Uo, m/s	0.4 ~ 4.56	3.5 ~ 3.7
Inlet sodium temperature Tin, °C	233 ~ 305	247 ~ 275
Heat flux at heated pin surface q, W/cm²	4.8 ~ 30.8	29.4 ~ 30.8

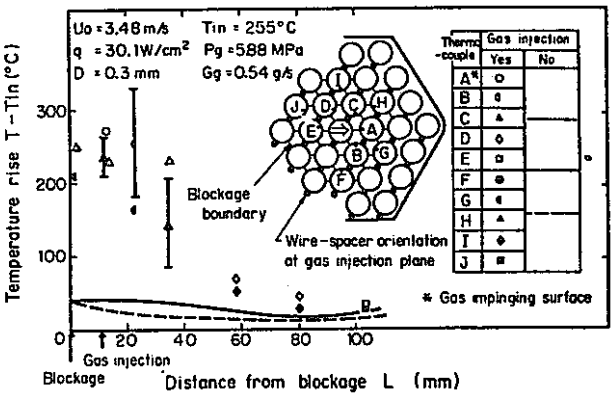

Fig. 4 Axial temperature profile behind blockage; Run GWL-2608

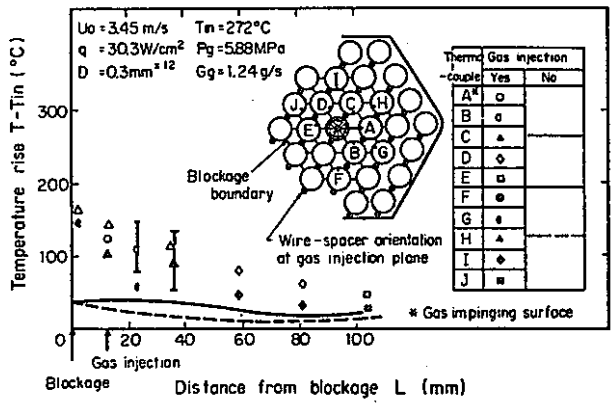

Fig. 5 Axial temperature profile behind blockage; Run GWL-6608

wake region and that the gas blanket area is wide, compared with gas release in the normal bundle. Further, Fukuzawa (11) comfirmed that released gas is concentrated in the blockage wake region and forms a gas accumulation region under certain coolant velocity and gas release rates. Thus, the high temperature rises, which were measured behind the blockage, indicate the formation of gas accumulation.

Figure 5 shows the result when gas was released through the multi-nozzle gas injector pin. The cooling disturbance due to gas release is not as bad as the results of single nozzle release (as shown in

Fig. 4). However, at a point more than 60 mm downstream from the blockage, the multi-nozzle gas release temperature rise is a bit higher than that of single nozzle gas release. The results, from a comparision between both figures, indicate that released gas distribution behind the blockage depends on the gas release direction.

Effects of Gas Injection Nozzle Diameter and Gas Plenum Pressure

Figure 6 shows the correlation between gas plenum pressure and temperature rise behind the blockage. Although all these data show no significant temperature rise at a point 100.3 mm downstream from the blockage, the temperature rise at points 12 mm and 22 mm downstream from the blockage increase with the gas plenum pressure. Temperature rises reached peak values at P_g=1.0MPa, when gas was released through the 0.5 mm and 0.8 mm diameter nozzle, while the temperature rise simply increased with the gas plenum pressure when gas was released through the 0.3 mm diameter nozzle. There was no significant difference between temperature rises measured 12 mm (gas impinging surface) and 22 mm downstream from the blockage. These data indicate that the temperature rise behind the blockage is characterized by the gas accumulation region.

From the above data, where released gas is concentrated behind the blockage, it should be considered that the temperature rise is governed by the gas release rate rather than by the nozzle diameter or the gas plenum pressure.

Coolant Velocity Effects

The normalized temperature rise, defined by Eq. (1), was introduced to evaluate cooling efficiency which was obtained under various experimental conditions.

$$\Xi = \frac{C_p \cdot \rho \cdot U_b \cdot (T - T_{in})}{\phi} = \frac{C_p \cdot \rho \cdot U_b \cdot (T - T_{in}) \cdot D_h}{4q} \qquad (1)$$

The physical meaning of the normalized temperature rise is represented by the equivalent axial distance which is required for the sodium to attain the same temperature rise when sodium flows in the normal bundle without gas release.

Figure 7 shows the normalized temperature rise at a point 22 mm downstream from the blockage as a function of coolant velocity at a blocked section. As can be seen in the figure, there are no significant differences in the normalized temperature rise between single phase flow (i.e., without gas release) and two phase flow (i.e., with gas release), when coolant velocity is less than 2 m/s. These data indicate that released gas flows away immediately due to buoyancy force at U_B < 2 m/s, since the recirculating flow within the wake region is very low or almost stagnant (12). Furthermore, agitation effect by injecting gas into sodium compensates for the deficiency in effective sodium thermal conductivity due to entrained gas.

As the recirculating velocity within the wake is proportional to the velocity at the blocked section (13), released gas is concentrated by the recirculating flow and forms the gas accumulation region at U_B > 2 m/s. Consequently, cooling efficiency decreases and significant temperature rise appears within the wake region. These data, presented in Fig. 7, show the lower limit of coolant velocity (2 m/s) for the gas accumulation.

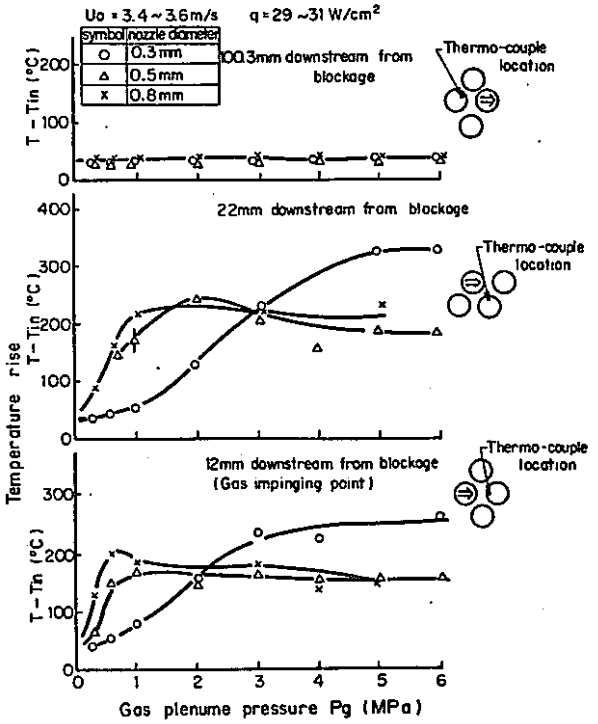

Fig. 6 Temperature rise behind blockage as a function of gas plenum pressure

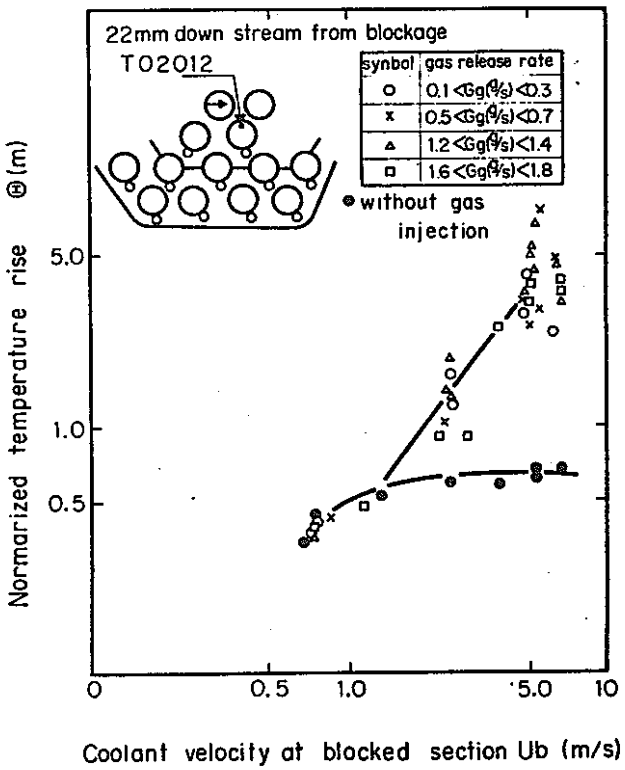

Fig. 7 Coolant velocity effect on the temperature rise due to gas release

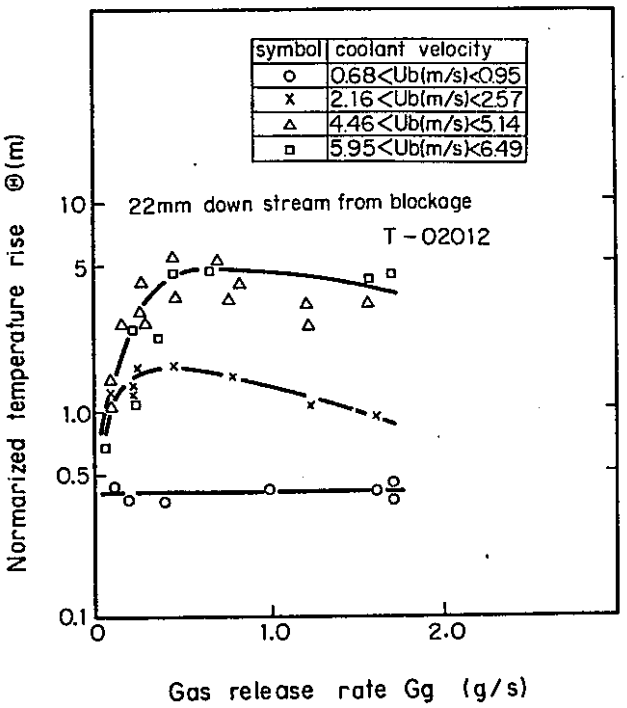

Fig. 8 Gas release rate effect on temperature rise in wake region.

Figure 8 presents a correlation between gas release rate and normalized temperature rise at a point 22 mm downstream from the blockage. The normalized temperature rise increases greatly with increasing gas release rate for $G_g < 0.6$ g/s (1 g/s = 556.8 Ncm^3/s), while for $G_g > 0.6$ g/s, the normalized temperature rise slightly decrease with increasing gas release rate. Three reasons for the reduction in temperature rise at $G_g > 0.6$ g/s can be considered: (a) There are upper limits to the gas inventory or void fraction within the wake region. (b) Gas jet reaches out of the blocked section and most of the gas flows away without re-entry to the wake. (c) Recirculation flow disappears since a large amount of gas is supplied to the wake region.

Transient Gas Release

As presented in Table 2, seven transient gas release experiments were carried out. In the present paper, two typical results are described.

A typical relationship is that in Fig. 9 where gas plenum pressure, temperature rise, void fraction and sodium velocity are shown versus transient time. Experimental conditions are presented in the figure. The gas plenum pressure decreases to 3.0 MPa at 6.5 seconds and 0.60 MPa at 21.5 seconds after the onset of gas release. In the transient gas release experiments, it is difficult to measure precise gas release rate by gas-flow-meter. The released gas flow rate, G_g, was, therefore, estimated from the following critical flow equation:

$$G_g(\tau) = \frac{\pi D^2}{4}\sqrt{\kappa\left(\frac{m-1}{\kappa-1}\right)\left(\frac{2}{m+1}\right)^{\frac{m+1}{m-1}} P_g(\tau)\rho_g} \quad . \quad (2)$$

where m, the gas release exponent, equals κ, the ratio of specific heat capacity when gas is released under isentropic flow. Generally, gas release exponent m does not equal κ, since gas flow through the nozzle

Table 2 A summary of transient gas release experiments

	GWL-1	GWL-2	GWL-3	GWL-4	GWL-5	GWL-6	GWL-7
Nozzle diameter D, mm	0.5	0.3	0.5	0.8	0.5	0.3	0.5
Number of nozzles	1	1	1	1	1	12	1
Gas plenum pressure P_g, MPa	5.39	6.17	2.94	5.88	5.88	5.88	7.84
Initial gas release rate G_g, g/s	1.6	0.373	0.69	2.65	1.23	1.06	1.38
Heat flux q, W/cm²	29.4	30.3	30.8	28.8	29.8	30.3	29.8
Sodium inlet velocity U_0, m/s	3.5	3.7	3.7	3.5	3.7	3.5	3.6

*1 Gas was released into pin gap (e.g., ○○ ⊙⊙ gas release direction)

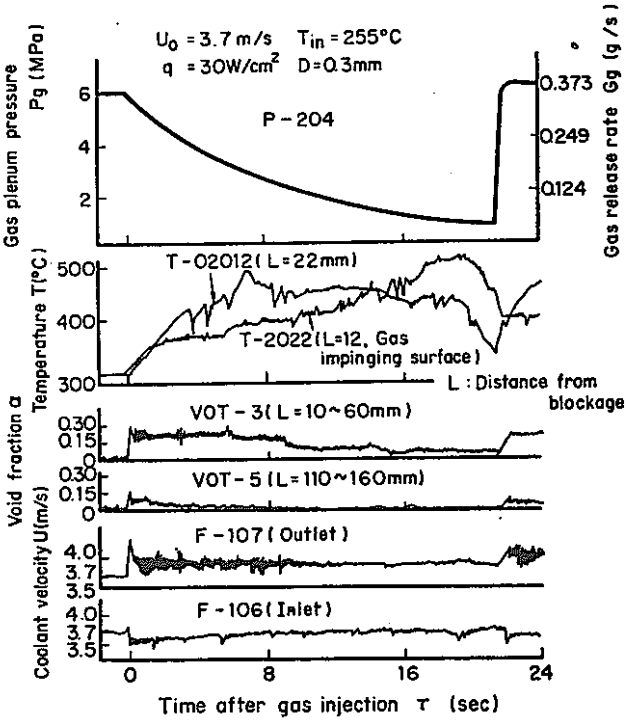

Fig. 9 Dynamic behavior for gas pressure, temperature, void fraction and coolant velocity; Run GWL-2.

is an irreversible flow, because of friction loss and turbulence. Thus, the actual gas release rate (i.e., irreversible flow) will be low, compared with that under idealized isentropic flow. In the present gas release experiments, the gas release exponent m of 1.10 was determined experimentally. Detailed information on the m value is described in reference (14). Once the value m is fixed, the applicability range of Eq. (2) is determined by the following equation:

$$\delta\, P_g(\tau) > P_a \ , \ \delta = \left(\frac{2}{m+1}\right)^{\frac{m}{m-1}} \quad (3)$$

Since the sodium pressure Pa is maintained around 0.13 MPa, the gas flows through the nozzle at critical velocity until the gas plenum pressure decreases less than 0.22 MPa. Therefore, in the transient gas re-

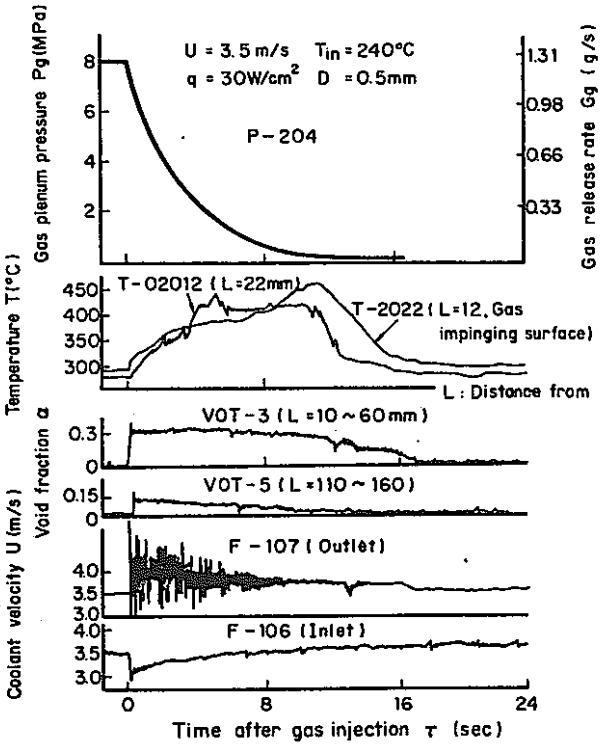

Fig. 10 Dynamic behavior for gas pressure, temperature, void fraction and coolant velocity; Run GWL-7.

lease experiments, most of the gas is released under critical flow condition.

Following the gas release, the temperature (T-2022) at the gas impinging surface initially increases rapidly at a rate of 44°C/s and then gradually increases at 7.5°C/s. The initial rate of temperature increase (44°C/s) is about the same magnitude as that under adiabatic condition (55°C/s). Since the spray cooling effect becomes more dominant at the gas impinging surface one second after gas release, the rate of temperature increase becomes flatter (7.5°C/s). The temperature (T-02012) at a point 22 mm downstream from the blockage increases at a rate of 35°C/s for 3.5 seconds and is higher than that at the gas impinging surface for 14 seconds after gas release.

Following the gas release, void tap VOT-3 indicates that, for 8 seconds after the onset of gas release, void fraction behind blockage remains constant (0.3) with decreasing gas plenum pressure, while the void tap VOT-5 indicates that void fraction simply decreases after an initial jump (0.15). These void fraction data show that released gas is accumulated in the wake region and that there is an upper limit of void fraction behind the blockage.

Figure 10 also shows the results of transient gas release experiment (GWL-7). In this case, initial pressure for the gas plenum is higher and the nozzle diameter is larger, than those in GWL-2 (Fig. 9). The gas release time is reduced and temperature rise is slightly lower than that of GWL-2. It is, therefore, concluded that a small cladding rupture can lead to a more severe condition with regard to fuel pin coolability than a large rupture.

Extrapolation to Reactor Condition

In order to evaluate the coolability in the MONJU fuel subassembly under the fission gas release associated with the local blockage, the normalized temperature rise data shown in Fig. 8 were extrapolated with the following equation:

$$T - Tin = \Xi \left(\frac{4q}{Dh \cdot Cp \cdot \rho \cdot Ut}\right)_{MONJU} \qquad (4)$$

where the blockage was assumed as the same one with the present 24-subchannel blockage (i.e., 6% central-type blockage of 169-pin bundle). In the extrapolation with Eq. (4), the proportional correlation between temperature rise due to gas release and heat flux is assumed. The other conditions which are necessary for the calculation are almost equivalent to that of the present experiments (see Table 3). Figure 11 shows the calculated results. Fission gas release at $Gg > 0.12$ g/s will raise the inside-wake coolant temperature up to saturation to cause local boiling.

There is no useful information to evaluate boiling behavior, when non-condensible gas such as fission gas is entrained in sodium, although single phase heat transfer is reduced by entrained non-condensible gas in sodium (15),(16). Thus, it is predicted that gas release associated with local blockage has a potential for dryout which leads to pin-to-pin failure propagation. However, as was noted earlier, the significant temperature rise which cause dryout is restricted to within the gas accumulation region. The temperature, out of gas accumulation region, would be the same magnitude as that of normal bundle gas release results (5). Hence, pin-to-pin failure propagation would be limited to the blockage affected region, even if local dryout is caused in the gas accumulation region.

The results from above discussion also indicate that consequence of pin-to-pin failure propagation depends on a blockage size. But in-core instruments, such as thermocouples and/or flow-meters would detect the anormal event due to local blockage, when the blockage area exceeds more than about half of total flow area (1). Therefore, as a consequence of fission gas release into the blockage wake region, no significant failure propagation which leads to subassembly-to-subassembly failure propagation would occur.

Table 3 Reactor conditions

Number of fuel pins	169
Hydraulic diameter in subchannel Dh, mm	4.1
Blocked subchannels	Central 24
Ratio of blocked area η, %	6 %
Heat flux at pin surface Q, W/cm	200
Coolant velocity at blocked section Ub, m/s	6.38
Coolant velocity at normal bundle Uo, m/s	6.0

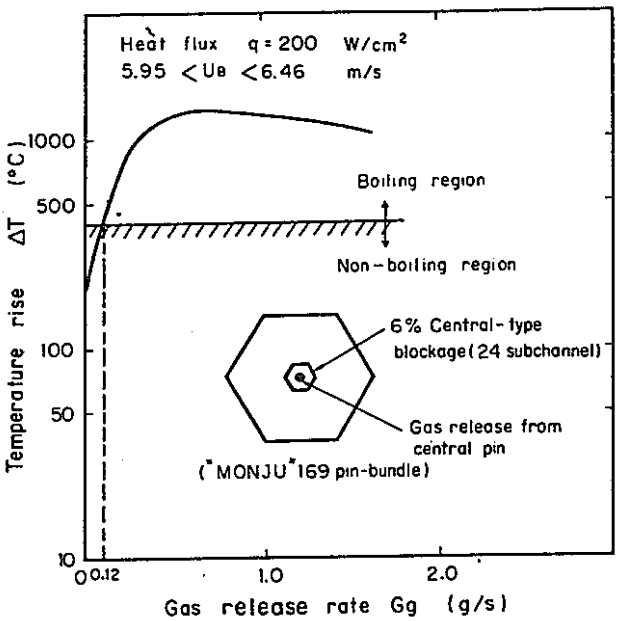

Fig. 11 Calculated temperature rise due to FP gas release into central blockage wake region under reactor conditions.

CONCLUSION

Based on the results of the present experiments, the following conclusions were obtained.

(1) Released gas is concentrated in a blockage wake region and results in gas accumulation region at Ub > 2m/s. In the gas accumulation region, temperature rise increases significantly. The low coolant flow condition of Ub < 2m/s, on the contrary, cause no additional cooling disturbance in the wake region, since released gas flows away immediately due to buoyancy force.

(2) The differences in temperature profile between single nozzle and muti-nozzle gas release indicate that the structure of the thermohydraulic field behind blockage may be affected by the gas release manner or the gas release direction.

(3) The temperature rise in the wake region increases rapidly with gas release rate at Gg < 0.6 g/s, while Gg > 0.6g/s, temperature rise decreases slightly with increasing gas release rate. These results indicate that there are upper limits to the gas invetory within the wake region.

(4) A small cladding rupture leads to a more severe condition with regard to fuel pin coolability than a large rupture, because of longer duration of gas release.

(5) Though the results of extrapolation to reactor conditions indicate that the inside-wake coolant temperature exceed its saturation temperature under reactor contions, out of wake region temperature would not increase significantly. Therefore, as a consequence of fission gas release into the blockage wake region, no significant failure propagation which leads to subassembly-to-subassembly failure propagation would occur.

The data obtained from these experiments are being used in computer model development for analytical studies on fission gas release events (17). The results of analytical predictions will be presented in a forthcoming paper.

ACKNOWLEDGEMENT

Those experiments could not have been successfully conducted without the support of many cooperators. The authors would like to especially thank Dr. Mochizuki, Dr.Ohtsubo and Mr. Hori for their sponsorship, and Dr. Kamei, Mr. Tamaoki and Mr. Mawatari for their kind encouragement, and Mr. Isozaki, Mr. Komaba, Mr. Sahashi and Mr. Uotani for their technical and engineering contribution.

REFERENCES

1 Nakamura, H., Miyaguchi, K. and Takahashi, J. "Hydraulic Simulation of Local Blockage in an LMFBR Fuel Subassembly-1," 1976 Fall Meeting of the Atomic Energy Society of Japan Oct. 1976, p.124.

2 Yamaguchi, K., et al., "Experimental Investigation of Local Cooling Disturbances in LMFBR Fuel subassemblies," to be presented at Heat Transfer Aspects of Reactor Safety Session of 1981 ASME Winter Annual Meeting, Nov. 1981.

3 Hubber, H. and Peppler, W., "Form and Development of Boiling behind a 49 % Central Blockage in 169 pin Bundle," 7th Liquid Metal Boiling Working Group Meeting, Jun., 1977.

4 Ishimaru, J., Yoshikawa, H. and Hori, M., "A Verification Study of ASFRE Code Through Experimental Analyses to Local Flow Blockage Tests," 9th Liquid Metal Boiling Working Group Meeting, Jun. 1980, pp.588-638.

5 Haga, K., et al., "Fission Gas Release Experiment in a Simulated LMFBR Subassembly," Trans. Am. Nucl. Soc., Vol.34, 1980, pp.494-495.

6 Bell, R., Boyce, B.E and Collier, J.G., "The Structure of a Submerged Impinging Gas Jet," Journal of British Nuclear Energy Society, Vol.77(2), 1972, pp.183-193.

7 Wilson, R.E., et al., "Experimental Evaluation of Fission Gas Release in LMFBR Subassemblies Using Electrically Heated Test Section with Sodium as Coolant," ANL-8036, 1973.

8 Van Erp, J.B., Chawla, T.C. and Fauske, H.K., "An Evaluation of Pin to Pin Failure Propagation due to Fission Gass Release in Fuel Subassemblies of Liquid-Metal-Cooled Fast Breeder Reactor" Nuclear Engineering and Design, Vol.31, Nov., 1974, pp.128-150.

9 Haga, K., et al., "Preliminary Results of Gas Injection into Sodium Flowing in a 37-pin Bundle," PNC-N-943-75-04 Sept., 1975.

10 Nakamura, H., et al., "Hydraulic Simulation of Local Blockage in an LMFBR Subassembly-3," 1980 Annual Meeting of the Atomic Energy Society of Japan, Mar., 1980, p.25.

11 Fukuzawa, Y., "Observations of the Behaviour of Gas in the Wake Behind a Corner Blockage in Fast Breeder Reactor Subassembly Geometry," KfK-2820, July, 1979.

12 Namekawa, F., Hashizume, K. and Mawatari, K., "Local Blockage Experiments in an LMFBR Fuel Subassembly-1," 1977 Fall Meeting of the Atomic Energy Society of Japan, Oct., 1977, p.37.

13 Nakamura, H., Miyaguchi and Takahashi., "Hydraulic Simulation of Local Blockage in an LMFBR Fuel Subassembly," Nuclear Engineering and Design, Vol.62 (1980) Nos. 1-3, Dec., 1980, pp.323-333.

14 Namekawa, F., et al., "Transient Fission Gas Release Experiments in LMFBRs' Subassemblies," to be presented 1981 Fall Meeting of the Atomic Energy Society of Japan, Oct., 1981.

15 Bishop, A.A, Engel and Markley, R.A., "Heat Transfer Effect on Entrained Gas in Liquid Sodium System" Nuclear Engineering and Design, Vol.52 (1979)

pp.1-13.
16 Hori, M. and Friedland, A.J., "Effect of Gas Entraiment on Thermal-hydraulic Performance of Sodium Reactor Core," Journal of Nuclear Science and Technology, Vol.7, May, 1970, pp.256-263.
17 Hirata, N., et al., "Recent Developments in ASFRE and TOPFRES," 9th Liquid Metal Boiling Working Group Meeting, June, 1980, pp.571-577.

APPENDIX: SCOPE OF PRESENTATION

1981 ASME WINTER ANNUAL MEETING

Out-of-pile Experiments for Fission Gas Release in LMFBR Fuel Subassemblies

----- Gas Release into Blockage in a Simulated LMFBR Fuel Bundle

F. Namekawa, K. Yamaguchi and K. Haga

Power Reactor and Nuclear Fuel Development Corporation
O-arai, Japan

INTRODUCTION

Thank you chairman.

In the LMFBR Safety design, it's very important to develop a detailed understanding of the accident progression due to local faults. It's generally believed that local blockage in a pin bundle is one of the most likely initiators of local faults, since pins are closely arrayed in the subassembly. The consequence of cooling disturbance due to local blockage within a fuel subassembly is an increase in the temperature of sodium, cladding and fuel. It's expected that the cooling disturbance might cause cladding rupture.

Thus, we carried out experimental studies to determine fuel pin cooling capability under fission gas release, as a consequence of pin failure caused by a local blockage.

Now, I'd like to present our experimental study.

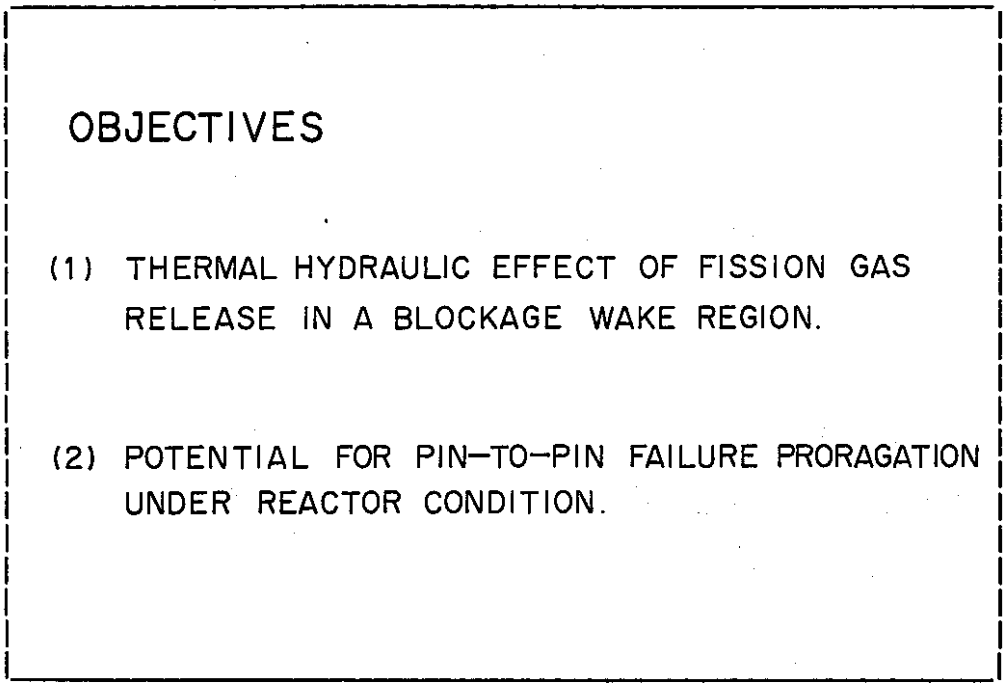

OBJECTIVES ..... (First slide, please. SLIDE No. 1)

There are two objectives for the present fission gas release experiments. As shown in this slide, the first objective is to clarify thermal hydraulic effect of fission gas release in a blockage wake region, in particular, to determine fuel pin cooling capability under fission gas release.

The second objective is to evaluate potential for pin-to-pin failure propagation under reactor conditions.

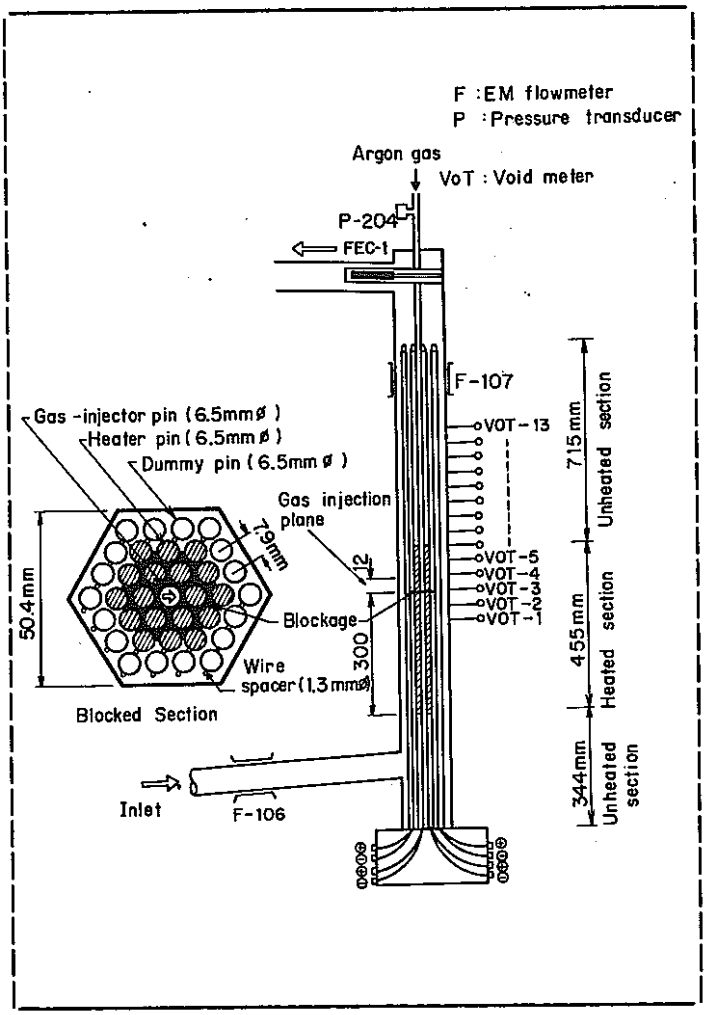

TEST SECTION ..... (Next slide please. SLIDE No. 2 i.e. Fig. 1)

This is a layout view of the test assembly that was used in the experiments.

A 37-pin bundle with wire spacers was installed in a hexagonal can. In this pin bundle, except for gas injector pin, 18 central pins (red colored) are electrically heated. A local blockage simulator (blue colored) which blocks the 24 central subchannels, is made of stainless steel which is impermeable and not heated. Blockage location is 300mm downstream from the start point of heated region.

The gas injector pin is installed at the center of the pin bundle. A gas injection nozzle is located at a point 12mm above the blockage model.

For temperature measurement in the pin bundle, thermocouples are embedded in the heated pin surface. On the other hand, void fractions were measured by using potential tap-type void meters, which are set on the hex-can surface.

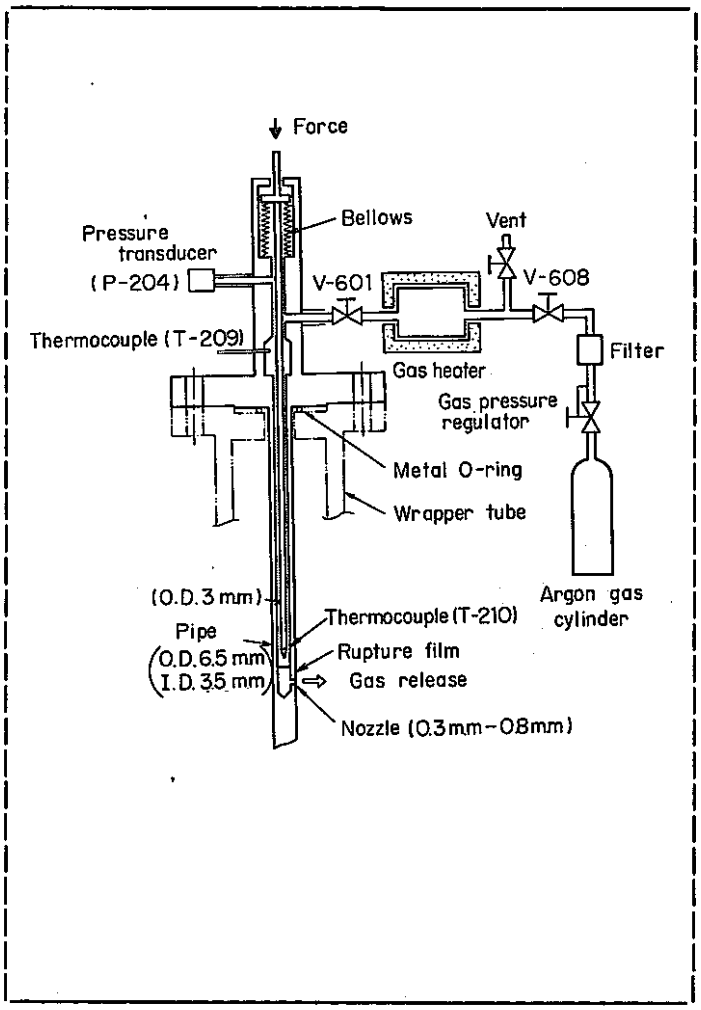

GAS INJECTOR PIN AND GAS SUPPLY SYSTEM ..... (Next slide please. SLIDE No. 3, i.e. Fig. 2)

This slide shows the gas injector pin and gas supply system. Argon was used, as simulated fission gas.

The gas injector pin has a 6.5mm outside diameter, the same diameter as other simulated fuel pins, and 3.5mm inside diameter. There is a rod in the gas injector pin. This rod is designed to break the rupture disc to cause transient gas release. In the transient gas release experiments, the isolation valve, V-601, was closed.

Following a transient gas release experiment, steady gas release experiments were carried out. In the steady gas release experiments, isolation valve, V-601 was opened, and then, gas was continuously supplied through the gas heater.

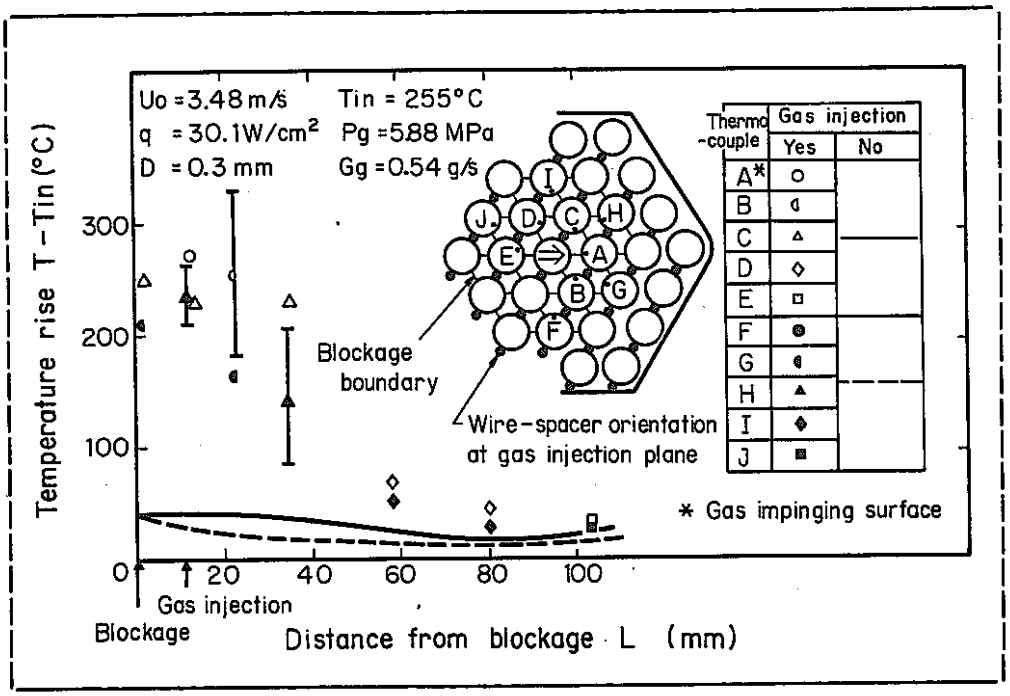

AXIAL TEMPERATURE PROFILE ..... (Next slide please. SLIDE No. 4, i.e. Fig. 4)

Now, I'll show you the results of the experiments. This first one is an axial temperature profile behind blockage under steady gas release experiments. Test conditions are shown in this figure.

Data on temperature rise without gas release are also shown with both solid and dashed lines. As shown in this figure, the temperature rise due to gas release increases extremely compared with that of no gas release. However, in the neighborhood of 80mm downstream from blockage, temperature rise decreases, the same as that of no gas release.

In the previous gas release experiments without local blockage, high temperature rise was not measured, except for the gas impinging surface. However, in the present experiment with local blockage, as shown in the figure, high temperature rise appears not only at the gas impinging surface, but also in most of the wake region.

The reasons for the significant temperature rise behind the blockage are explained by a gas accumulation region being formed behind the blockage.

Normalized Temperature Ⓗ

$$Ⓗ = \frac{Cp \cdot \rho \cdot Ub\ (T - Tin)}{\phi}$$

$$= \frac{Cp \cdot \rho \cdot Ub \cdot (T - Tin) \cdot Dh}{4q}$$

DEFINITION OF NORMALIZED TEMPERATURE RISE ..... (Next slide, please.

SLIDE No. 5)

The normalized temperature rise, as defined here, was introduced to evaluate cooling efficiency which was obtained under various experimental conditions.

The physical meaning of the normalized temperature rise is represented by the equivalent axial distance, which is required for the sodium to attain the same temperature rise when sodium flows in the normal bundle without gas release.

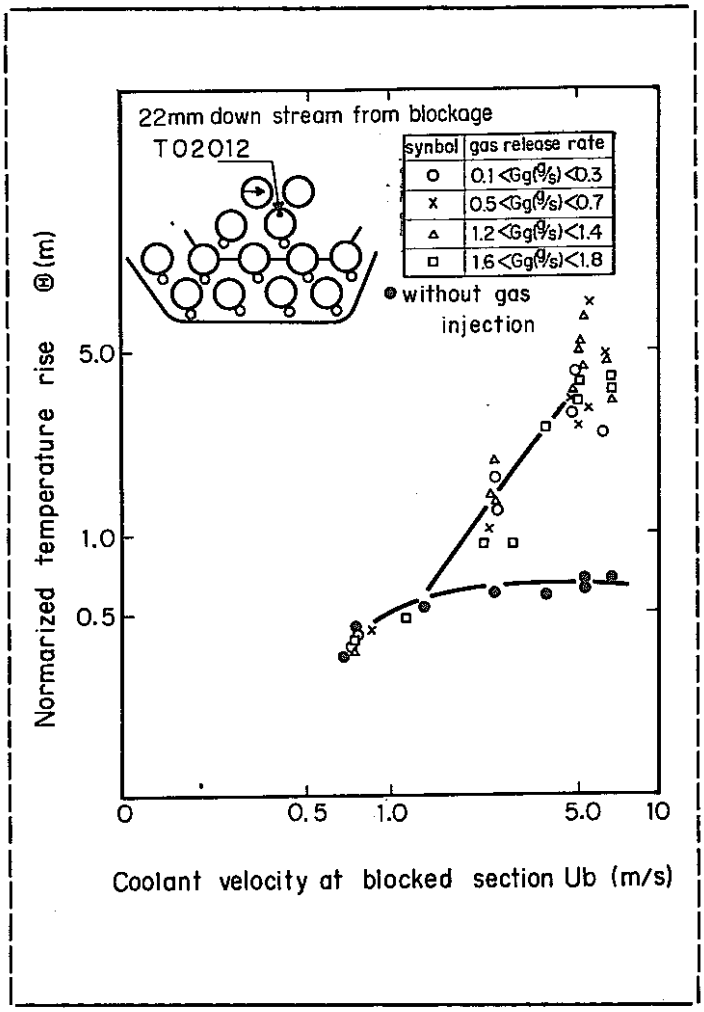

COOLANT VELOCITY EFFECT ..... (Next slide, please. SLIDE No. 6, i.e. Fig. 7)

This figure shows the normalized temperature rise at a point 22mm downstream from the blockage as a function of coolant velocity at a blocked section.

In this figure, black dots indicate no gas release condition. As can be seen in the slide, there are no gas release effects on the normalized temperature rise, when coolant velocity is less than about 2m/s. These data indicate that released gas flows away immediately due to buoyancy force, because the reversal flow within the wake region is very low or almost stagnant.

On the other hand, when coolant velocity is greater than 2m/s, the normalized temperature rise increases extremely with coolant vcelocity. The reason is that the reversal flow increases with the coolant velocity at blocked section. Consequently, released gas is concentrated and forms a gas accumulation region behind the blockage.

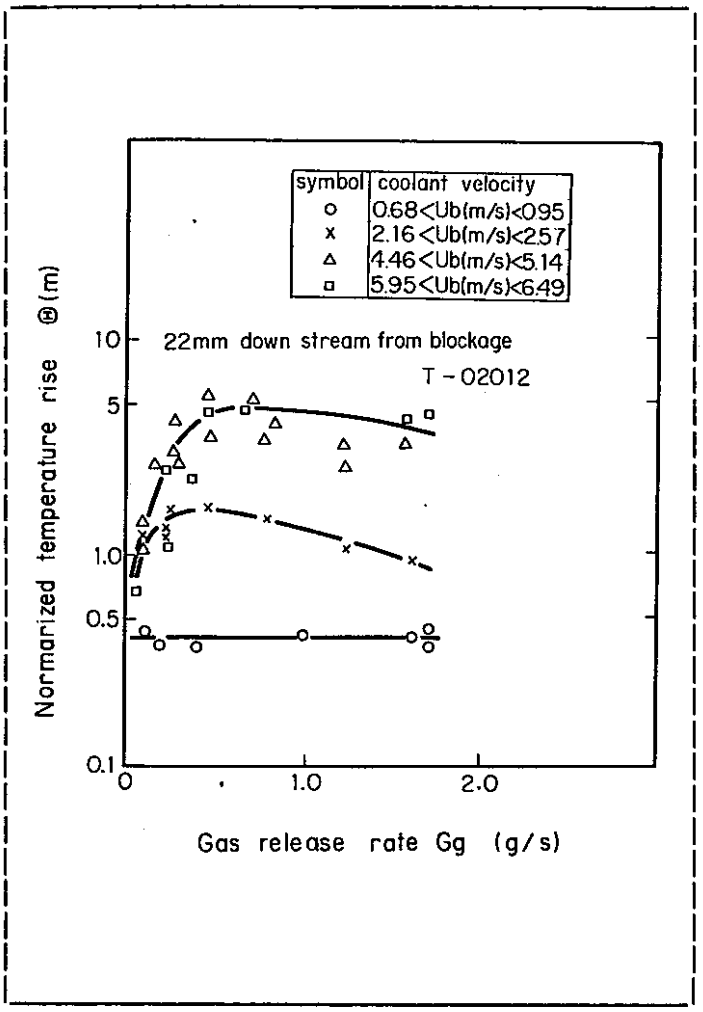

EFFECT OF GAS RELEASE RATE ..... (Next slide, please. SLIDE No. 7, i.e. Fig. 8)

This slide shows a correlation between gas release rate and normalized temperature rise at a point 22 mm downstream from the blockage. As shown in the figure, the normalized temperature rise increases greatly with increasing gas release rate when gas release rate is less than 0.6g/s, however, when gas release rate is greater than about 0.6g/s, the normalized temperature rise slightly decreases with increasing gas release rate.

Then, why does the temperature rise decrease with increasing gas release rate? There are three reasons we can consider. First, there are upper limits to the gas inventory or void fraction within the wake. Second, gas jet reaches outside the blocked section and some of the gas flows away without re-entry to the wake. Third, recirculating flow disappears, since a large amount of gas is supplied to the wake region.

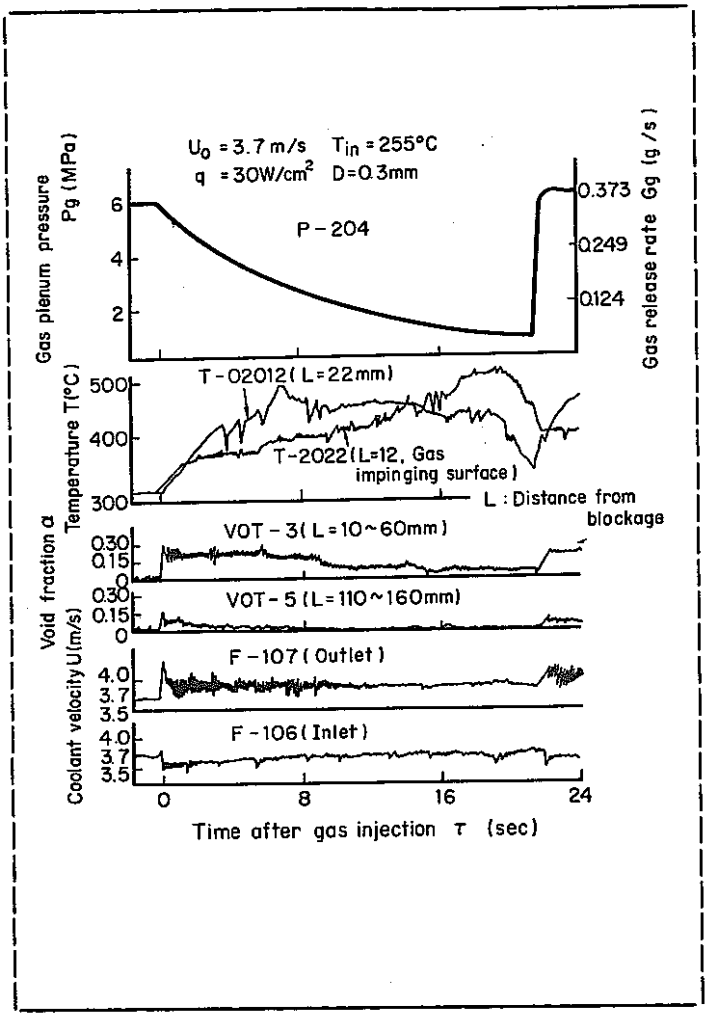

TRANSIENT TEST ..... (Next slide, please. SLIDE No. 8, i.e. Fig. 9)

I have presented the steady gas release experiment results, so far. Now, let me show you the results of transient gas release experiments. These data represent a typical relationship between gas plenum pressure, temperature, void fraction and coolant velocity, as a function of transient time.

As shown in the slide, following the inception of gas release, the temperature at the gas impinging surface, shown by the red colored line, increases at a rate of 44°C/s. The initial rate of temperature increase rate of 44°C/s is about the same magnitude as that under adiabatic conditions.

However, about one second after the gas release, the temperature increase rate gradually becomes flatter, because the spray cooling effect becomes more dominant at the gas impinging surface.

The temperature at a point 22mm downstream, shown by the blue colored line, increases at a rate of 35°C/s for 3.5 seconds. Then, it becomes higer than at the gas impinging surface 15 seconds after the gas release.

The peak values for both temperatures are about the same magnitude as that of the steady gas release under the same initial conditions. Therefore, the steady gas release results can be applied to an evaluation on the fuel pin cooling capability, as a conservative estimation.

On the other hand, for void signal, as can be seen in these figures, at a point 10 to 50mm downstream from blockage, void fraction remains constant with decreasing gas plenum pressure for 8 seconds after gas release. However, at a point 110 to 160mm downstream, void fraction simply decreases after the initial jump. These void fraction data indicate that the released gas is accumulated in the wake region.

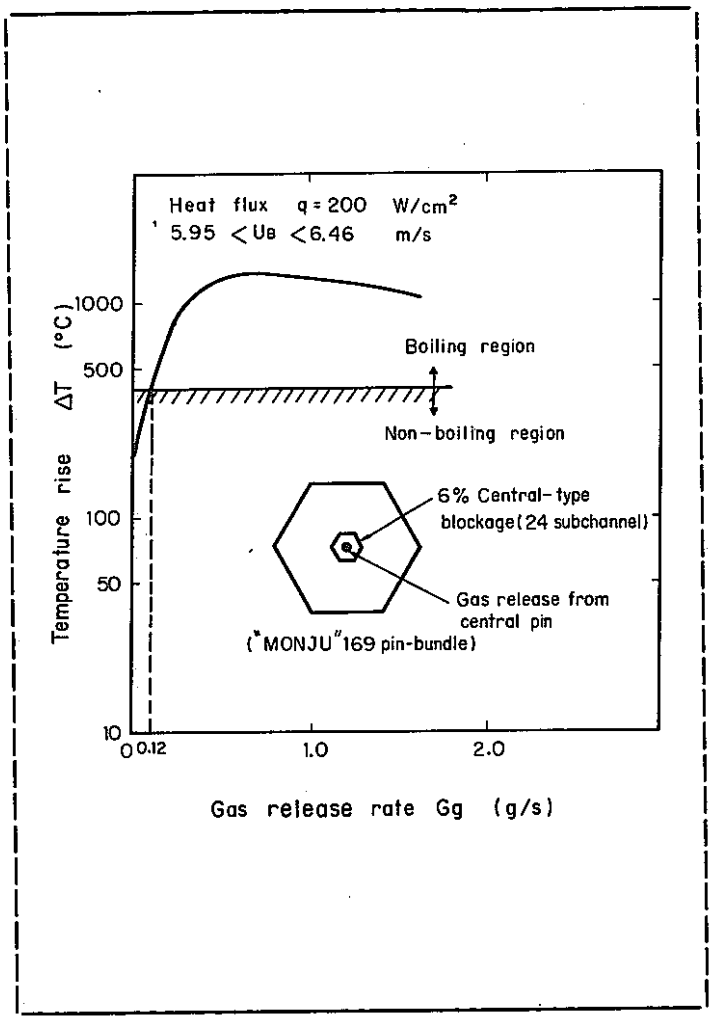

ESTIMATION OF REACTOR CONDITION ..... (Next slide, please. SLIDE No. 9, i.e. Fig. 11)

In order to evaluate the potential for pin-to-pin failure propagation, fuel pin cooling capability in the gas accumulation region were estimated under reactor conditions.

In the estimation, the blockage is assumed the same one as for the 24 subchannel blockage. There are 169 pins in the Monju fuel subassembly, therefore, 24 subchannel blockage equals a blocked ratio of 6% in the 169 pin bundle. In addition to this assumption, a proportional correlation between temperature rise due to gas release and heat flux is assumed. The other conditions which are necessary for the calculation are presented in our paper.

This slide shows the estimated results for temperature rise in the gas accumulation region under Monju operating condition. As shown here, when gas release rate is greater than 0.12g/s, fission gas release will raise the temperature in the gas accumulating region up to saturation to cause local boiling.

Therefore, it is predicted that gas release associated with the local blockage has a potential for dryout which may lead to pin-to-pin failure propagation. However, the temperature, outside the gas accumulation region, would be very low, of the same magnitude as that of normal bundle gas release. Thus, pin-to-pin failure propagation would be limited to the blockage affected region, even if dryout is caused in the gas accumulation region.

CONCLUSIONS

(1) ONLY AT GAS ACCUMULATION REGION IN THE WAKE OF BLOCKAGE, DID TEMPERATURE INCREASES SIGNIFICANTLY.

(2) FORMATION OF GAS ACCUMULATION IS DOMINATED BY COOLANT VELOCITY AND GAS RELEASE RATE.

(3) NO SIGNIFICANT PIN FAILURE PROPAGATION WOULD OCCUR UNDER REACTOR CONDITION, EVEN IF LOCAL DRYOUT OCCURED IN A GAS ACCUMULATION REGION.

CONCLUSIONS ..... (Next slide, please. SLIDE No. 10)

Based on the results of present experiments, the following conclusions are reached.

First, when coolant velocity is greater than 2m/s, released gas is accumulated in the blockage wake region.

Second, at the gas accumulation regions did temperature increase significantly, however, outside the wake region, there are no gas release effects on temperature field.

Third, beased on the extrapolated results to the reactor condition, no significant pin failure propagation would occur under Monju operating condition, even if local dryout occurred in the gas accumulation region due to fission gas release.

That's all, thank you for your attention.

3. 1981 ANS WINTER MEETING

4 Local Boiling Behind a Central Blockage in a Simulated LMFBR Fuel Bundle

M. Uotani, K. Yamaguchi and K. Haga

Edited by M. Uotani

This paper is compiled in the Transactions of ANS Volume 39, pp. 657-658.

6. Local Boiling Behind a Central Blockage in a Simulated LMFBR Fuel Bundle, *M. Uotani,* K. Yamaguchi, K. Haga (PNC-Japan)*

It is expected that local sodium boiling will occur when a large flow area is blocked in a liquid-metal fast breeder reactor (LMFBR) fuel bundle. For the safety evaluation of local faults, it is important to understand the margin of coolability of fuel pins under boiling conditions. To this end, an experimental study was carried out on local sodium boiling in a simulated fuel pin bundle.

The test bundle consisted of a central section with 19 electrically heated pins surrounded by 18 dummy pins. Simulating the prototype reactor MONJU's fuel bundle, the pin diameter and the pin pitch were 6.5 and 7.9 mm, respectively. The heated length was 450 mm with uniform heat flux. A 1.3-mm-diam spacer wire was wrapped around each pin, with a helical pitch of 265 mm. The central 24 flow subchannels were blocked by a 5-mm-thick stainless steel plate located 300 mm downstream from the start of the heated section. The fraction of flow area that was blocked was 26%.

The pin surface and sodium temperatures were measured by many Chromel-Alumel thermocouples. The inlet flow rate was measured by an electromagnetic flowmeter. In the present experiment, the inlet temperature and flow rate were held constant, and the heat flux was increased step by step. The system pressure at the heated section was 0.13 MPa.

Figure 1 shows the isotherms of sodium and boiling boundaries during a local boiling test, Run 37 WLB-114, where the inlet sodium flow velocity was 1.70 m/s and the inlet temperature was 734 K. In this run, six steady-state boiling steps were performed under different heat flux conditions. At the pin surface heat flux of 127 W/cm^2 (time t = 0), the maximum temperature within the wake region reached the saturation level of 1200 K. No incipient boiling superheat was measured in this case. After the first step of heat input increase (t = 16 s, 135 W/cm^2), the boiling mode changed to oscillatory, as has been observed in Refs. 1 and 2. The frequency was ~9 Hz. A small amount of vapor bubble always survived during the oscillations.

As the heat flux was increased up to 161 W/cm^2 (t = 76 s), the amplitude of oscillatory signals damped little by little. Figure 2 indicates that the gradual radial and axial growth of the high-temperature region reduced the temperature difference in the wake, and that the growth reduced the oscillation frequency. When the heat flux reached 167 W/cm^2 at 82 s, the oscillatory behavior disappeared; then the pin surface and sodium temperatures 22 mm downstream from the blockage showed steep increases due to the occurrence of

---

*Present Address: Central Research Institute of Electric Power Industry.

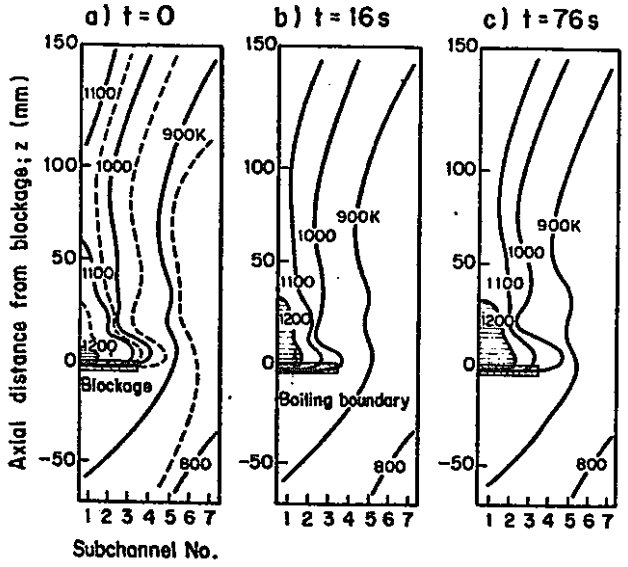

Fig. 1. Transition of isotherms and boiling boundary behind central blockage, run No. 37 WLB-114.

dryout. The abrupt growth of the voided region was observed, accompanied by cladding melting. The voided region, however, was limited locally, and flow reduction was hardly measured. The margin from boiling inception to dryout was 30% in terms of the power-to-flow ratio.

To evaluate the oscillatory frequency observed in the present test bundle, an analytical model has been developed. The bundle behavior was coupled with the displacement of a liquid column under the following assumptions:

1. The bubble is expressed by a single sphere.
2. In the bubble expansion process, vapor pressure is represented by the Gast[3] model. (A linear temperature profile is assumed here, whereas a parabolic one is used by Gast.)
3. In the bubble contraction phase, the vapor pressure is based on a polytropic change.

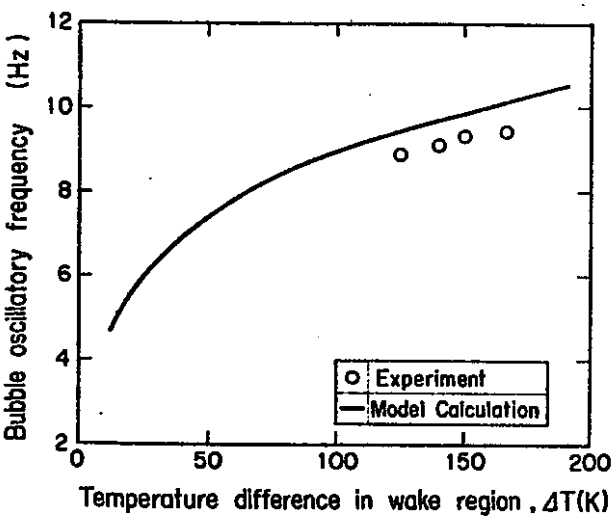

Fig. 2. Effect of temperature difference in wake region on bubble oscillatory frequency.

The mean bubble volume was estimated experimentally. The polytropic index was also fixed through the interpretation of measured data.

Fig. 2 shows the comparison of observed oscillatory frequencies with the model calculation. The horizontal axis is the temperature difference within the wake. The same tendency can be seen from the figure between the calculations and the experimental results, that is, the oscillatory frequency reduces in keeping with the decrease of temperature difference within the wake.

From the present experiment, it seems that the local boiling pattern transfers in the following manner with increasing value of power-to-flow ratio:

1. oscillatory boiling–coolability of fuel pins is maintained
2. boiling pattern changes from oscillatory to stationary
3. dryout occurs soon after the appearance of stationary boiling.

Further study is needed to clarify the conditions of the boiling pattern transition.

1. F. HUBER and W. PEPPLER, "Form and Development of Boiling Behind a 49% Central Blockage in a 169 Pin Bundle," presented at 7th Liquid Metal Boiling Working Group Mtg., Petten, Netherlands, June 1-3, 1977.
2. B. DORR and J. E. DEBRIES, "The ECN/KfK Local Boiling Experiments in Petten," presented at 8th Liquid Boiling Working Group Mtg., Mol, Belgium, October 11-13, 1978.
3. K. GAST, "Die Ansbreitung örtlicher Störungen im Kern Schneller Natriumgekuhlter Reacktoren und ihre Bedeutung für die Reaktorsicherheit," KFK-1380, Kernforschungszentrum Karlsruhe (1971).

APPENDIX: SCOPE OF PRESENTATION

1981 ANS Winter Meeting

November 29-December 3, 1981, San Francisco

Local Boiling Behind a Central Blockage in a Simulated LMFBR Fuel Bundle

M. Uotani, K. Yamaguchi and K. Haga

Power Reactor and Nuclear Fuel Development Corporation
O-arai, Japan

INTRODUCTION

It is expected that local sodium boiling will occur when a large flow area is blocked in an LMFBR fuel pin bundle. For the safety evaluation of local faults, it is important to examine boiling behavior and dryout mechanism behind a flow blockage. Knowledge of bubble behavior in a partially blocked fuel subassembly is indispensable to develop an anormaly detection system. Furthermore knowledge of dryout mechanism in the two phase region is also required to evaluate the margin of fuel pin coolability.

For these reason, we have conducted sodium boiling experiments in a wire-wrapped 37-pin bundle simulating a fuel subassembly of the Japanese prototype LMFBR.

LOCAL BOILING BEHIND A CENTLAL BLOCKAGE
IN A SIMULATED LMFBR FUEL BUNDLE

M.Uotani,K.Yamaguchi,K.Haga
(PNC-JAPAN)

OBJECTS

EXAMINE THE SODIUM BOILING BEHIND
A FLOW BLOCKAGE IN A FUEL PIN BUNDLE
(1) BOILING PATTERN
(2) DRYOUT MECHANISM
(3) DRYOUT REGION

OBJECTIVES ..... (First slide, please. SLIDE No. 1)

The objectives of the present study are as follows. (Pointing the slide,) Examine the sodium boiling behind a flow blockage in a fuel pin bundle. The needed informations on local boiling are the first, boiling pattern, the second, dryout mechanism, and the third, dryout region.

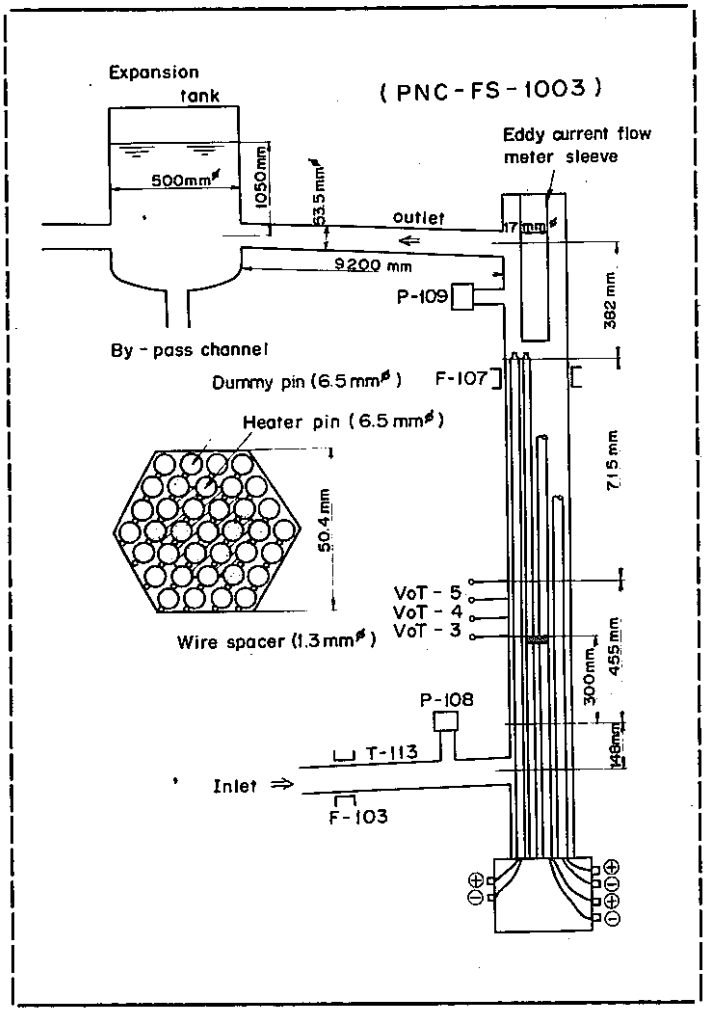

TEST SECTION ..... (Next slide, please. SLIDE No. 2)

This is the test section used in the present study. A thirtyseven-pin bundle is centered in a hexagonal tube. The flat to flat distance is 50.4mm. The bundle consisted of 19 electrically heated pins which located within the blockage boundary and other dummy pins. The diameter of each pin is 6.5mm and the pin-pitch is 7.9mm. Each pin was wrapped with a spacer wire of 1.3mm diameter in a clockwise direction with a 265mm pitch. The central 24 subchannels were blocked by a 5mm thick stainless-steel plate located at nearly middle axial position of the heated section. The blockage covered 27% of the total flow area. The pin surface and sodium temperatures were measured by many chromel-almel thermocouples. The inlet and outlet sodium flow rates were measured by electro-magnetic flow-meters. The average void fractions of some axial spans were measured with registance type void-meters.

EXPERIMENTAL CONDITIONS
(Run No. 37WLB114)

MEAN FLOW VELOCITY;	1.78m/sec
INLET SODIUM TEMPERATURE;	461°C
HEAT FLUX;	127～167W/cm
COVER GAS PRESSURE;	1.05 bar.

EXPERIMENTAL CONDITIONS ..... (Next slide, please. SLIDE No. 3)

This slide shows the experimental conditions. Mean flow velocity, inlet sodium temperature, heat flux and cover gas pressure were in these range. In the present experiment, the inlet temperature flow velocity and cover gas pressure were held constant and the heat flux was gradually increased step by step.

We now move on to the experimental results.

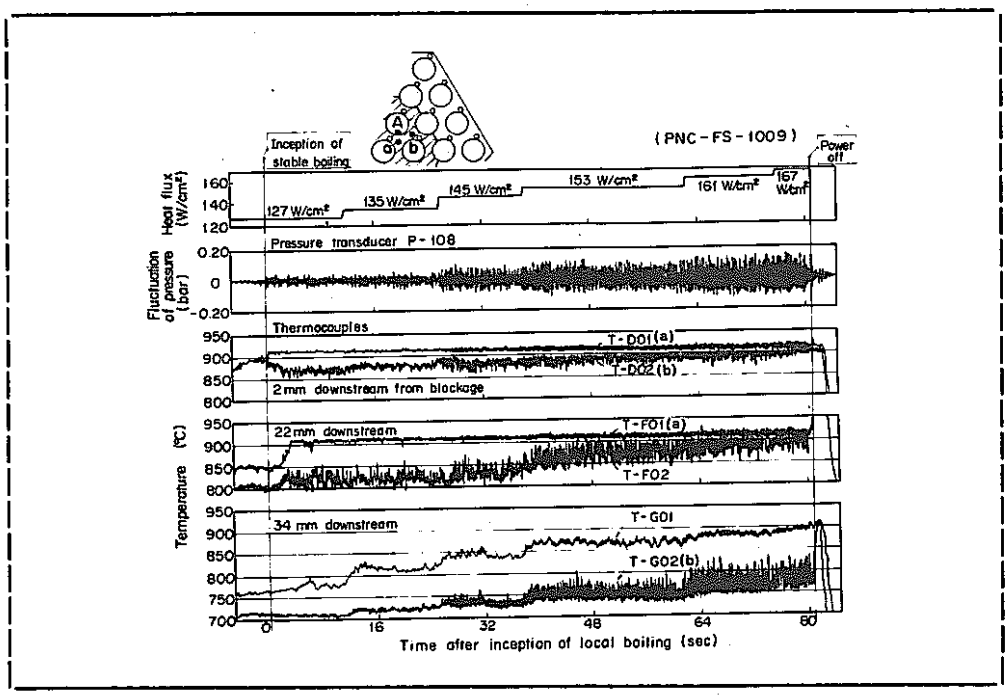

TEMPERATURE SIGNALS DURING ALL RUN ..... (Next slide, please.

SLIDE No. 4)

This figure shows the signals of pressure and sodium temperatures at 3 different axial planes from boiling inception to the pin power shutdown in a typical run. The horizontal axis is the time from boiling inception, which was caused at the heat flux of 127W/cm^2. After boiling inception, the central subchannel temperature reached to the saturated level of sodium at 2mm downstream, then the temperature at 22mm showed the same level. They remained to the saturated temperature level of sodium with small fluctuation, while that of adjacent subchannels increased with large fluctuation. A few seconds after last power-up, the fluctuation decreased gradually, and several heater pins were subjected to burn-out caused by pin surface dryout.

Let's examine the boiling behavior in more detail at stages, of boiling inception, steady oscillatory boiling and occurence of dryout.

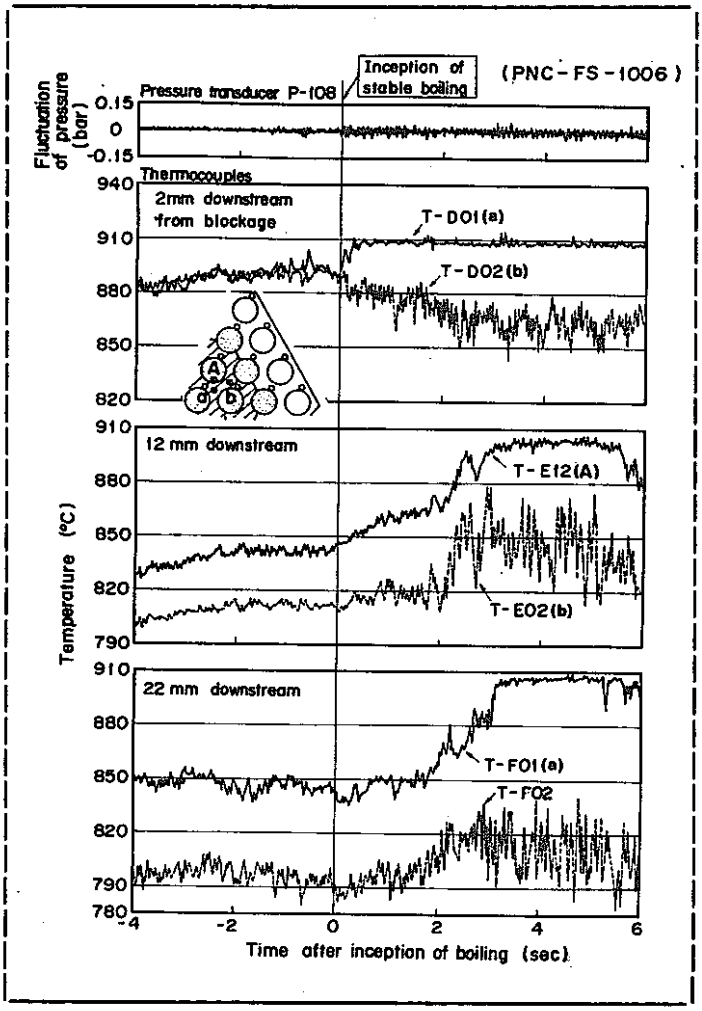

TEMPERATURE SIGNALS AT BOILING INCEPTION ..... (Next slide, please.

SLIDE No. 5)

This figure shows the temperature histories observed at 2mm, 12mm, and 22mm downstream from blockage at boiling inception. Radial locations of the thermocouples are illustrated here. Pressure signal is also shown in this figure. A few seconds after power-up, continuous oscillation of pressure was observed, and saturated region of central subchannels expanded axially in two or three seconds. On the other hand, adjacent subchannels remained in subcooled temperature. No large incipient boiling super heat was observed in each run, so the void region never expanded rapidly.

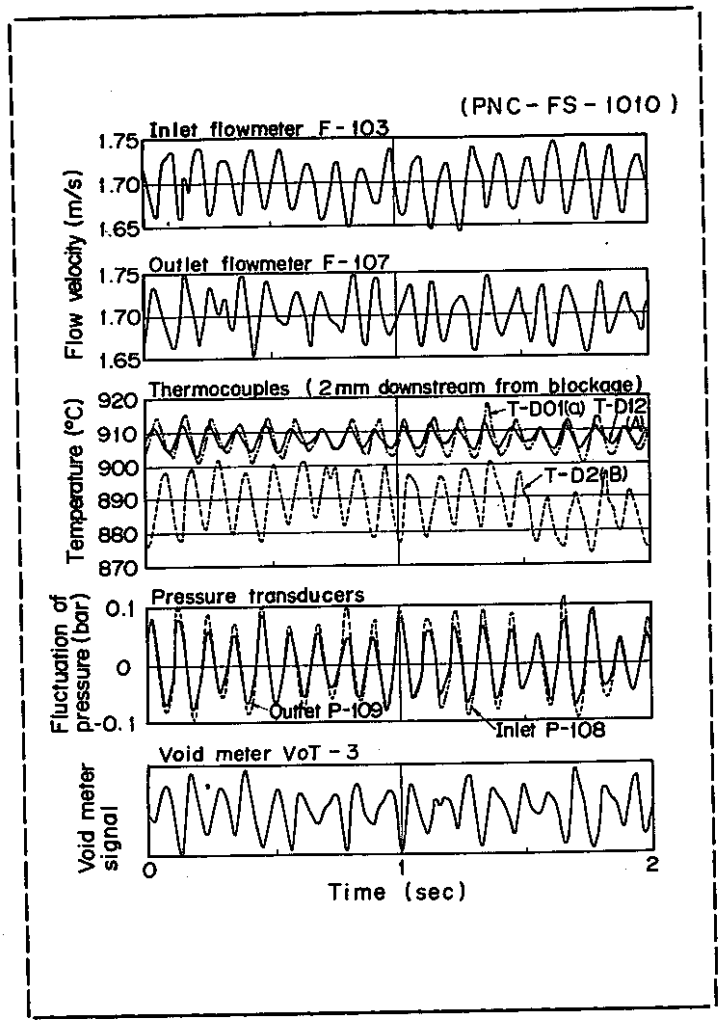

TEMPERATURE SIGNAL IN OSCILLATORY BOILING ..... (Next slide, please.

SLIDE No. 6)

After the first step increase of heat input, the boiling mode changed to oscillatory. This mode was reported in KfK and ECN experiments.

This slide shows the typical signals of inlet and outlet flowmeters, thermocouples at 2mm downstream from blockage, pressure transducer and void-meter for 2 seconds. As you can see in the figure, each signals oscillated regulatory with the frequency of about 9 Hz. The temperature oscillation is in a reverse phase to the voidmeter signal, which corresponds to the size of voiding region. This fact means that a small amount vapor bubble always survived during the oscillation.

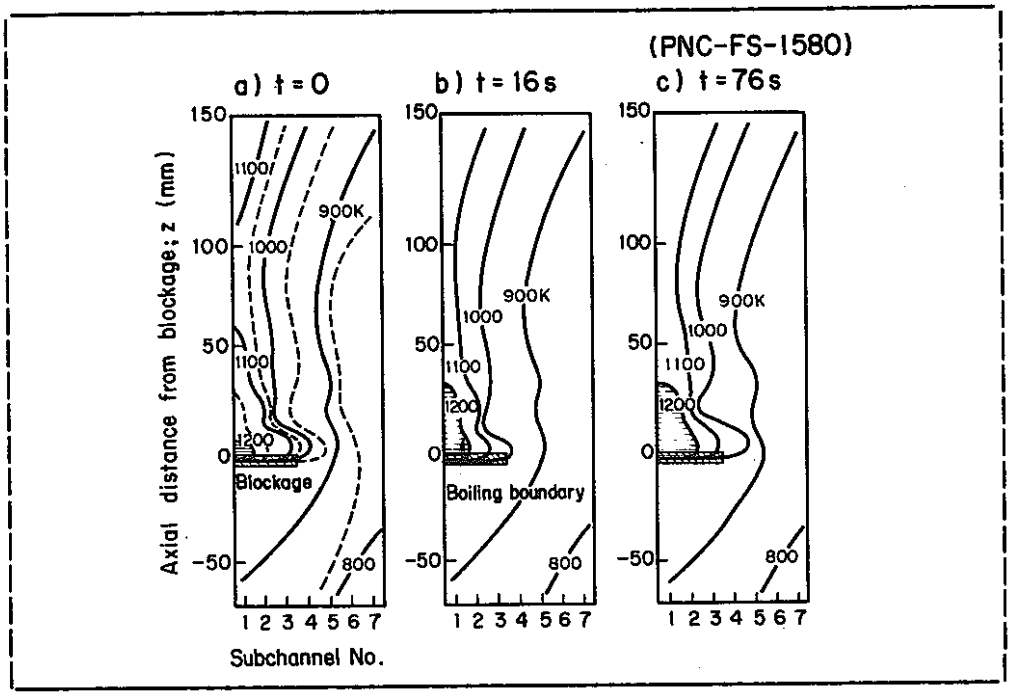

ISOTHERM MAPS ..... (Next slide, please. SLIDE No. 7, i.e. Fig. 1)

This figure shows the isotherms of sodium and boiling boundaries for each step. During oscillatory boiling, the voided region was limited within the wake region.

BUBBLE OSCILLATION MODEL

* SINGLE SPHERICAL BUBBLE
* ONE DIMENSIONAL MOMENTUM EQ. OF LIQUID COLUMN
* LINEAR TEMPERATURE FIELD
* VAPOR PRESSURE
  EXPANSION-----GAST'S MODEL
  CONTRACTION---POLYTROPIC CHANGE (ref. Isotharmal contraction in GAST and Fauske models)
* POLYTROPIC INDEX and MEAN VAPOR VOLUME are obtained from EXPERIMENT

BUBBLE OSCILLATION MODEL ..... (Next slide, please. SLIDE No. 8)

In order to evaluate the oscillatory frequency observed in the test bundle, an analytical model has been developed. One dimensional momentum equation of liquid column was formulated based on the single spherical bubble model. Dynamic behavior of the ordinaly differential equation. The linear perturbation method was applied in this process and the linear temperature profile was assumed within the wake region. Concerning the change of the vapor pressure, Gast's model was applied to the expanding bubble, and the polytropic change was assumed for the contracting bubble. Gast and Fauske considered that the voided region contracts isothermally, but the experimental results conflicted with their model. The politropic index was found from the vapor volume experimentally. The proper value was from 0.1 to 0.2.

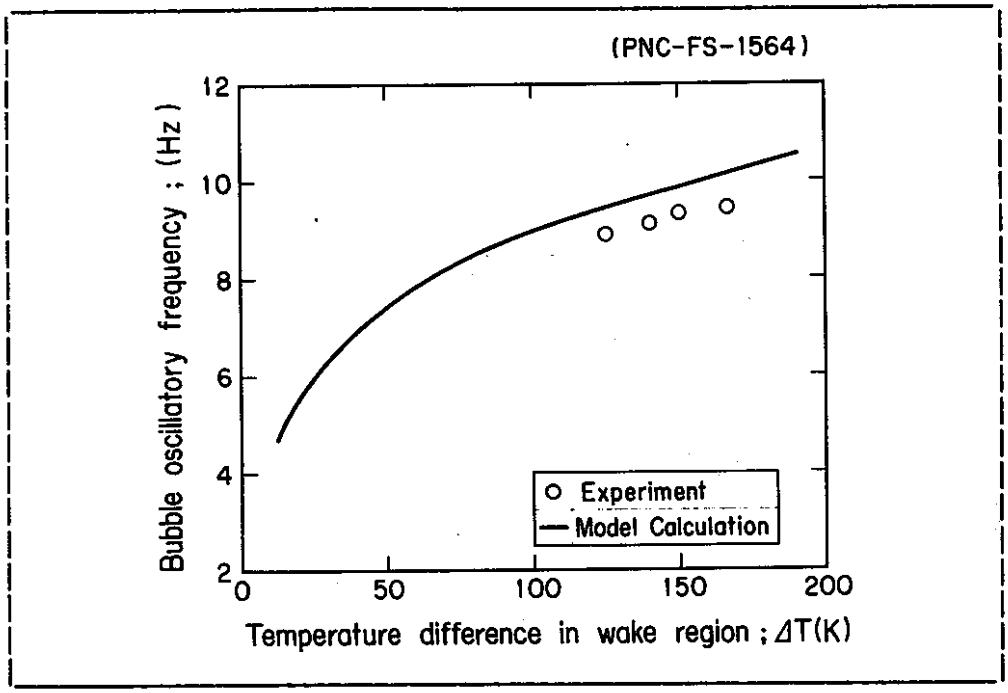

BUBBLE OSCILLATORY FREQUENCY ..... (Next slide, please. SLIDE No. 9, i.e. Fig. 2)

This figure shows the comparison of observed oscillatory frequencies with the model calculation. The horizontal axis is the temperature difference within the wake. The same tendency can be seen from the figure between the calculations and the experimental results, that is to say, the oscillatory frequency reduces in keeping with the decrease of temperature difference within the wake.

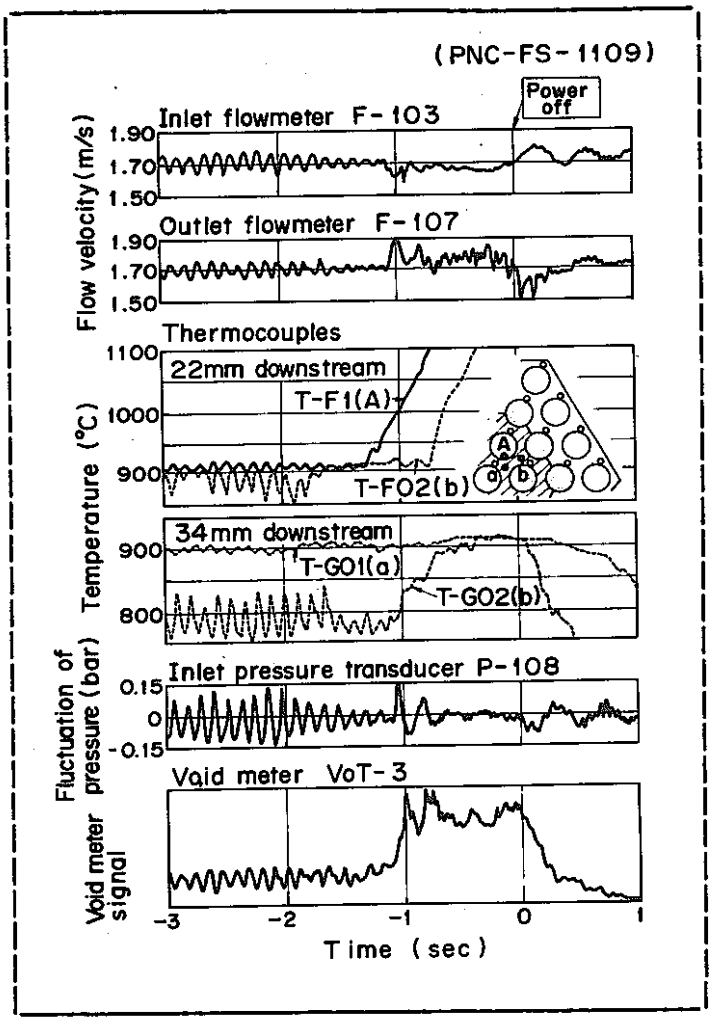

TEMPERATURE SIGNALS AT DRYOUT PHASE ..... (Next slide, please.

SLIDE No. 10)

This figure shows the signals at the instance of permanent dryout. As the heat flux was increased up to 167W/cm^2, the amplitude of oscillatory signals damped little by little during the time from -2 to -1 seconds. It was obvious that the gradual growth of radial and axial high temperature region forced the oscillatory movement to be stabilized, as shown in the previous figure. As soon as the transition of boiling pattern appeared, the pin surface temperature at 22mm downstream showed steep increase due to occurrence of permanent dryout. The abrupt growth of the voided region was observed, accompanied by cladding melting. The voided region was, however, limited locally and flow reduction was hardly measured.

From the present experiment it seems that the local boiling pattern transfers in the following manner with increasing the value of power-to-flow ratio: (1) Boiling inception with irregular nucleate boiling, (2) Oscillatory boiling--coolability of fuel pins is maintained in this mode, (3) Dryout occurs soon after the appearance of stationary boiling.

The transition condition of boiling pattern was thought to depend on the temperature and pressure gradients in the wake region, the volume of saturated region and the inertia mass of test section. But further study is needed to clarify the conditions of the boiling pattern transition.

CONCLUSION

(1) OSCILLATORY BOILING IMPROVED THE COOLABILITY OF LOCALIZED BUBBLY REGION
(2) OSCILLATION OF VOIDING REGION WAS ESTIMATED BY A SIMPLE MODEL
(3) DECREASE OF TEMPERATURE GRADIENT IN WAKE REGION CAUSED TRANSITION OF BOILING PATTERN TO STATIONARY MODE
(4) PERMANENT DRYOUT WAS FOLLOWED BY TRANSITION OF BOILING PATTERN

CONCLUSIONS ..... (Next slide, please. SLIDE No. 11)

Now I would like to summarize the present work.

First; Oscillatory boiling improved the coolability of localized bubbly region.

Second; Oscillation of voided region was estimated by a simple model.

Third; Decrease of temperature gradient in the wake region caused the transition of boiling pattern to a stationary mode.

Fourth; Permanent dryout was followed by the transition of boiling pattern.

4. PNC-UKAEA SPECIALISTS' MEETING ON SAFETY AND INSTRUMENT

5 Recent Progress of the Transient Sodium Boiling and Fuel Failure Propagation Tests

Edited by K. Yamaguchi

RECENT PROGRESSES OF THE TRANSIENT SODIUM BOILING AND FUEL FAILURE PROPAGATION TESTS

FOR THE PRESENTATION AT THE
UK-PNC SAFETY SPECIALISTS' MEETING,
OEC/PNC, OCT. 20-23, 1981

PREPARED BY THE
FBR SAFETY SECTION, OEC/PNC, JAPAN

INTRODUCTION

..... (Turn on the light of OHP, OHP No. 1)

I would like to present the recent progresses of the experimental works which have been conducted in the FBR Safety Section of O-arai Engineering Center, PNC.

ORGANIZATION OF THE OEC (FBR R&DS)

- EXPERIMENTAL FAST REACTOR DIVISION
  (MANAGER: Y. MATSUNO)
- FUEL AND MATERIAL DIVISION
  (" : M. WATANABE)
- SODIUM ENGINEERING DIVISION
  (" : Y. MIMOTO)
  - FLUID DYNAMICS SECTION
  - SODIUM TECHNOLOGY SECTION
  - SODIUM COMPONENTS SECTION
  - SODIUM ANALYSIS SECTION
- STEAM GENERATOR DIVISION
  (" : M. HORI)
  - 50 MW STEAM GENERATOR SECTION
  - STEAM GENERATOR SAFETY SECTION
  - DYNAMICS ANALYSIS SECTION
  - FAST REACTOR SAFETY SECTION

ORGANIZATION OF OEC ..... (Change the OHP sheet, OHP No. 2)

First of all, I would like to begin with the explanation of the organization of O-arai Engineering Center (OEC). The PNC makes efforts to develop a Fast Breeder Reactor and an Advanced Thermal Reactor. The required technologies have been studied chiefly at the OEC. There are two lines of commands from the Headquarters to the OEC, in accordance with the concerning reactor types. I would like to limit my speech to the FBR project, which is covered by a total of four divisions listed here.

First, the Experimental Fast Reactor Division operates JOYO. Several items have been tested, such as the performance, operation and maintenance of all equipments and components. The reactor power reached 75 MWth in July 1979, and will be raised up to 100 MWth in the near future.

Second, the Fuel and Material Division examines fuel and materials irradiated in JOYO to develop FBR fuels. The irradiated fuel

subassemblies are first delivered to the Fuel Monitoring Facility, where they are subjected to nondestructive examinations. Then they are disassembled into fuels and materials and are sent to the Alpha-Gamma Facility and the Material Monitoring Facility for detailed physical, chemical, metallurgical and mechanical tests.

Third, the Sodium Engineering Division organized by these four sections covers the design studies of many reactor components except for the steam generator. The covering items are material strength tests in high-temperature sodium, sodium mixing tests in simulational fuel subassemblies, performance and endurance tests of in-sodium components, and developments of practical and reliable detectors and instrumentation circuits.

Fourth, the Steam Generator Division is organized by these four sections. The 50 MW Steam Generator Section operates a demo-plant to attain a high heat transfer efficiency of the steam generator, and also to have a reliable construction and performance. The safety of the steam generator is investigated at the Steam Generator Safety Section by conducting sodium-water interaction experiments. The Dynamics Analysis Section examines the dynamic characteristic of the FBR plant to ensure proper controllability of the steam generator.

The FBR Safety R&Ds are progressed in the FBR Safety Section. Experiments and analyses are being made to determine to what extent the fuel elements are damaged when the sodium flow is lost or when the reactor power is run away; and whether or not radioactivity escapes from the reactor under hypothetical anomaly conditions. The MONJU licensing work is powerfully supported by the results of these investigations.

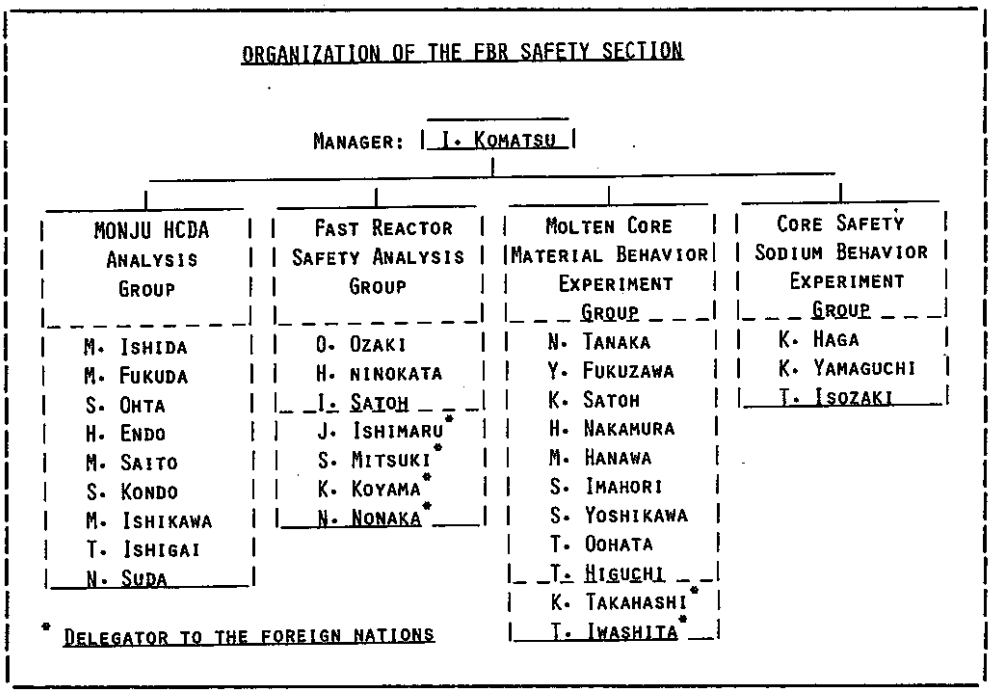

FBR SAFETY SECTION ..... (Change the OHP sheet, OHP No. 3)

Next, I would like to account for the organization of the FBR Safety Section in detail. The section manager, I. Komatsu, exercises general control over the activities of the FBR Safety Section.

There are four sub-groups in the FBR Safety Section: They are the MONJU HCDA Analysis (MHA) Group, the Fast Reactor Safety Analysis (FSA) Group, the Molten Core Material Behavior Experiment (FSI) Group, and the Core Safety Sodium Behavior Experiment (FSB) Group. Here, you can see the names of the members of each group.

The PNC has been in cooperation with a number of foreign nations in the development of FBR safety. Based on the agreements with the United States and Germany/France, several persons are delegated to various laboratories, such as the SANDIA, HEDL, BNL, ANL, and CABRI.

ACTIVITIES OF THE FBR SAFETY SECTION

- MONJU HCDA Analysis Group
  - Calculations for MONJU licensing
    - SAS, SIMMER, PISCES ....
- Fast Reactor Safety Analysis Group
  - Code developments
    - ASFRE, TOPFRES, ...
  - Analyses of in-pile tests
    - CABRI, SLSF, TREAT ....
- Molten Core Material Behavior Experiment Group
  - Fuel-sodium interaction experiment
    - FSI Facility
  - Analysis of in-pile PAHR tests
    - SANDIA
  - Code modification
    - SSC
- Core Safety Sodium Behavior Experiment Group
  - Sodium boiling and fuel failure propagation experiments
    - SIENA Facility
  - HCDA bubble experiments
    - SIENA Facility and BBT Rigs

ACTIVITIES ..... (Change the OHP sheet, OHP No. 4)

The activities of each group are listed here.

The MONJU HCDA analysis Group was temporary organized in 1979 to buckup HCDA calculations required for the MONJU licensing work. The SAS-3D, SIMMER and PISCES codes are introduced from USA and used for these calculations. The project planning and management are controlled by the staff of the headquarters under the personnel contact with the project teams assigned to individual codes.

The Fast Reactor Safety Analysis Group is in charge of the code developments. The thermo-hydrodynamics of sodium flow within the subassembly has been analized by the self-deviced codes, such as ASFRE and TOPFRES. The experimental data measured by the Core Safety Sodium Behavior Experiment Group and the other laboratories are used as benchmark examples in the code validation exercises. Another activity of this group is the international cooperations with the CABRI, SLSF and TREAT projects. The accident analysis code PAPAS is developed and used

for the pre- and post-calculations of the CABRI runs.

The Molten Core Material Behavior Experiment Group studies the fuel-sodium interaction and associated phenomena. The test loop, FSI, can heat UO_2 inserted pins with the transient power excursion manner. At the beginning of this year, this group was reinforced its activity to be capable of analyzing the SANDIA in-pile PAHR test data. Also added was the LOPI calculation team. For this aim, the SSC code was introduced from USA and its modification is under way with keeping in contact with developers to device a PNC-MONJU version.

The Core Safety Sodium Behavior Experiment Group covers transient sodium boiling and fuel failure propagation tests. The experimental facility SIENA can receive various pin bundles to examine critical conditions which could lead to sodium boiling, dryout, cladding melting and movement, and so on. Recently, the Bubble Behavior Test Rig was attached to the SIENA Facility. The behavior of a large sodium bubble will be examined in the future to obtain basic data for the source term assessment of the possible radioactivity escape accidents.

SODIUM BOILING AND FUEL FAILURE PROPAGATION TESTS

FBR SAFETY SECTION, OEC/PNC, JAPAN

CONTENTS

SCOPE OF THE FSB ACTIVITIES ..... (Change the OHP sheet, OHP No. 5)

Now, I would like to explain the activities of our Core Safety Sodium Behavior Experiment Group in detail.

We have two subjects classified by fund lines. The first one is the Transient Sodium Boiling Test. It is further divided into three: LOF without Scram, Decay Heat Sodium Boiling, and CDA Bubble Behavior. The second one is the Fuel Failure Propagation Test. It is divided into five: Pin Contact, Local Flow Blockage, Molten Clad Relocation, Code Development for Anomaly Detection, and Inter-Subassembly Heat Transfer.

We have a mother loop named SIENA. Each subject has been carried out by changing its test section.

Now, I will show you our future status, too. The LOF experiments were completed one year ago, and this subject will be restarted in the Clad Relocation test in 1982. The first-phase Pin Contact Test which focused on the MONJU geometry was also finished and the results will be used in developing a new version of analysis code. The basic soft of Anomaly Detection is already devised. Hence, we can treat this subject as being succeeded in the Local Flow Blockage Test. The final experiments of Local Flow Blockage will be continued till the end of next year. The examination of the Inter-Subassembly Heat Transfer problems will be followed in a few years. Consequently, the six subjects will be continued in the future.

A total of three staffs, two engineers and one technicians, have been in action. At present, we have two subcontract technicians and one temporary employed programmer. Total budget of our group is about $ 0.4 M/year, including the pays for the regular subcontract technicians. The lack of fund and personnel is partially sufficed by making contracts with some industries so that they can temporary apply their man power to our works, and by diverting the other PNC funds to our purposes. However, we must work too hard due to the assistant and miscellaneous works associated with their introductions.

Next, let us go into individual details.

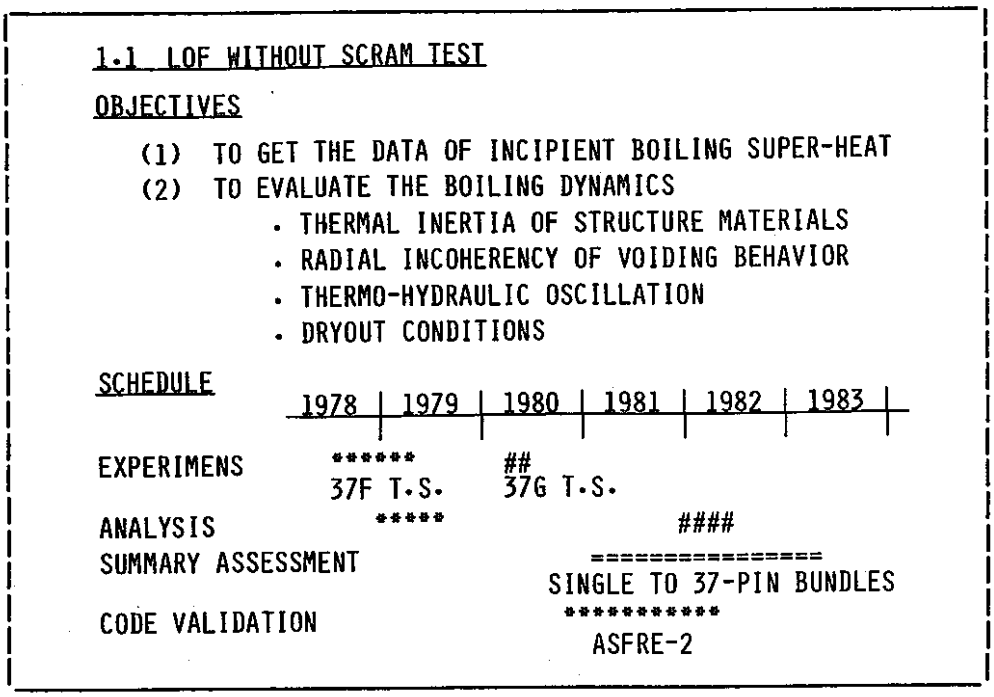

INDIVIDUAL DISCUSSIONS

1.1 LOF without Scram Test ..... (Change the OHP sheet, OHP No. 6)

You can see the objectives of our LOF Test. The First one is to get the I.B. super-heat data as many as possible. The second one is to evaluate the boiling dynamics. Our interests lie in the following four problems: thermal inertia of structure materials, radial incoherency of voiding behavior, thermo-hydraulic oscillation, and dryout conditions. The last one is what we want to know ultimately.

The time schedule of the LOF Test is shown below. This program is started with the single-pin test geometry. The bundles made of 7, 19 and 37 pins were tested in the followed experiments. All of the experiments were completed. These results will be used for the summary assessment work of the LOF-driven consequences. Some of the test data with the 37F test section have been used for the code validation exercise of the ASFRE-2 wire-wrapped version in the Fast Reactor Safety Analysis Group.

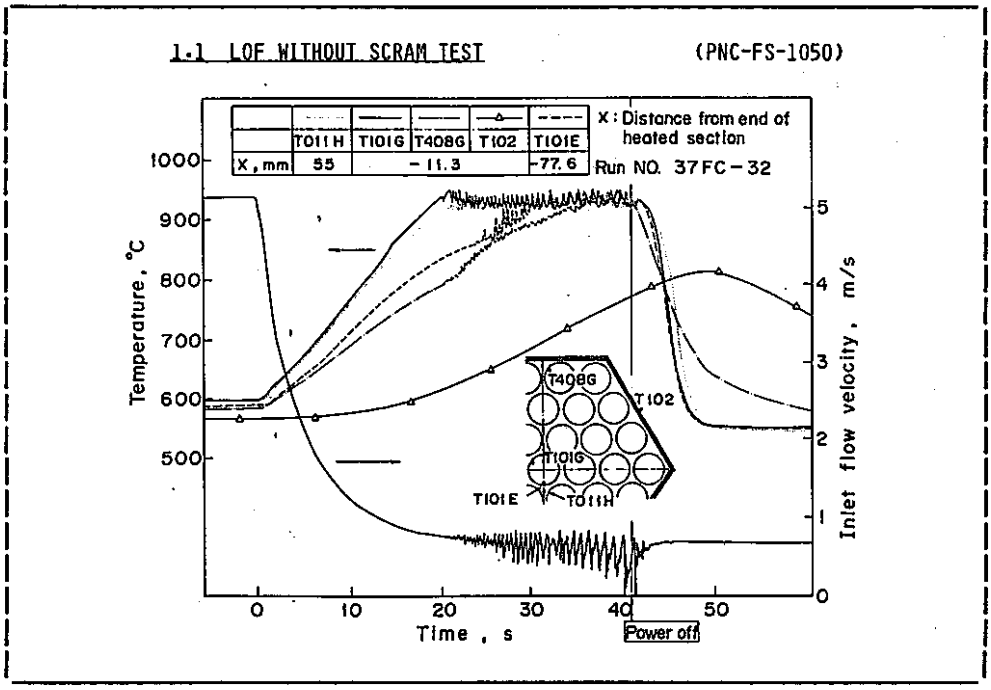

..... (Change the OHP sheet, OHP No. 7, i.e. Fig. 1)

I would like to show you a typical result obtained by the test before last. Concerning the I.B. super-heat, the observed values were very small. No effects could be identified of the experimental parameters except for the pin bundle size. So, it will be reasonable to consider that the onset of sodium boiling in the bundle is similar to that in usual working fluid.

For the boiling dynamics, the story is summarized as follows: After a few seconds into boiling, the saturated temperature region expands axially around the central subchannels, although it is not shown in this figure. At the same time, the thermo-hydraulic oscillation synchronized with a repetitive bubble formation and collapse is initiated. For LOF conditions, you can easily understand that the oscillation is not stable but divergent due to the reducing pressure drop and inlet flow restriction.

During a gradual growth of the oscillation, a cluster of bubbles or a vapor slug will become to form a high-quality vapor core at the center of the bubbly region. When the vapor core grows up large enough to obstruct sodium entry during the oscillation, the pin surfaces covered by the vapor core will be soon dried out. The actual cladding melting is followed after a few times' repetetions of dryout and rewetting.

1.1 LOF WITHOUT SCRAM TEST (CONTINUED)

RESULTS

(1) MEASURED INCIPIENT BOILING SUPER-HEAT DATA HAD A DECREASING TENDENCY WITH THE BUNDLE SIZE

(2) • A SLUG-EJECTION TYPE VOID BEHAVIOR WAS OBSERVED IN A SINGLE-PIN GEOMETRY TEST
• A MULTI-PIN GEOMETRY FORCED THE VOID TO EXPAND AXIALLY AT FIRST, THEN RADIALLY

(3) DRYOUT OCCURRED AS THE INLET FLOW REDUCED ENOUGH TO CAUSE ITS BRIEF VALUE TO REACH ALMOST ZERO

(4) MANY TEMPERATURE DISTRIBUTION DATA OF THE STEADY-STATE SINGLE-PHASE FLOWS WERE OBTAINED IN VARIOUS SIZE BUNDLE EXPERIMENTS

..... (Change the OHP sheet, OHP No. 8)

The summary assessment of the LOF data is under way. All data which were obtained in every bundle geometries are reviewed. The applicability of analysis codes, such as SAS-3D, to the experimental results will be also examined during the assessment work. The following qualitative evaluations will be added to the results of this exercise.

First, the measured incipient boiling super-heat data had a decreasing tendency with the bundle size. In the 37-pin bundle tests, almost all wall super-heat data were less than 50 °C. Second, A slug-ejection type void behavior was a characteristic phenomena which is usually appeared in a single-pin geometry test. A multi-pin geometry forced the void to expand axially at first, then radially. When the void occupies full plane, the void behavior seems to resemble that in the single-pin test. Third, dryout occurred as the inlet flow reduces to cause violent flow oscillation.

In addition to these findings, many temperature distribution data of the steady-state single-phase flows were obtained in various size bundle experiments. For example, a trapezoidal radial temperature profile was obtained in the 37-pin bundle test.

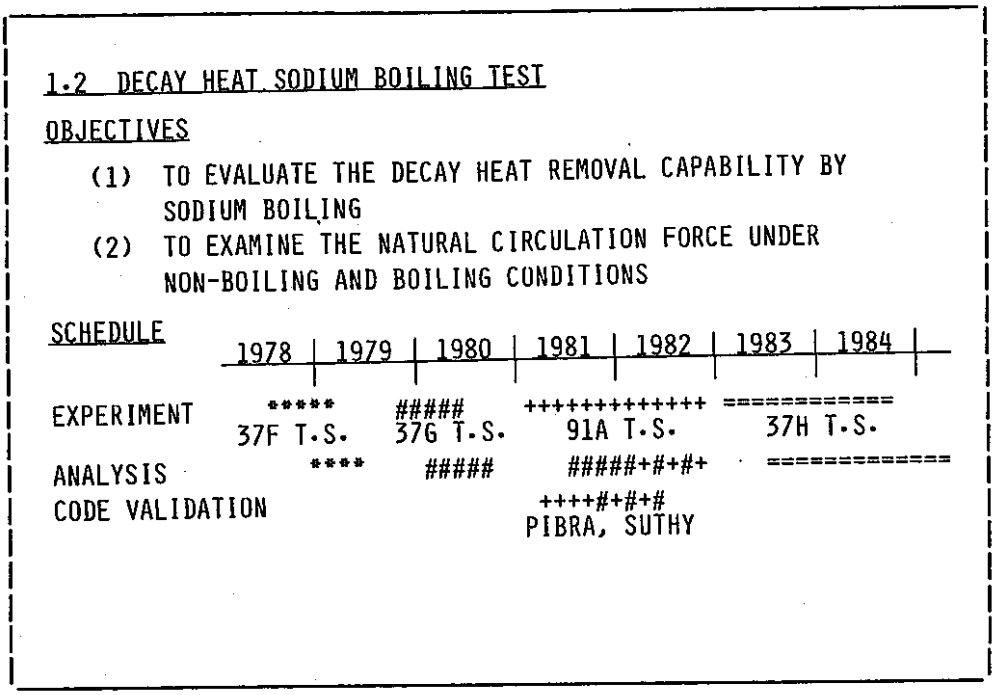

1.2 Decay Heat Sodium Boiling Test

..... (Change the OHP sheet, OHP No. 9)

Next is the Decay Heat Sodium Boiling Test. It has two objectives. The first one is to evaluate the dryout criteria under low heat flux and low flow conditions. The second one is to examine the selfsustaining safety aspect of natural circulation.

The time schedule is shown below. This program was started three years ago using the same 37-pin bundle with that used for the LOF experiment. The similar experiments were carried out again with the next 37-pin bundle to make a dryout data base applicable to the MONJU LOPI transient conditions. The analysis of these data is now under way.

Besides these boiling experiments, the long term LOF-driven natural circulation characteristic in the SIENA Facility was preliminarily examined at the beginning of this year, using the locally blocked 91-pin bundle. We are now analizing the measured data by the PIBRA code which is developed in Toshiba Corp. for the LOPI calculations of the MONJU primary loops. Based on the prompt result of this exercise, some additional sensors are going to be equipped to the loop in the next year. Then, the parametric runs of the LSHRS will be conducted.

We are now planning the further advanced program, where not only the reversal flow under better simulations of LOPI transients but also the natural circulation boiling under LSHRS transient condition can be attained.

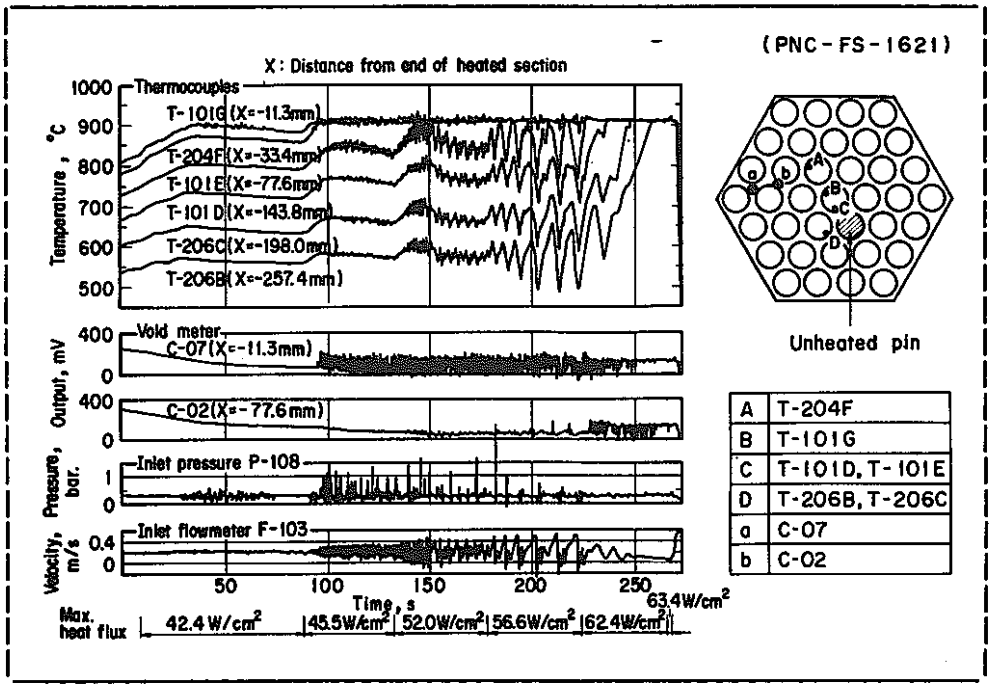

..... (Change the OHP sheet, OHP No. 10, i.e. Fig. 2)

This figure shows an example of a dryout run. It was presented at the 9th meeting of the Liquid Metal Boiling Working Group (LMBWG). The sodium flow was driven by natural circulation of our test facility. Sodium boiling was first started, here, and was restarted by the additional heat up. In the latter half of this run, you can identify the regular oscillation caused by the slug flow and its termination. Prior to the instance of dryout, the flow pattern was changed to annular or annular-mist flow. The estimated average exit quality at dryout was greater than 0.5.

1.2 DECAY HEAT SODIUM BOILING TEST (CONTINUED)

RESULTS

(1) SODIUM BOILING ACCELERATED NATURAL CIRCULATION FLOW BY A GREAT AMOUNT TO YIELD LESS VOIDED SITUATION WITH TIME

(2) THE DECAY HEAT REMOVAL IS POSSIBLE FOR A WIDE RANGE OF EXIT QUALITY

(3) THE SLUG FLOW HAD EXTREMELY HIGHER DECAY HEAT REMOVAL CAPABILITY THAN THE ANNULAR FLOW BECAUSE OF THE REPETITIVE REWETTING OF THE DRIED PIN SURFACES

..... (Change the OHP sheet, OHP No. 11)

During the last experiments, we have got additional 20 points dryout data at the heat flux range from about 4% to 15% of reactor condition. The results are summarized here with a general idea about the foregoing test results.

Sodium boiling has a large potential of accelerating natural circulation flow. Therefore, it is reasonable to consider that the most severe situation for the decay heat removal during the LOPI or LSHRS accident will appear at an early stage of a possible power-to-flow mismatching. However, such a situation might permit the decay heat being removed, unless the exit quality exceeds a critical value of 0.5.

It has been said that the temporary flow run down might cause rapid dryout. But, an unstable flow oscillation or a slug flow pattern were found to have an extremely higher capability of decay heat removal than that during an annular or annular-mist flow pattern. It suggested us that we should examine why the oscillation was terminated in many runs and why such a flow regime transition was not attained in very low flow runs.

For the decay heat conditions, dryout did not necessarily cause unlimited pin temperature excursion. In other words, the heat transfer during the long term repititive dried condition was not so bad. This fact implies that the spray cooling by a large amount of entrained droplets plays an important role in the heat transfer during the dryout.

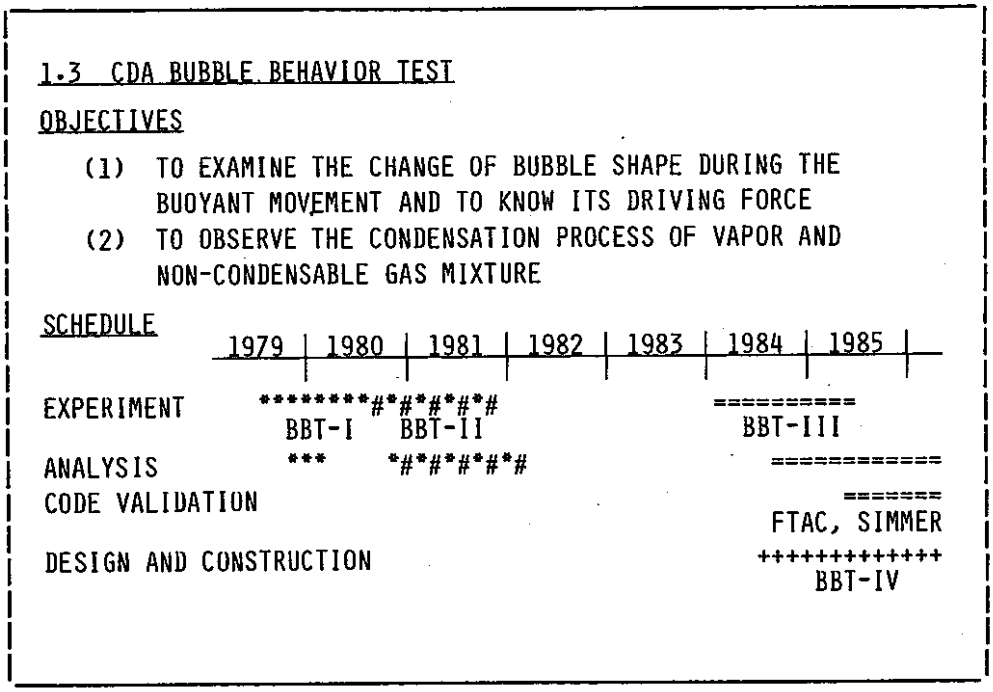

1.3 CDA Bubble Behavior Test .... (Change the OHP sheet, OHP No. 12)

The last item of the Transient Sodium Boiling Tests is the CDA Bubble Behavior Test. Its objectives are shown here. We are going to examine two problems: the change of the shape of a large bubble during its buoyant movement, and the condensation of it. The similar tests are conducted as the FAST program in USA and the EXCOBULLE test in France.

As are shown in the time schedule, this program was started two years ago. A small scale in-sodium test vessel BBT-III Rig is designed and manufactured last year. Quite recently, it was installed in the SIENA Facility. Besides this in-sodium test, two mockup tests are running in parallel using cold and hot water pools, BBT-I and BBT-II Rigs. The results are expected to be used to backup the interpretation of in-sodium test results we will have.

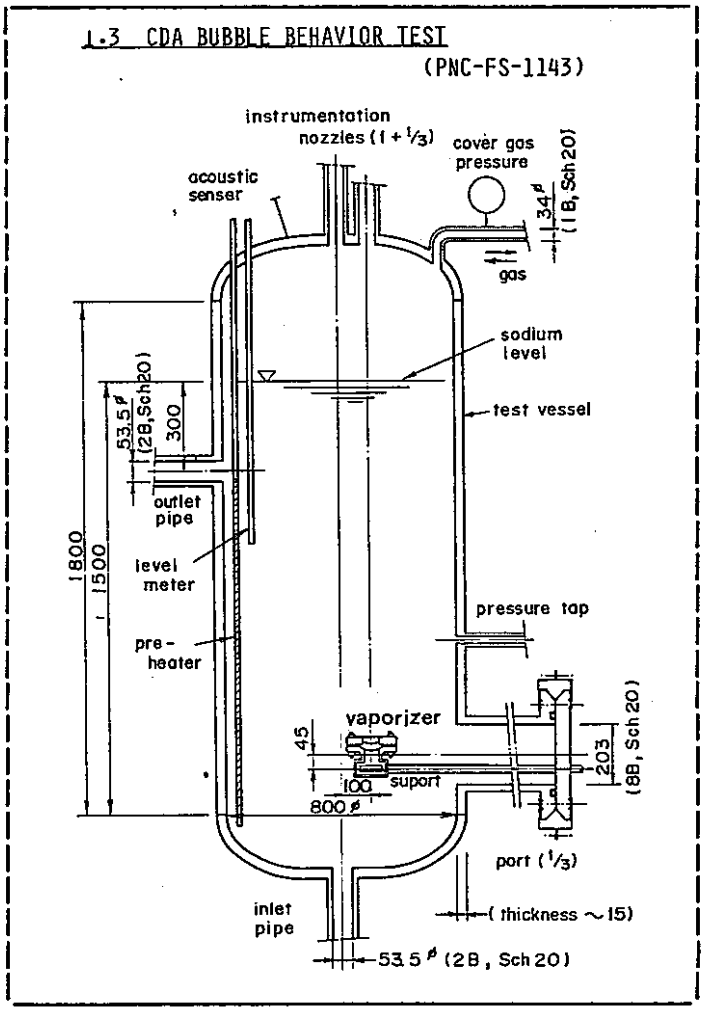

..... (Change the OHP sheet, OHP No. 13, i.e. Fig. 3)

This is the test vessel BBT-III. We are planning to make a large bubble of sodium vapor and noncondensable gas mixture by a vaporizer unit. The capability of this method will be preliminarily checked in water.

Two important problems are left unsolved: One is the scale effects of bubble and in-vessel structures. The other is the effect of the initial condition of bubble formation. We have a plan to construct a next large scale in-sodium test vessel.

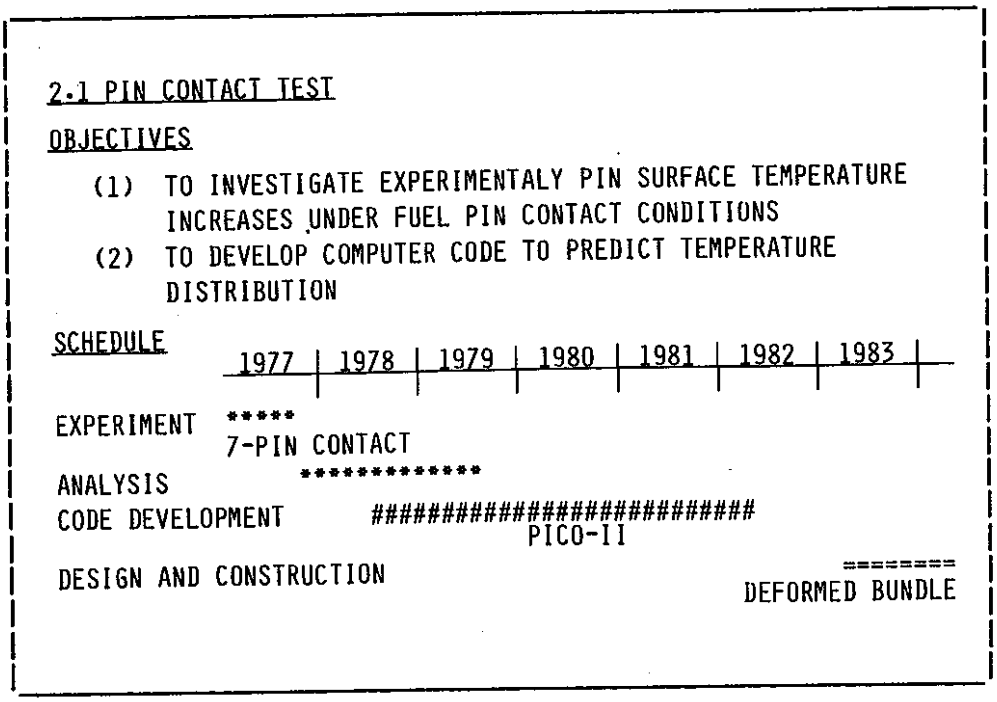

2.1 Pin Contact Test ..... (Change the OHP sheet, OHP No. 14)

The first item of the Fuel Failure Propagation Tests is the Pin Contact Test. Its first objective is to estimate experimentally the temperature increases under fuel pin contact conditions. The second is to develop a computer code to predict temperature distributions around the contacted pins.

The time schedule of the Pin Contact experiments is shown below. Four kinds of experiments for MONJU fuel subassembly geometry, such as a 2-pin point contact, a 2-pin line contact, a 3-pin point contact, a 7-pin point contact, were conducted and completed already in 1977.

An advanced project which uses a deformed bundle for a future demonstration reactor geometry is planned to be started in 1983.

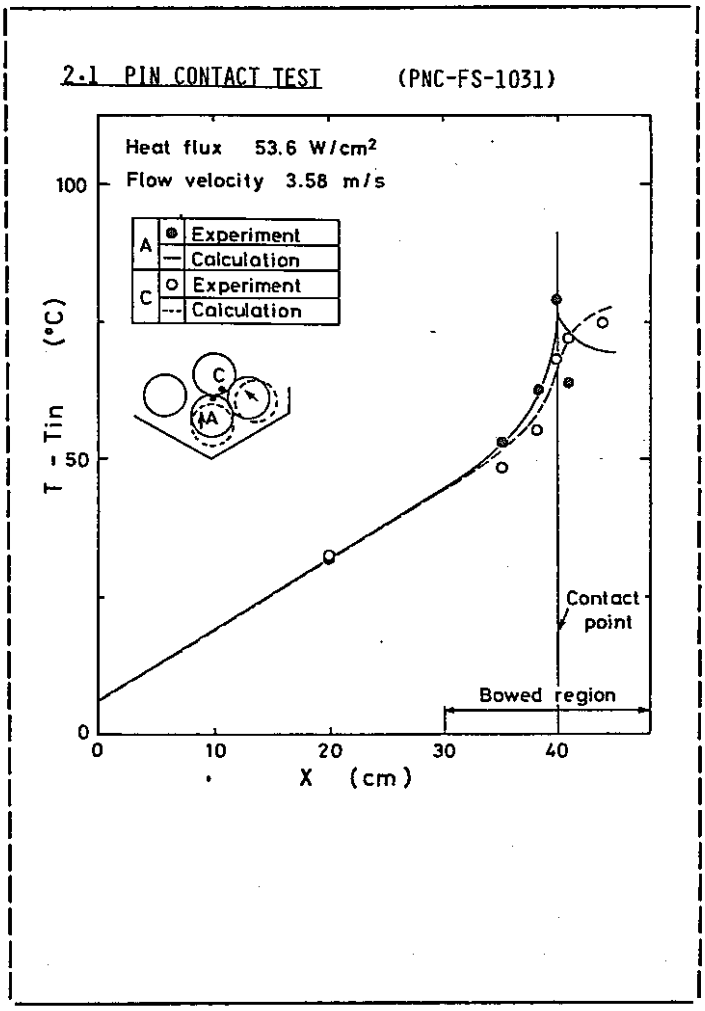

..... (Change the OHP sheet, OHP No. 15, i.e. Fig. 4)

This figure shows an example of the three-pin point contact test. The pin surface temperature was measured along typical two vertical lines, a line through a pin contact point and a line facing a three-pin enclosing subchannel.

As the pin gap decreases along the vertical direction, the pin surface located between two bowed pins raises its temperature most steeply to reach a maximum temperature at the contact point. After that, the temperature decreases sharp due to the cross-flow cooling behind the contact point. On the other hand, the pin surface facing the subchannel takes nearly constant temperatures for a long axial region downstream from the pin contact plane. The prediction by the PICO-I code gives reasonable tendencies of these temperature distributions up to the contact point. The difference between local temperatures along these two lines will gradually disappear at downstream planes from the bowed region.

2.1 PIN CONTACT TEST (CONTINUED)

RESULTS

(1) LOCAL TEMPRTATURE INCREASES UNDER MONJU DESIGN.CONDITION WERE EXTRAPOLATED BY THE PICO-I CODE

CONTACT MODE	2-PIN POINT	2-PIN LINE	3-PIN POINT	7-PIN POINT
MAXIMUM TMPERATURE INCREASES	40 °C	70 °C	100 °C	150 °C

(2) PICO-II IS UNDER DEVELOPMENT, ADDING FUEL PIN BOWING MODEL AND CROSS FLOW CALCULATION MODEL TO THE ORIGINAL PICO-I CODE

..... (Change the OHP sheet, OHP No. 16)

Experimental results were extrapolated to the reactor condition by the PICO-I code. The results are summarized here. For instance, the three-pin point contact will raise cladding temperature by 100 °C at the contact point, when the MONJU operating conditions are concerned. These results are used for the assessment of the fuel pin's integrity.

The PICO-I code is under revision now. The improvement enables to predict realistic flow redistribution in the downstream region of the pin contact plane. Furthermore, an updated PICO-II code will have a routine to calculate the inner temperature profile of the pins. This code development work will be completed at the end of this finantial year.

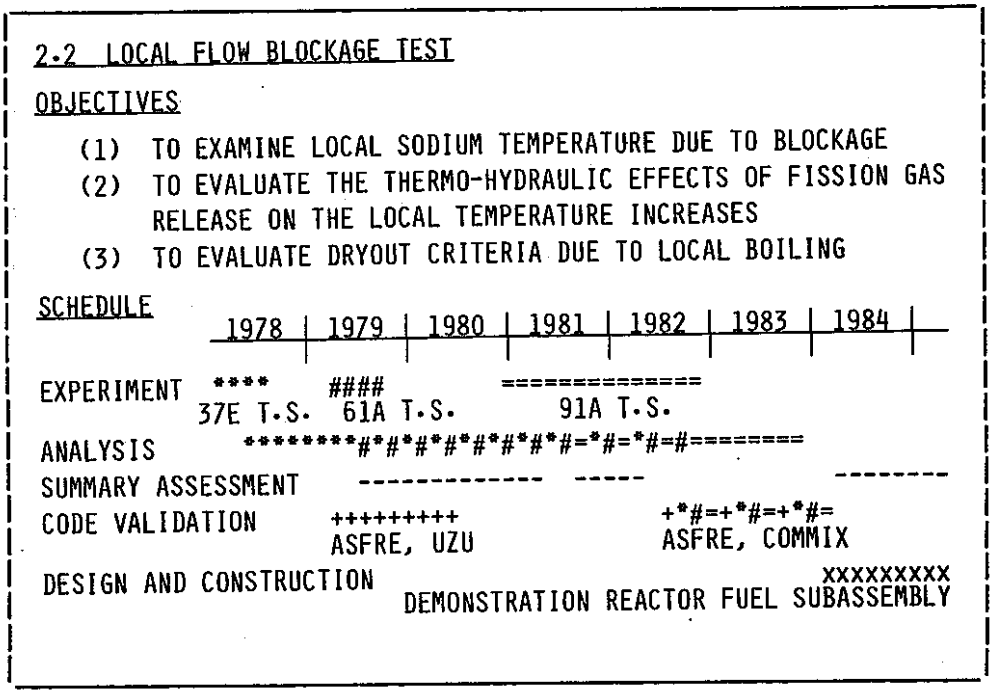

2.2 Local Flow Blockage Test .... (Change the OHP sheet, OHP No. 17)

Next item is the Local Flow Blockage Test. We have following three objectives: The first one is to examine local sodium temperature increases caused by the blockage. The second one is to evaluate the thermo-hydraulic effects of fission gas release on the local temperature increases. The last one is to evaluate dryout criteria under local boiling condition.

This program was started in 1974. The final experiment for the MONJU fuel subassembly geometry has started at the beginning of this year, using a 91-pin bundle with 50% edge blockage. The single-phase runs and the first series of FP gas release runs have been completed. In the next year, we are going to conduct additional gas release runs and local boiling runs.

The summary assessment of these test results was started in 1979 as a cooperative work with Toshiba Corporation. The initial conclusion with some general ideas about the remainding test results was attained on June, 1981. It was used for the MONJU licensing work.

Now, we are proposing to the Headquarters that at least an additional test with a new test section simulating a demonstration reactor fuel subassembly should be conducted in the future. This plan has a strong connection with the Inter-Subassembly Heat Transfer Test, because the estimation of the heat loss from the failed subassembly to the neighboring ones is required in the event tree analysis of local faults.

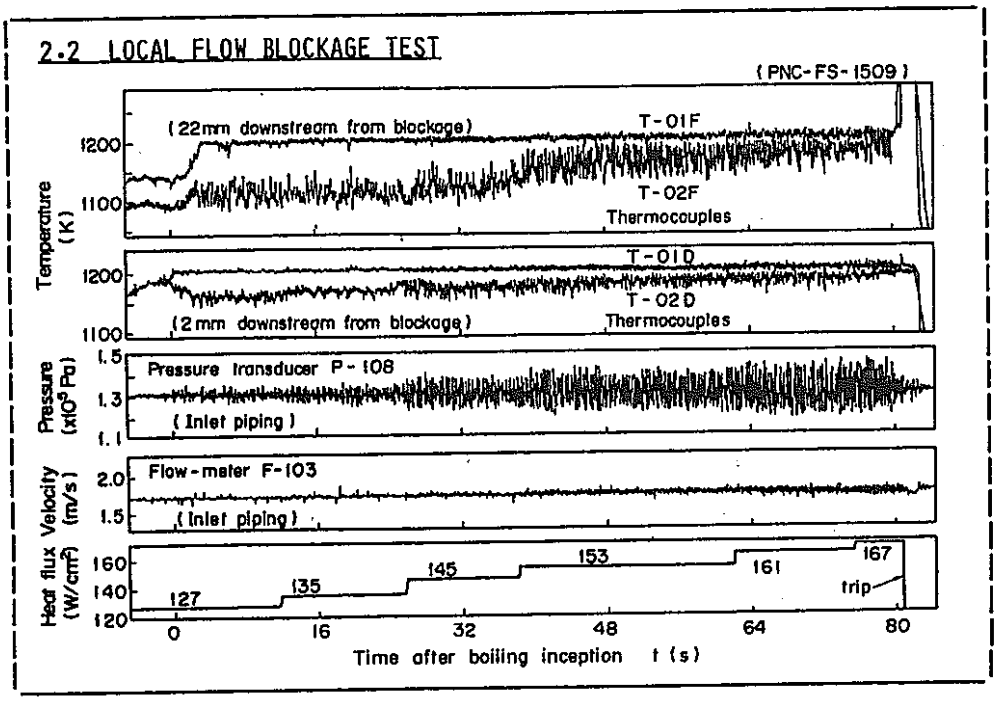

..... (Change the OHP sheet, OHP No. 18, i.e. Fig. 5)

This figure shows an example of the local boiling/dryout run conducted with the 37D wire-wrapped and centrally 26% blocked test section. The permanent dryout appeared at the fifth step of power increase after boiling inception step. In the almost all time periods of these boiling steps, the oscillatory boiling pettern governed the phenomena. However, when the power-to-flow ratio was raised up to 131% of the initial value at the boiling inception step, the oscillation damped gradually into a stabilized state, and the dryout was reached.

It can be considered that the oscillation could not attain a new effectively cooled condition at the last step. In such a case, the stabilization cannot, of cause, relieve the pins from melting.

2.2 LOCAL FLOW BLOCKAGE TEST (CONTINUED)

RESULTS

(1) · UNIVERSAL EMPIRICAL CORRELATIONS WERE OBTAINED TO EVALUATE LOCAL TEMPERATURE INCREASES

· UNDETECTED SODIUM BOILING WOULD NOT OCCUR IN A CENTRALLY BLOCKED SUBASSEMBLY, WHILE AN EDGE BLOCKAGE WILL CAUSE SODIUM BOILING

(2) GAS RELEASE INTO WAKE REGION CAUSES SEVERE TEMPERATURE INCREASES

(3) · BOTH STABLE AND OSCILLATORY BOILING MODES WERE OBSERVED DEPENDING ON THE TESTED CONDITIONS

· THE MARGIN FROM BOILING INCEPTION TO BOILING CRISIS DEPENDS ON THE BOILING MODE

..... (Change the OHP sheet, OHP No. 19)

The results obtained up to now are shown here.

For single-phase flow, universal empirical correlations were obtained to evaluate the local temperature increases behind central- and edge-type blockages. The paper describing details of the basic idea for this is submitted to the 1981 ASME Winter Annual Meeting. Extrapolation of the experimental results to the MONJU condition leads to the conclusion that the undetected sodium boiling would not occur in a centrally blocked subassembly, while an edge blockage whose area is more than a quarter of the normal flow area will cause sodium boiling for the MONJU design case.

For simulant FP gas release, it was found that the gas release into the wake region would cause severe temperature rise, because of the gas accumulation in the wake. Experimental results have been analyzed to evaluate the effects of gas release rate and sodium flow velocity on the gas concentration in the wake region. The evaluation leads to a prospect that the one-pin failure within the wake has sufficient potential to cause pin-to-pin failure propagation within the gas accumulated region. For more detail, you can refer our ASME paper which is submitted to the same meeting as above.

For local boiling, the theoretical excess temperature at the occurrence of dryout was evaluated. It indicates that there is a margin of about 30% from boiling inception to boiling crisis, when the continuous oscillatory boiling is expectable in the wake region. On the

other hand, the margin will be reduced to about 15% in the case of stable boiling. Therefore, whether the boiling pattern is stable or not becomes very important for the assessment of the coolability. For this aim, the analytical model of oscillatory boiling has been examined as one of the possible methods to know why the oscillation is initiated and why it is terminated. Future efforts are needed on this field.

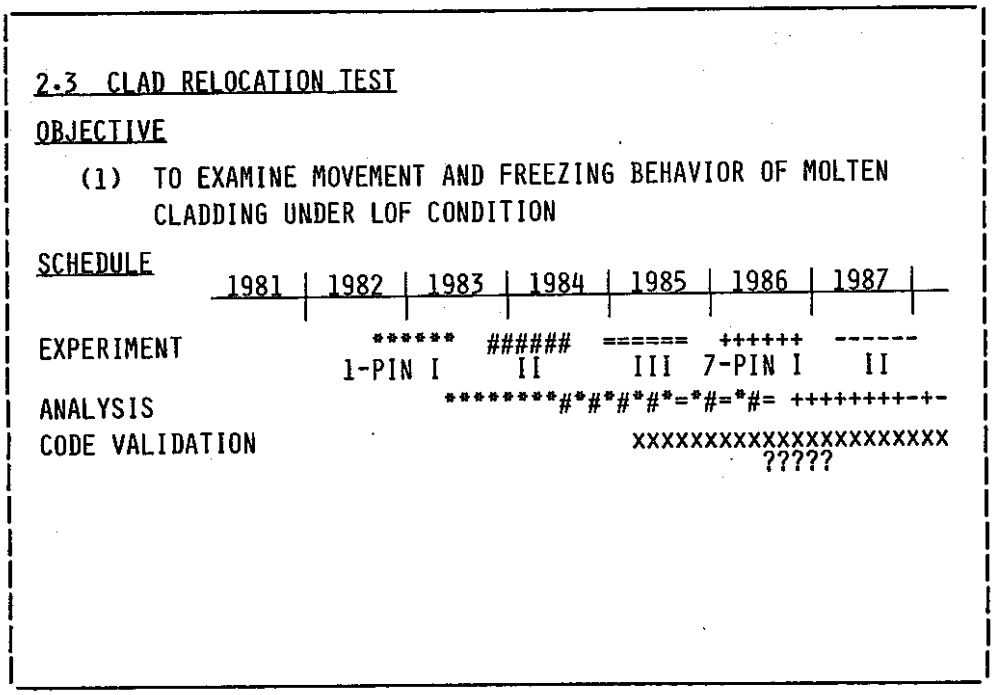

2.3 Clad Relocation Test ..... (Change the OHP sheet, OHP No. 20)

The third item is the Clad Relocation Test. The objective is to examine the movement and freezing behavior of molten cladding under LOF condition, and to provide a physical model to improve computer codes.

At present, single-pin test sections are under manufacturing. The first run will be carried out in the next year. The 7-pin bundle test will be followed in a few years.

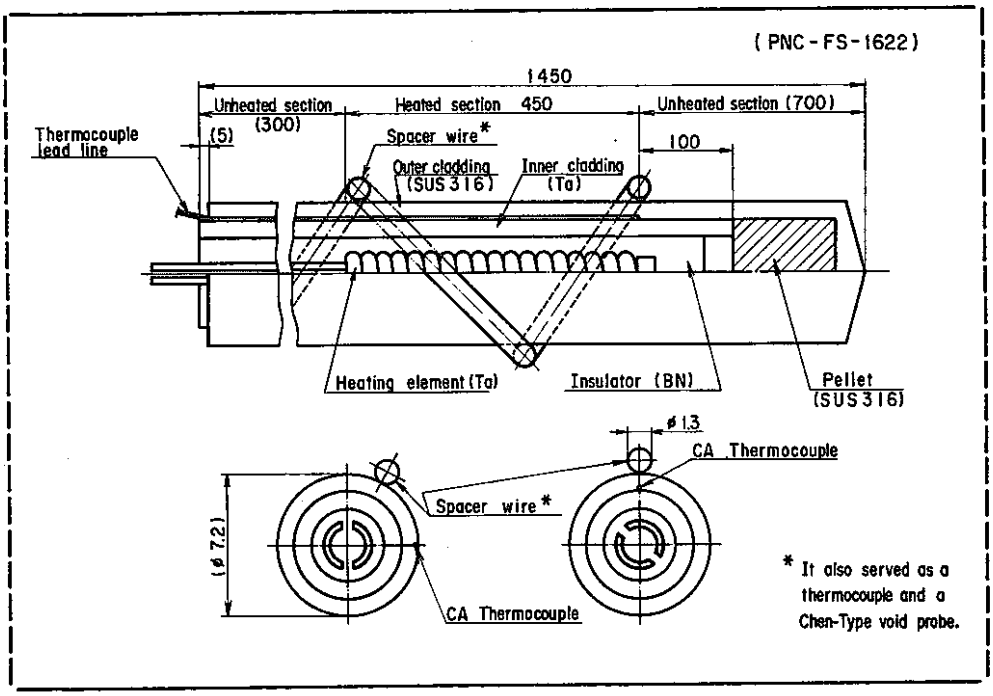

..... (Change the OHP sheet, OHP No. 21, i.e. Fig. 6)

This is a sketch of the test pin under manufacturing. The outer cladding is made of a stainless steel and the inner one is made of a tantalum. The outer diameter is 7.2 mm. The heating length is 450 mm. The test pin is wrapped with a spacer wire, and is inserted in a hexagonal or circular tube.

Following preliminary test in air, in-sodium test will be carried out.

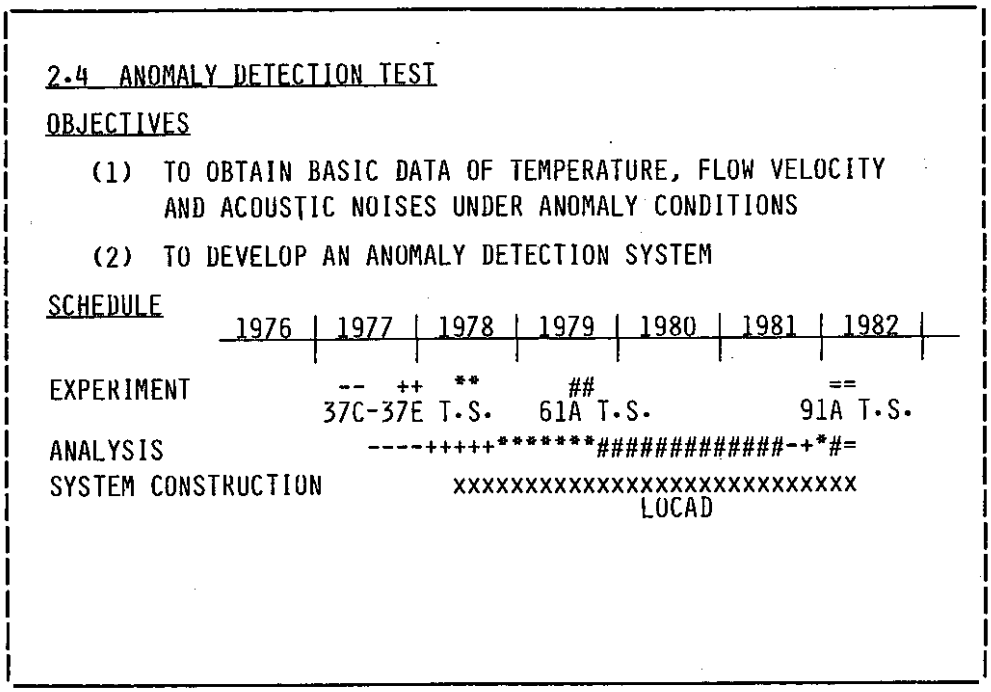

2.4 Anomaly Detection Test ..... (Change the OHP sheet, OHP No. 22)

The fourth item is the Anomaly Detection Test. Its first objective is to obtain basic data of temperature, flow velocity and acoustic noises under anomaly conditions, such as local cooling disturbance without boiling local boiling, FP gas release. The second objective is to develop an anomaly detection system. Development of a new detector is not included in our project, but is a subject of the Sodium Technology Section of the Sodium Engineering Division, OEC/PNC.

This program has been progressed in parallel to the local boiling experiments, as a joint research between PNC and Mitsubishi Electric Company. In addition, the coming first series local boiling runs will be conducted as a cooperative work with the Sodium Technology Section. These parties introduces various sensors and instrumentation circuits to our site to satisfy their data logging demands. A topical one is an acoustic sensor developed at ANL. After finishing the construction of a new instrumentation system, the test will be carried out until the spring of next year.

The code development of the Anomaly Detection was started four years ago. It will be completed in the next year.

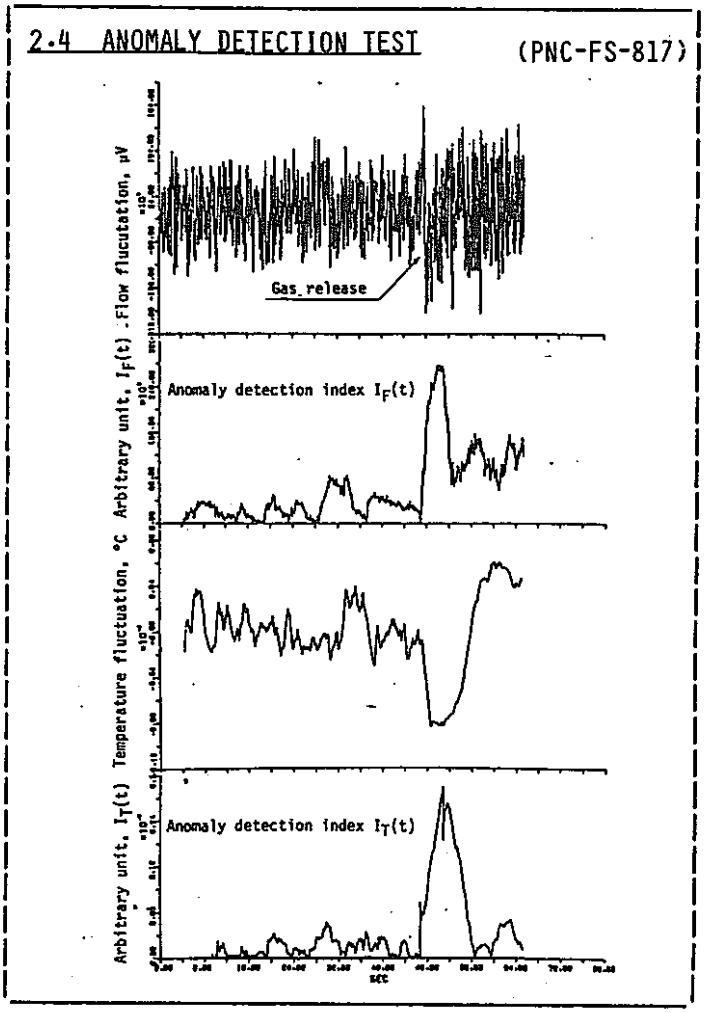

..... (Change the OHP sheet, OHP No. 23, i.e. Fig. 7)

This figure shows a typical result of the Anomaly Detection which uses the Whiteness Test Method. In this run, the grid spacer type 37-pin bundle with central 39% blockage was used. The flow fluctuation was measured by the Mark-II type probe which was developed in PNC for the MONJU in-core monitoring. The temperature fluctuation was measured so that the specification of the instrumentation system is equalized to that of MONJU.

This figure reveals that the FP gas release accident is well detectable when the anomaly detection indices submitted from the Anomaly Detection System are used for the judgement. The LOCAD System includes all functions required for this purpose.

2.4 ANOMALY DETECTION TEST (CONTINUED)

RESULTS

(1) • THE WHITENESS TEST METHOD APPLIED TO THE FLOW AND TEMPERATURE FLUCTUATIONS CAN DETECT AN INTENSIFIED OSCILLATORY BOILING

• BOILING DETECTION BY AN ACOUSTIC NOISE IS PROMISSING

• FP GAS RELEASE DUE TO A BURST TYPE ONE-PIN FAILURE CAN BE DETECTED BY FLOW FLUCTUATION

(2) • THE LOCAD SYSTEM WHICH USES THE WHITENESS TEST METHOD HAS BEEN DEVELOPED TO ATTAIN A REAL-TIME MONITORING

..... (Change the OHP sheet, OHP No. 24)

Here is the summary of the results.

First of all, we can say that the local cooling disturbance in the absence of boiling is very difficult to detect by use of outlet temperature fluctuation, because of the strong flow mixing at the upper end of the bundle. By the same reason, an early detection of the local boiling is difficult when the temperature and flow fluctuation are used for the anomaly detection. However, the Whiteness Test method is more suitable than the RMS method, and may find an anomaly state in the case of an intensified oscillatory boiling. On the other hand, the utilization of the acoustic noise is promising for the boiling detection, although there are some unsolved problems relevant to the signal transmittance and the resonant response in the equipped plant.

Third, the FP gas release due to a burst-type one-pin failure can be detected by use of flow fluctuation.

Anomaly Detection System, named LOCAD, has been developed. Its main specifications are as follows: First, it can be applied to a real-time monitoring. Second, the system consists of several sub-programs, each of which has a function of anomaly detection, signal diagnosis, and anomaly pattern classification.

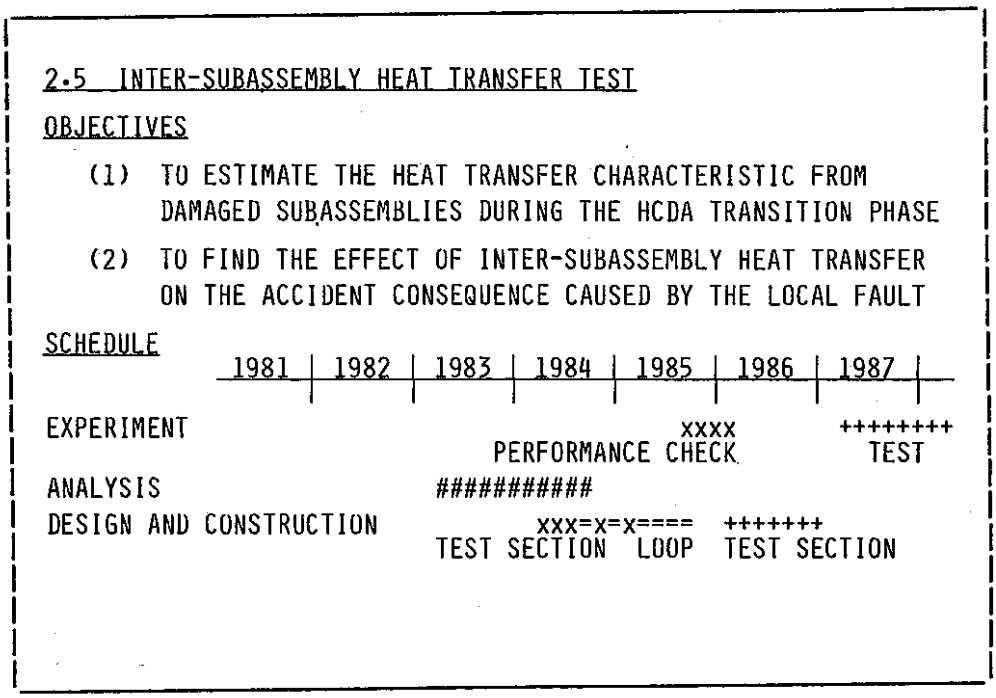

2.5 Inter-Subassembly Heat Transfer Test

..... (Change the OHP sheet, OHP No. 25)

The last item of the Fuel Failure Propagation Tests is the Inter-Subassembly Heat Transfer Test. It belongs to the unapproved future plan.

The Inter-Subassembly Heat Transfer plays an important role in the heat removal from a damaged subassembly. Especially, it becomes a dominant mechanism of possible heat removal during the hypothetical transition phase, where the decay heat of molten subassemblies must be removed by the natural circulation flow of the neighboring subassemblies. In the assessment of local faults, a similar situation can be considered, while the heat is removed not by the natural circulation flow but by the forced convection flow. The exact treatment of the inter-subassembly heat transfer leads an accident consequence to result in a less severer state than that estimated by neglecting this safety contributor.

For realizing this plan, not only a new conceptual design of the test section but also a modification of the test loop is required. A preliminary study for this purpose will be started in 1983.

END REMARKS ..... (Turn off the light of OHP)

That is all I have to say. Thank you for your attension.

5. END REMARKS

During October through December 1981, experimental studies in the Fast Reactor Safety Section were presented at one international conference and two meetings in USA. The former is the Third Specialist's Meeting on Reactor Noise (SMORN III) at Tokyo. The possibility of anomaly ditection using in-core monitor sensors was investigated in the paper. The latters are the 1981 American Society of Mechanical Engineers (ASME) Winter Annual Meeting and the 1981 American Nuclear Society (ANS) Winter Meeting. Two papers were submitted to the ASME meeting and one to the ANS. They discussed the heat transfer problems caused by local blockage, that is, the temperature rise behind blockage including the effect of released fission product gases, and local boiling phenomena. Because these items are main objectives of R & D on local faults, many experiments have been conducted using locally blocked bundle in our section. The experimental results and efforts of the data analysis are making possible to establish the evaluation methods of local blockage effect in an accident senario. Although the establishment is under way, the basic ideas are described in these papers.

On the other hand, in this time period, the PNC-UKAKA specialists' meeting on safety and instrument was held at OEC[1]. Chapter 4 covers the presentation on the recent progresses of the transient sodium boiling and fuel failure propagation tests.

The objective of this report lies in publishing the detailed scope of the presentations by a PNC "N" number report. The author(s) of a submitted paper ought to write required matters in his (their) paper. However, it is, sometimes, insufficient because of the limitation of pages assigned to the paper and the dead line of the manuscript preparation. It was considered that the supplemental remarks and the pointed explanation presented at the meeting should not be lost to provide essential informations for future advanced studies.

The records of presentations before October 1981, are compiled in "Scope of Presentation(I)"[2] and "Scope of Presentations(II)"[3].

(1) Edited by K. Haga, Records of PNC-UKAKA Specialists' Meeting on Safety and Instrument, PNC SB 042 81-02, December 1981
(2) Edited by K. Yamaguchi, PNC N 960 81-10, July 1981
(3) Edited by K. Haga, PNC N 960 81-12, September 1981